

GENERAL INSTRUCTION

- Authors: Please check and confirm whether the name of the corresponding author is correct as set.
- Authors: Carefully check the page proofs (and coordinate with all authors); additional changes or updates WILL NOT be accepted after the article is published online/print in its final form. Please check author names and affiliations, funding, as well as the overall article for any errors prior to sending in your author proof corrections.
- Authors: We cannot accept new source files as corrections for your article. If possible, please annotate the PDF proof we have sent you with your corrections and upload it via the Author Gateway. Alternatively, you may send us your corrections in list format. You may also upload revised graphics via the Author Gateway.

QUERIES

- Q1. Author: Please confirm or add details for any funding or financial support for the research of this article.
- Q2. Author: Please check and confirm whether the author affiliations in the first footnote are correct as set.
- Q3. Author: Please provide the expansions for IFAS, if applicable.
- Q4. Author: Please update Refs. [15], [24], and [33], if already published.
- Q5. Author: Please provide the complete bibliographic details for Ref. [21].
- Q6. Author: Please provide the page range for Ref. [36].
- Q7. Author: Please provide the subjects in which the author Shizhao Zhou received his respective degrees.

Control-Oriented Modeling of Effective Bulk Modulus and Online Compensation for Hydraulic Manipulator Motion Control

Yangxiu Xia , Jiajia Liu , Litong Lyu , Manzhi Qi , Shizhao Zhou ,
and Zheng Chen , Senior Member, IEEE

Abstract—Model-based control methods have been acknowledged as powerful solutions for hydraulic manipulators through compensating nonlinear dynamics. Hydraulic oil, as the working medium for energy transfer, significantly affects the system's rigidity and control performance. In most studies, the effective bulk modulus of oil is either treated as a constant or estimated as an unknown parameter. However, it is closely related to working pressure and can vary several times under different pressures. Although several theoretical models for the effective bulk modulus exist, their complexity and dependence on specific measurement equipment limit models' application in hydraulic manipulator control. In this study, a control-oriented model for the effective bulk modulus is developed, balancing the feasibility of control design and the accuracy of the model description. A model-based controller is then synthesized for a multi-degree-of-freedom hydraulic manipulator. Through an especially designed X-swapping scheme, the primary parameters of the manipulator, including those in the bulk modulus model, can be updated online without additional hardware dependencies. Theoretical analysis and experiment results demonstrate that the method improves the dynamic performance of hydraulic manipulators under varying pressures. Notably, this represents the first instance where a hydraulic manipulator controller accounts for the nonlinear characteristics of the effective bulk modulus.

Index Terms—Effective bulk modulus, hydraulic manipulator, motion control, parameter estimation, X-swapping.

I. INTRODUCTION

HYDRAULIC manipulators are widely used in applications including construction, underwater operations, and various other scenarios [1], [2]. With the trends toward automation and intelligence, closed-loop control of the hydraulic manipulators becomes increasingly important, no matter the machine is controlled through human-aided teleoperation or fully automated processes [3], [4], [5]. To achieve desired control performance, model-based control methods, such as virtual decomposition control [6], robust integral of the sign of the error [7], [8], and adaptive robust control (ARC) [9], [10], have been acknowledged as powerful solutions. And there have been numerous research achievements in modeling and compensating for factors such as payload inertia [11], [12], dynamic friction force/torque [13], and contacting force [3]. The essence of such model-based control method lies on precise model compensation of the nonlinear dynamics of the hydraulic manipulator, which means that more precise model compensation leads to enhanced control performance [14], [15].

The bulk modulus of hydraulic oil, as the primary working medium for energy transfer in hydraulic manipulators, determines the system's rigidity and is a key parameter influencing its dynamic performance [16]. The bulk modulus of pure oil is very large, making it approximately incompressible in most hydraulic transmission systems. However, due to entrained insoluble air in oil and the radial deformation of hydraulic hoses, the characterization of the effective bulk modulus is quite complicated and strongly nonlinear. Changes in working pressure can cause its value to vary by several times [17], [18], significantly affecting the efficiency and operational stability of hydraulic manipulators.

Therefore, numerous studies have focused on the measurement and theoretical modeling of the effective bulk modulus. Yang et al. [19], [20] derived a tangent bulk modulus model for oil with entrapped air and developed a measurement device to validate the model's accuracy. Murrenhoff et al. [21], [22] proposed the IFAS model, accounting for factors such as low pressures, varying temperature, and entrained air content, and

Q1 Received 26 November 2024; revised 11 April 2025; accepted 25 May 2025. Recommended by Technical Editor S. Jeong and Senior Editor H. Fujimoto. This work was supported in part by the Zhejiang Provincial Natural Science Foundation of China under Grant LR23E050001; in part by the Science and Technology Project of Hebei Education Department under Grant BJ2025200; in part by the Youth Talent Program Supported by China Railway Society; and in part by the National Natural Science Foundation of China under Grant 52105065. (Corresponding author: Zheng Chen.)

Q2 Yangxiu Xia, Jiajia Liu, Manzhi Qi, and Zheng Chen are with the State Key Laboratory of Ocean Sensing, Zhejiang University, Hangzhou 310058, China, and also with Ocean College, Zhejiang University, Zhoushan 316021, China (e-mail: yx.xia@zju.edu.cn; jiajia_liu@zju.edu.cn; manzhi.q@zju.edu.cn; zheng_chen@zju.edu.cn).

Litong Lyu is with the School of Mechanical Engineering, Shijiazhuang Tiedao University, Shijiazhuang 050043, China (e-mail: litong_lyu@stdt.edu.cn).

Shizhao Zhou is with the School of Mechanical Engineering and Automation, Fuzhou University, Fuzhou 350108, China (e-mail: zhoushizhao@zju.edu.cn).

Color versions of one or more figures in this article are available at <https://doi.org/10.1109/TMECH.2025.3583563>.

Digital Object Identifier 10.1109/TMECH.2025.3583563

verified the consistency of the model using three different methods (mass change, volume change, and soundspeed methods). With advances in measurement technology, subsequent studies have further validated the effectiveness of these two models through experimentation and demonstrated a strong relationship between the effective bulk modulus and working pressure [23], [24]. Particularly at low pressure, the effective bulk modulus of elasticity is significantly lower than at high pressure, indicating that the rigidity of the hydraulic system undergoes substantial changes with pressure variations [25], [26].

However, the mathematical formulation of the effective bulk modulus model is complex, and some states cannot be obtained in real time, making it challenging to apply in real-time control of hydraulic manipulators. Specifically, the acquisition of internal states (such as air content and the polytropic constant) in these models relies on specialized measurement equipment [27], which complicates the deployment of hydraulic systems in practice. Moreover, with continuous operation, parameters such as air content and temperature change in real time, resulting in offline results that cannot be directly applied to online pressure control. In addition, such a complex model significantly increases both the design and computational complexity of the controller. Consequently, there is limited research effectively applying these models to control. This also explains why most current research on hydraulic control either regards it as a known parameter or approaches it as an unknown lumped parameter for online estimation [28], [29], [30].

The actuators of hydraulic manipulators frequently undergo stop-and-go situations and the pressure changes quickly [31]. Considering the nonlinear characteristics of the effective bulk modulus will improve the control performance of the hydraulic manipulator, especially when there are rapid changes in working pressure. On one hand, this can improve control performance by enhancing the accuracy of feedforward model compensation. On the other hand, in most model-based control methods, the effective bulk modulus serves as a parameter in the feedback control law. Accurately accounting for its variations is crucial for tuning feedback gains, optimizing control, and other related tasks. In addition, the use of independent metering systems allows for individual adjustment of cylinder pressure in each chamber, enabling functions such as energy conservation [32], [33], [34]. The pressure within each chamber may vary significantly, leading to distinct effective bulk modulus values. Therefore, the primary challenge lies in the mathematical formulation used to capture this relationship, which must not only accurately reflect the underlying mechanism of the effective bulk modulus but also account for the feasibility of control design and enable online adaptation of key parameters whenever possible.

In this study, a control-oriented effective bulk modulus compensation method is proposed, which balances the feasibility of control design and the accuracy of the model description. The contributions of this study can be summarized as follows:

1) A control-oriented model for the effective bulk modulus is developed, which is feasible for model compensation and accurately reflects its nonlinear relationship with working pressure.

2) A model-based adaptive robust motion controller is synthesized for the multi-degree-of-freedom (DOF) hydraulic manipulator. Through an especially designed X-swapping

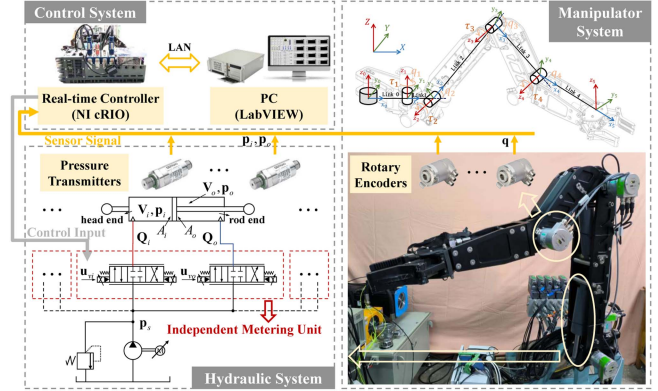


Fig. 1. Schematic diagram of a general hydraulic manipulator.

scheme, the primary parameters of the hydraulic manipulator, including those in the proposed bulk modulus model, can be updated online without additional sensors or other hardware dependencies.

3) The performance is evaluated both theoretically and through comparative experiments. The results demonstrate that the proposed method effectively enhances the dynamic performance of hydraulic manipulators across different pressure conditions.

II. PROBLEM STATEMENT AND PRELIMINARIES

A. Modeling of Hydraulic Manipulator

Consider an n -DOF hydraulic manipulator (as shown in Fig. 1), where each hydraulic cylinder is controlled by an independent metering unit [35], [36]. The rigid body dynamics can be represented as

$$\mathbf{M}(\mathbf{q})\ddot{\mathbf{q}} + \mathbf{C}(\mathbf{q}, \dot{\mathbf{q}})\dot{\mathbf{q}} + \mathbf{G}(\mathbf{q}) = \boldsymbol{\tau} - \mathbf{f}_F + \Delta_F \quad (1)$$

where $\mathbf{q} \in \mathbb{R}^n$, $\dot{\mathbf{q}} \in \mathbb{R}^n$, and $\ddot{\mathbf{q}} \in \mathbb{R}^n$ denote the joint angle position, velocity, and acceleration, respectively. The mass matrix $\mathbf{M}(\mathbf{q}) \in \mathbb{R}^{n \times n}$, the Coriolis and centrifugal matrix $\mathbf{C}(\mathbf{q}, \dot{\mathbf{q}}) \in \mathbb{R}^{n \times n}$, and the vector of gravity $\mathbf{G}(\mathbf{q}) \in \mathbb{R}^n$ are defined accordingly. $\Delta_F \in \mathbb{R}^n$ represents the lumped uncertain nonlinearities, including external interference and other hard-to model terms. $\mathbf{f}_F \in \mathbb{R}^n$ is modeled as Stribeck friction

$$\mathbf{f}_F = \Lambda_{\mathbf{q}} \mathbf{f}_v + \Lambda_{\mathbf{S}_f} (\mathbf{f}_c + \Lambda_{\mathbf{e}_f} \mathbf{f}_s) \quad (2)$$

with $\mathbf{f}_c \in \mathbb{R}^n$, $(\mathbf{f}_c + \mathbf{f}_s) \in \mathbb{R}^n$, and $\mathbf{f}_v \in \mathbb{R}^n$ representing the coefficients of the Coulomb friction, the static friction, and the viscous friction, respectively. $\Lambda_{\bullet} = \text{diag}(\bullet)$ represents the vector \bullet expanded into a diagonal matrix. $\mathbf{e}_f = e^{-(\dot{\mathbf{q}}/\dot{q}_s)^2}$, where \dot{q}_s is the Stribeck velocity threshold. $\mathbf{S}_f = \tanh(k_f \dot{\mathbf{q}})$ serves as an approximation of the sign function, with k_f chosen to be sufficiently large.

The net moment vector $\boldsymbol{\tau} \in \mathbb{R}^n$ in (1) is defined as

$$\boldsymbol{\tau} = \mathbf{J}_h(\mathbf{q}) (\Lambda_{\mathbf{A}_i} \mathbf{p}_i - \Lambda_{\mathbf{A}_o} \mathbf{p}_o) \quad (3)$$

in which $\mathbf{J}_h(\mathbf{q}) \in \mathbb{R}^{n \times n}$ is the nonsingular joint Jacobian matrix. $\mathbf{A}_i \in \mathbb{R}^n$ and $\mathbf{A}_o \in \mathbb{R}^n$ denote the piston areas at each chambers. $\mathbf{p}_i \in \mathbb{R}^n$ and $\mathbf{p}_o \in \mathbb{R}^n$ are the chamber pressure of

164 each cylinder, whose dynamics can be further expressed as

$$\begin{aligned} \Lambda_{\mathbf{V}_i} \Lambda_{\beta_{ei}^{-1}} \dot{\mathbf{p}}_i &= -\Lambda_{\mathbf{A}_i} \mathbf{J}_h \dot{\mathbf{q}} + \mathbf{Q}_i + \Delta_{Qi} \\ \Lambda_{\mathbf{V}_o} \Lambda_{\beta_{eo}^{-1}} \dot{\mathbf{p}}_o &= \Lambda_{\mathbf{A}_o} \mathbf{J}_h \dot{\mathbf{q}} - \mathbf{Q}_o + \Delta_{Qo} \end{aligned} \quad (4)$$

165 where $\mathbf{V}_i \in \mathbb{R}^n$ and $\mathbf{V}_o \in \mathbb{R}^n$ are the total compressible volumes. $\Delta_{Qi} \in \mathbb{R}^n$ and $\Delta_{Qo} \in \mathbb{R}^n$ denote the modeling errors, 166 including flow leakages and valve flow mapping errors. β_{ei} and 167 β_{eo} represent the effective bulk modulus, which will be further 168 explained later.

170 $\mathbf{Q}_i \in \mathbb{R}^n$ and $\mathbf{Q}_o \in \mathbb{R}^n$ in (4) are the supplied flow rates, 171 which can be derived from the valve flow mappings

$$\mathbf{Q}_i = \Lambda_{\mathbf{k}_{qi}} \Lambda_{\mathbf{h}_i} \mathbf{u}_{vi}, \quad \mathbf{Q}_o = \Lambda_{\mathbf{k}_{qo}} \Lambda_{\mathbf{h}_o} \mathbf{u}_{vo} \quad (5)$$

172 in which $\mathbf{k}_{qi} \in \mathbb{R}^n$ and $\mathbf{k}_{qo} \in \mathbb{R}^n$ denote the valves' flow gain 173 coefficient. $\mathbf{u}_{vi} \in \mathbb{R}^n$ and $\mathbf{u}_{vo} \in \mathbb{R}^n$ are the control commands 174 for each valve. $\mathbf{h}_i \in \mathbb{R}^n$ and $\mathbf{h}_o \in \mathbb{R}^n$ are defined as

$$\begin{aligned} \mathbf{h}_i &= \Lambda_{S(\mathbf{u}_{vi})} \sqrt{\mathbf{p}_s - \mathbf{p}_i} + \Lambda_{S(-\mathbf{u}_{vi})} \sqrt{\mathbf{p}_i - \mathbf{p}_r} \\ \mathbf{h}_o &= \Lambda_{S(\mathbf{u}_{vo})} \sqrt{\mathbf{p}_o - \mathbf{p}_r} + \Lambda_{S(-\mathbf{u}_{vo})} \sqrt{\mathbf{p}_s - \mathbf{p}_o} \end{aligned} \quad (6)$$

175 with \mathbf{p}_s and \mathbf{p}_r being the supply pressure of the pump 176 and the tank reference pressure, respectively. $S(\bullet) = [S_1(\bullet_1), \dots, S_n(\bullet_n)]^T$ is an elementwise selective function, 177 whose m th element is defined as

$$S_m(\bullet_m) = \begin{cases} 1, & \bullet_m > 0 \\ 0, & \bullet_m \leq 0. \end{cases} \quad (7)$$

179 The following notations are used throughout this article: $\tilde{\mathbf{x}} =$
180 $\hat{\mathbf{x}} - \mathbf{x}$ denotes the estimation error, with $\hat{\mathbf{x}}$ being the estimate of
181 vector \mathbf{x} . $\lambda_{\mathbf{X}} = \min(\text{eig}(\mathbf{X}))$ and $\bar{\lambda}_{\mathbf{X}} = \max(\text{eig}(\mathbf{X}))$ mean
182 the minimum and maximum eigenvalues of matrix \mathbf{X} .

183 *Property 2.1:* The inertia matrix $\mathbf{M}(\mathbf{q})$ is a symmetric positive definite (s.p.d.) matrix, and satisfies

$$\underline{\lambda}_{\mathbf{M}} \|x\|^2 \leq x^T \mathbf{M}(\mathbf{q}) x \leq \bar{\lambda}_{\mathbf{M}} \|x\| \quad \forall x \in \mathbb{R}^n. \quad (8)$$

185 *Property 2.2:* $\dot{\mathbf{M}}(\mathbf{q}) - 2\mathbf{C}(\mathbf{q}, \dot{\mathbf{q}})$ is a skew-symmetric matrix, i.e.,

$$x^T [\dot{\mathbf{M}}(\mathbf{q}) - 2\mathbf{C}(\mathbf{q}, \dot{\mathbf{q}})] x = 0 \quad \forall x \in \mathbb{R}^n. \quad (9)$$

187 *B. Modeling of Effective Bulk Modulus*

188 As discussed in the introduction, almost all existing studies
189 focusing on hydraulic control systems treated the effective bulk
190 modulus as a known parameter or as an unknown lumped parameter
191 to be estimated online [28], [29]. However, hydraulic oil,
192 as the primary working medium for energy transfer, determines
193 the system's rigidity and is a key parameter influencing control
194 performance [37]. To figure out the real characteristic of the
195 effective bulk modulus, some studies tried to derive theoretical
196 models through some specific experiments aided by additional
197 measuring equipment. Two representative studies have
198 constructed the tangent bulk modulus model and the IFAS model,
199 respectively, which are outlined as follows:

200 1) tangent bulk modulus model [19], [38]:

$$\beta_e = \frac{(V_{a0} - V'_a) \chi^{1/\kappa} + V_{f0} e^{-\varsigma}}{(V_{a0} - V'_a) \kappa^{-1} p_{atm}^{-1} \chi^{\frac{\kappa+1}{\kappa}} + V_{f0} \beta_0^{-1} e^{-\varsigma}}. \quad (10)$$

201 2) IFAS model [21], [22]:

$$\beta_e = \frac{\varpi \chi^{1/\kappa} + (1 - \varpi) (1 + m\varsigma)^{-1/m}}{\varpi (\kappa p_{atm})^{-1} \chi^{\frac{\kappa+1}{\kappa}} + (1 - \varpi) \beta_0^{-1} (1 + m\varsigma)^{\frac{m-1}{m}}}. \quad (11)$$

202 With $\varsigma = (p_{abs} - p_{atm})/\beta_0$ and $\chi = p_{atm}/p_{abs}$. p_{abs} and p_{atm}
203 are the absolute pressure and the atmospheric pressure, respectively.
204 ϖ means the entrained air content and m is the
205 pressure-related term in the bulk modulus of oil. κ represents
206 the polytropic constant of air, ranging from 1.0 to 1.4. β_0 and
207 V_{f0} are the bulk modulus and the volume of pure oil. V_{a0} and
208 V'_a denote the total volume of bubbles at atmosphere and the
209 dissolved volume of air when pressure changes from p_{atm} to p .
210 It is worth noting that $\gamma_b \leq 2\%$ is typically observed in general
211 hydraulic systems [22], where $\gamma_b = (V_{a0} - V'_a)/V_{f0}$.

212 While models mentioned previously have demonstrated good
213 agreement with experimental results, they are not suitable for
214 use in controllers for model compensation. This limitation
215 arises from their noninvertible structures, which prevent the
216 construction of a model compensation law, and the requirement
217 for specific measurements of internal states. Therefore, in this
218 study, we try to develop a control-oriented model based on these
219 theoretical models. According to (10) and (11), considering the
220 fact that $\beta_0 \gg (p_{abs} - p_{atm})$ and $\chi^{-1/\kappa} \gg \gamma_b$, the reciprocal of
221 the effective bulk modulus $\beta_{e\bullet}$ (with $\bullet \in \{i, o\}$) can be modeled
222 as

$$\beta_{e\bullet}^{-1} = \beta_0^{-1} + \gamma_b \kappa^{-1} p_{atm}^{-1} (\chi_{\bullet})^{\frac{\kappa+1}{\kappa}} \quad (12)$$

223 where $\chi_{\bullet} = p_{atm} \mathbf{p}_{\bullet}^{-1}$ with \mathbf{p}_{\bullet} being the elementwise reciprocal
224 of \mathbf{p}_{\bullet} . Then, to address the unmeasurable state γ_b and polytropic
225 constant κ , a third-order polynomial expansion is utilized as an
226 approximation, which is depicted by

$$\beta_{e\bullet}^{-1} = \theta_{\beta\bullet} + R_n(\chi_{\bullet}), \quad \theta_{\beta\bullet} \triangleq \phi_{\chi_{\bullet}}^T \vartheta_{\alpha_{\bullet}} \quad (13)$$

227 with $\phi_{\chi_{\bullet}}^T = [\Lambda_{\chi_{\bullet}}^0, \dots, \Lambda_{\chi_{\bullet}}^3]$. $\vartheta_{\alpha_{\bullet}} = [\alpha_{\bullet,0}^T, \dots, \alpha_{\bullet,3}^T]^T \in \mathbb{R}^{4n}$ is the
228 internal parameter set to be estimated later, where $\alpha_{\bullet,0}$ corre-
229 sponds to the bulk modulus of pure oil. $\alpha_{\bullet,1}$, $\alpha_{\bullet,2}$, and $\alpha_{\bullet,3}$ reflects
230 the influence of entrained air content and temperature on the
231 effective bulk modulus together. $R_n(\chi_{\bullet})$ represents the Peano
232 remainder. The proposed model for the effective bulk modulus
233 in (13) is constructed by simplification of the theoretical models
234 considering practical conditions. This model adopts a parametric
235 polynomial structure that is invertible, enabling its use for model
236 compensation with only pressure measurements required. The
237 process of utilizing the model for compensation and updating
238 the parameters online will be detailed in Section III-F.

239 *C. Model Parameterization*

240 The uncertain nonlinearities in (1), (4), and (13) can be split
241 into the nominal value $\Delta_{\bullet,n}$ with slow variation and the bounded

deviation value $\tilde{\Delta}_o$, which are given by

$$\begin{aligned}\Delta_{Fn} + \tilde{\Delta}_F &\triangleq \Delta_F \\ \Delta_{Qin} + \tilde{\Delta}_{Qi} &\triangleq \Delta_{Qi} - \Lambda_{Vi} \Lambda_{\dot{p}_i} R_n(\chi_i) \\ \Delta_{Qon} + \tilde{\Delta}_{Qo} &\triangleq \Delta_{Qo} - \Lambda_{Vo} \Lambda_{\dot{p}_o} R_n(\chi_o)\end{aligned}\quad (14)$$

Define $\theta_1 = \mathbf{f}_v$, $\theta_2 = \mathbf{f}_c$, $\theta_3 = \mathbf{f}_s$, $\theta_4 = \Delta_{Fn}$, $\theta_5 = \Delta_{Qin}$, $\theta_6 = \Delta_{Qon}$. The sets of the parameters to be estimated online are grouped as $\Theta_F = [\theta_1^T, \theta_2^T, \theta_3^T, \theta_4^T]^T$, $\Theta_{Qi} = [\vartheta_{\alpha_i}^T, \theta_5^T]^T$, and $\Theta_{Qo} = [\vartheta_{\alpha_o}^T, \theta_6^T]^T$. Referring back to (13), the dynamics model can be parameterized as

$$\begin{aligned}M\ddot{\mathbf{q}} + C\dot{\mathbf{q}} + G &= \tau - \phi_F^T \Theta_F + \tilde{\Delta}_F \\ \Lambda_{V_i} \Lambda_{\theta_{\beta_i}} \dot{\mathbf{p}}_i &= -\Lambda_{A_i} \mathbf{J}_h \dot{\mathbf{q}} + \mathbf{Q}_i + \theta_5 + \tilde{\Delta}_{Qi} \\ \Lambda_{V_o} \Lambda_{\theta_{\beta_o}} \dot{\mathbf{p}}_o &= \Lambda_{A_o} \mathbf{J}_h \dot{\mathbf{q}} - \mathbf{Q}_o + \theta_6 + \tilde{\Delta}_{Qo}\end{aligned}\quad (15)$$

with $\phi_F^T = [\Lambda_{\dot{\mathbf{q}}}, \Lambda_{S_f}, \Lambda_{S_f} \Lambda_{e_f}, -I_n]$.

Assumption 2.1: The bounds of parametric uncertainties and uncertain nonlinearities are known, i.e.,

$$\begin{aligned}\Theta_F &\in \Omega_{\Theta_F}, \Theta_{Qi} \in \Omega_{\Theta_{Qi}}, \Theta_{Qo} \in \Omega_{\Theta_{Qo}} \\ \|\tilde{\Delta}_F\| &\leq \delta_F, \|\tilde{\Delta}_{Qi}\| \leq \delta_{Qi}, \|\tilde{\Delta}_{Qo}\| \leq \delta_{Qo}\end{aligned}\quad (16)$$

where $\Omega_{\bullet} \triangleq \{\bullet : \bullet_{\min} \preceq \bullet \preceq \bullet_{\max}\}$. δ_F , δ_{Qi} , δ_{Qo} , \bullet_{\min} , and \bullet_{\max} are known scalars (with $\bullet \in \{\Theta_F, \Theta_{Qi}, \Theta_{Qo}\}$). Especially, $\bar{\theta}_{\beta_i}$ and $\underline{\theta}_{\beta_o}$ represent the known upper and lower bounds of θ_{β_i} (with $\bullet \in \{i, o\}$), respectively.

D. Control Objective

The task for the controller is to generate the control commands \mathbf{u}_{vi} and \mathbf{u}_{vo} for the valves such that the joint angles $\mathbf{q}(t)$ track a set of desired trajectories $\mathbf{q}_d(t) \in \mathbb{R}^n$ as closely as possible, which are assumed to be known, bounded, and at least third-order differentiable. In addition, since the independent metering configuration is used to control the hydraulic manipulator [35], [36], the flexibility should be handled properly to keep the cylinder working pressure at a low level.

I2. CONTROL DESIGN

The control framework is illustrated in Fig. 2. Through the reference pressure generation module, one chamber is required to maintain low pressure, while the other generates the necessary net moment. What is more, to address nonlinear variations in effective elastic modulus under low pressure, an X-swapping-based online parameter estimation method is proposed.

A. Projection Type Adaptation Law With Rate Limits

The parameter estimation $\hat{\Theta}$ will be updated by the structure

$$\dot{\hat{\Theta}} = \text{sat}_{\dot{\hat{\Theta}}_M}(\text{Proj}_{\hat{\Theta}}(\Gamma\nu)) \quad (17)$$

in which $\dot{\hat{\Theta}}_M$ is a preset rate limit, and Γ is any continuously differentiable s.p.d. matrix. ν is an adaptation function to be synthesized later. For any ν , the properties $\hat{\Theta} \in \Omega_{\Theta}$ and $\|\dot{\hat{\Theta}}\| \leq \dot{\hat{\Theta}}_M$ will always be satisfied.

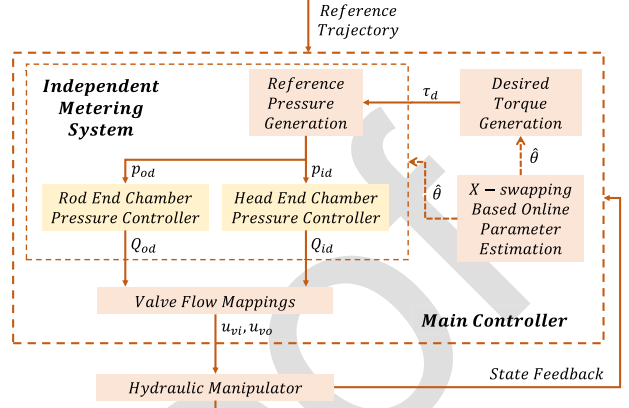


Fig. 2. Overall control framework.

The saturation function $\text{sat}_{\dot{\hat{\Theta}}_M}(\bullet)$ is expressed as

$$\text{sat}_{\dot{\hat{\Theta}}_M}(\bullet) = \begin{cases} \frac{\dot{\hat{\Theta}}_M}{\|\bullet\|} \bullet, & \|\bullet\| > \dot{\hat{\Theta}}_M \\ \bullet, & \text{otherwise.} \end{cases} \quad (18)$$

The projection-type adaptation law for $\hat{\Theta}$ is defined as

$$\text{Proj}_{\hat{\Theta}}(\bullet) = \begin{cases} \bullet - \Gamma \frac{n_{\hat{\Theta}} n_{\hat{\Theta}}^T}{n_{\hat{\Theta}}^T \Gamma n_{\hat{\Theta}}} \bullet, & \hat{\Theta} \in \partial\Omega_{\Theta} \text{ and } n_{\hat{\Theta}}^T \bullet > 0 \\ \bullet, & \text{otherwise} \end{cases} \quad (19)$$

where $\partial\Omega_{\Theta}$ represents the boundary of Ω_{Θ} . $n_{\hat{\Theta}}$ denotes the outward unit normal vector at $\hat{\Theta} \in \partial\Omega_{\Theta}$.

In addition, an gradient descent-based projection-type adaptation law for $\hat{\mathbf{d}} \in \mathbb{R}^n$ is defined as

$$\dot{\hat{\mathbf{d}}} = \text{Proj}_{\hat{\mathbf{d}}}(\Gamma \mathcal{H} \nu) \quad (20)$$

in which $\text{Proj}_{\hat{\mathbf{d}}}(\bullet) = [\text{Proj}_{\hat{d}_1}(\bullet_1), \dots, \text{Proj}_{\hat{d}_n}(\bullet_n)]^T$ is an elementwise operations projection function, whose m th element is designed as

$$\text{Proj}_{\hat{d}_m}(\bullet_m) = \begin{cases} 0, & |\hat{d}_m| = d_M \text{ and } \hat{d}_m \nu_m > 0 \\ \bullet_m, & \text{otherwise} \end{cases} \quad (21)$$

with d_M being a preset bound.

$\mathcal{H}(\hat{\mathbf{d}}, \nu, \mathcal{Q}) = \text{diag}([h_1, \dots, h_n])$ in (20) is a diagonal matrix, where $h_m = -\bar{\lambda}_{\mathcal{Q}} \text{sgn}(\hat{d}_m \nu_m)$ is a possible choice, such that (20) satisfies the following properties:

$$(P1) \|\dot{\hat{\mathbf{d}}}\| \leq d_M \quad \forall t$$

$$(P2) \hat{\mathbf{d}}^T [\Gamma^{-1} \text{Proj}_{\hat{\mathbf{d}}}(\Gamma \mathcal{H} \nu) - \mathcal{Q} \nu] \leq 0 \quad \forall \nu \quad (22)$$

in which $\mathcal{Q} \in \mathbb{R}^{n \times n}$ is any positive definite diagonal matrix and $\text{sgn}(\bullet)$ denotes the sign function.

B. Desired Torque Generation

Let $\mathbf{z}_1 = \mathbf{q} - \mathbf{q}_d$ denote the angle tracking error, a switching function can be defined as

$$\mathbf{z}_2 = \dot{\mathbf{z}}_1 + \Lambda_{k_1} \mathbf{z}_1 = \dot{\mathbf{q}} - \dot{\mathbf{q}}_{eq}, \dot{\mathbf{q}}_{eq} \triangleq \dot{\mathbf{q}}_d - \Lambda_{k_1} \mathbf{z}_1 \quad (23)$$

with $k_1 = [k_{11}, \dots, k_{1n}]^T$ being a positive constant gain vector. It can be obtained that $\mathcal{L}[\mathbf{z}_2] = \Lambda_{G(s)}\mathcal{L}[\mathbf{z}_1]$ and $G(s) = [1/(s + k_{11}), \dots, 1/(s + k_{1n})]^T$, where $\mathcal{L}[\bullet]$ means the Laplace transform of \bullet . Therefore, as long as the $\mathbf{z}_2 \rightarrow 0$, the tracking error \mathbf{z}_1 will be very small or converge to zero.

Differentiating (23) and noting (15), it has

$$\begin{aligned} \mathbf{M}\dot{\mathbf{z}}_2 + \mathbf{C}\mathbf{z}_2 &= \boldsymbol{\tau}_d - \phi_F^T \Theta_F - \mathbf{G} + \mathbf{z}_3 \\ &\quad + \tilde{\Delta}_F - (\mathbf{M}\ddot{\mathbf{q}}_{eq} + \mathbf{C}\dot{\mathbf{q}}_{eq}) \end{aligned} \quad (24)$$

in which $\mathbf{z}_3 = \boldsymbol{\tau} - \boldsymbol{\tau}_d$. $\boldsymbol{\tau}_d$ denotes the desired torque, which is designed as

$$\begin{aligned} \boldsymbol{\tau}_d &= \boldsymbol{\tau}_{da1} + \boldsymbol{\tau}_{ds1} + \boldsymbol{\tau}_{da2} + \boldsymbol{\tau}_{ds2} \\ \boldsymbol{\tau}_{da1} &= \phi_F^T \hat{\Theta}_F + \mathbf{M}\ddot{\mathbf{q}}_{eq} + \mathbf{C}\dot{\mathbf{q}}_{eq} + \mathbf{G} \\ \boldsymbol{\tau}_{ds1} &= -\Lambda_{k_F} \mathbf{z}_2 \end{aligned} \quad (25)$$

with Λ_{k_F} being a s.p.d. gain matrix. The details about $\boldsymbol{\tau}_{da2}$ and $\boldsymbol{\tau}_{ds2}$ will be given later.

By substituting (25) into (24), all parameter estimation discrepancies $\tilde{\Theta}_F$ and uncertain nonlinearities $\tilde{\Delta}_F$ can be lumped into

$$\mathbf{d}_F + \tilde{\mathbf{d}}_F^* \triangleq \phi_F^T \tilde{\Theta}_F + \tilde{\Delta}_F \quad (26)$$

where \mathbf{d}_F and $\tilde{\mathbf{d}}_F^*$ denote the static component and the high-frequency component, respectively.

Then, $\boldsymbol{\tau}_{da2}$ in (25) is designed to compensate \mathbf{d}_F as

$$\boldsymbol{\tau}_{da2} = -\hat{\mathbf{d}}_F, \dot{\hat{\mathbf{d}}}_F = \text{Proj}_{\hat{\mathbf{d}}}(\Lambda_{\gamma_F} \mathcal{H}_F \mathbf{z}_2), \|\hat{\mathbf{d}}_F\| \leq d_{FM} \quad (27)$$

with $\mathcal{H}_F = \mathcal{H}(\hat{\mathbf{d}}_F, \mathbf{z}_2, \mathbf{I})$. Λ_{γ_F} is a s.p.d. matrix and d_{FM} is a preset bound.

Select $\boldsymbol{\tau}_{ds2} = -\eta_F^{-1} h_F^2 \mathbf{z}_2 / 4$ to ensure that the following two conditions are met:

- 1) $\mathbf{z}_2^T \boldsymbol{\tau}_{ds2} \leq 0$
- 2) $\mathbf{z}_2^T (\boldsymbol{\tau}_{ds2} - \tilde{\mathbf{d}}_F + \tilde{\mathbf{d}}_F^*) \leq \eta_F$

in which $\eta_F > 0$ is an arbitrarily small parameter and h_F can be any smooth function so that

$$h_F \geq \|\phi_F^T \tilde{\Theta}_F\| + d_{FM} + \delta_F. \quad (29)$$

Using (25) and (27), the resulting error dynamics of \mathbf{z}_2 can be written as

$$\mathbf{M}\dot{\mathbf{z}}_2 + \mathbf{C}\mathbf{z}_2 = -\Lambda_{k_F} \mathbf{z}_2 + \mathbf{z}_3 + \boldsymbol{\tau}_{ds2} - \tilde{\mathbf{d}}_F + \tilde{\mathbf{d}}_F^*. \quad (30)$$

C. Generation of Reference Pressure for Each Chamber

Define the reference pressure trajectories for both chambers as \mathbf{p}_{id} and \mathbf{p}_{od} , which will be given later and must satisfy the following conditions:

$$\mathbf{J}_h (\Lambda_{\mathbf{A}_i} \mathbf{p}_{id} - \Lambda_{\mathbf{A}_o} \mathbf{p}_{od}) = \boldsymbol{\tau}_d. \quad (31)$$

By defining the pressure tracking errors as $\mathbf{z}_{pi} = \mathbf{p}_i - \mathbf{p}_{id}$ and $\mathbf{z}_{po} = \mathbf{p}_o - \mathbf{p}_{od}$, \mathbf{z}_3 in (30) can be expressed further as

$$\mathbf{z}_3 = \mathbf{J}_h (\Lambda_{\mathbf{A}_i} \mathbf{z}_{pi} - \Lambda_{\mathbf{A}_o} \mathbf{z}_{po}). \quad (32)$$

Referring back to (7), \mathbf{p}_{od} for the rod end chamber is designed as

$$\mathbf{p}_{od} = \Lambda_{S(\xi_{po})} \mathbf{p}_c + \Lambda_{S(-\xi_{po})} \Lambda_{\mathbf{A}_o}^{-1} (\Lambda_{\mathbf{A}_i} \mathbf{p}_c - \mathbf{J}_h^{-1} \boldsymbol{\tau}_d) \quad (33)$$

with $\xi_{po} = \Lambda_{\mathbf{A}_i}^{-1} (\Lambda_{\mathbf{A}_o} \mathbf{p}_c + \mathbf{J}_h^{-1} \boldsymbol{\tau}_d) - \mathbf{p}_c$. \mathbf{p}_c represents the desired low pressure, while avoiding occasional pressure fluctuations that could cause the local pressure to drop below the air separation pressure, potentially leading to cavitation.

Then, \mathbf{p}_{id} for the head end chamber can be integrated as

$$\mathbf{p}_{id} = \Lambda_{\mathbf{A}_i}^{-1} (\Lambda_{\mathbf{A}_o} \mathbf{p}_{od} + \mathbf{J}_h^{-1} \boldsymbol{\tau}_d). \quad (34)$$

Remark 3.1: The independent metering unit shown in Fig. 1 enables numerous reference pressure configurations that satisfy (29). According to (31) and (32), the reference pressure in both chambers will not fall below the preset pressure \mathbf{p}_c , while at least one chamber reaches \mathbf{p}_c , thereby minimizing the overall working pressure. In addition, the proposed generation method ensures that the desired torque $\boldsymbol{\tau}_d$ remains unchanged, thus maintaining the required high-precision motion control performance.

D. Pressure Controller for Head End Chamber

The error dynamics of \mathbf{z}_{pi} is expressed as

$$\Lambda_{\theta_{\beta_i}} \dot{\mathbf{z}}_{pi} = \Lambda_{\mathbf{V}_i}^{-1} (\mathbf{Q}_i - \Lambda_{\mathbf{A}_i} \mathbf{J}_h \dot{\mathbf{q}} + \theta_5 + \tilde{\Delta}_{Qi}) - \Lambda_{\theta_{\beta_i}} \dot{\mathbf{p}}_{id}. \quad (35)$$

Given the sufficiently high bandwidth of the control valve, the dynamics of the valve spool motion can be neglected [10], allowing the assumption $\mathbf{Q}_i = \mathbf{Q}_{id}$. Referring back to (13) and noting $\Lambda_{\theta_{\beta_i}} \dot{\mathbf{p}}_{id} = \Lambda_{\dot{\mathbf{p}}_{id}} \phi_{\chi_i}^T \dot{\vartheta}_{\alpha_i}$, \mathbf{Q}_{id} can be designed as

$$\begin{aligned} \mathbf{Q}_{id} &= \mathbf{Q}_{ida1} + \mathbf{Q}_{ids1} + \mathbf{Q}_{ida2} + \mathbf{Q}_{ids2} + \Upsilon_{Qi} \\ \mathbf{Q}_{ida1} &= \Lambda_{\mathbf{A}_i} \mathbf{J}_h \dot{\mathbf{q}} - \hat{\theta}_5 + \Lambda_{\mathbf{V}_i} \Lambda_{\dot{\mathbf{p}}_{id}} \phi_{\chi_i}^T \dot{\vartheta}_{\alpha_i} \\ \mathbf{Q}_{ids1} &= -\Lambda_{\mathbf{V}_i} \Lambda_{k_{Qi}} \mathbf{z}_{pi}, \quad \Upsilon_{Qi} = -\Lambda_{\mathbf{V}_i} \mathcal{F}_i \Lambda_{\mathbf{A}_i} \mathbf{J}_h^T \mathbf{z}_2 \end{aligned} \quad (36)$$

with $\Lambda_{k_{Qi}}$ being an s.p.d. gain matrix. \mathcal{F}_i is designed as $\mathcal{F}_i = \mathcal{F}(\mathbf{z}_{pi}, \Lambda_{\mathbf{A}_i} \mathbf{J}_h^T \mathbf{z}_2, \bar{\theta}_{\beta_i})$, where the specific definition and property of \mathcal{F} will be demonstrated in the *Lemma 3.1*. Substituting (36) into (35), all uncertainties can be lumped into

$$\mathbf{d}_{Qi} + \tilde{\mathbf{d}}_{Qi}^* \triangleq \Lambda_{\mathbf{V}_i}^{-1} (-\hat{\theta}_5 + \tilde{\Delta}_{Qi}) + \Lambda_{\dot{\mathbf{p}}_{id}} \phi_{\chi_i}^T \tilde{\vartheta}_{\alpha_i} \quad (37)$$

where \mathbf{d}_{Qi} and $\tilde{\mathbf{d}}_{Qi}^*$ denote the static component and the high-frequency component, respectively.

Then, \mathbf{Q}_{ida2} in (36) is designed as

$$\mathbf{Q}_{ida2} = -\Lambda_{\mathbf{V}_i} \hat{\mathbf{d}}_{Qi}, \quad \dot{\hat{\mathbf{d}}}_{Qi} = \text{Proj}_{\hat{\mathbf{d}}}(\Lambda_{\gamma_{Qi}} \mathcal{H}_{Qi} \mathbf{z}_{pi}) \quad (38)$$

with $\mathcal{H}_{Qi} = \mathcal{H}(\hat{\mathbf{d}}_{Qi}, \mathbf{z}_{pi}, \Lambda_{\theta_{\beta_i}}^{-1})$. $\Lambda_{\gamma_{Qi}}$ is a s.p.d. matrix and $\|\hat{\mathbf{d}}_{Qi}\| \leq d_{QiM}$, where d_{QiM} being a preset bound.

Select $\mathbf{Q}_{ids2} = -\eta_{Qi}^{-1} h_{Qi}^2 \Lambda_{\mathbf{V}_i} \mathbf{z}_{pi} / 4$ to ensure that the following two conditions are met:

$$1) \mathbf{z}_{pi}^T \Lambda_{\theta_{\beta_i}}^{-1} \Lambda_{\mathbf{V}_i}^{-1} \mathbf{Q}_{ids2} \leq 0$$

$$2) \mathbf{z}_{pi}^T \Lambda_{\theta_{\beta_i}}^{-1} (\Lambda_{\mathbf{V}_i}^{-1} \mathbf{Q}_{ids2} - \tilde{\mathbf{d}}_{Qi} + \tilde{\mathbf{d}}_{Qi}^*) \leq \underline{\theta}_{\beta_i} \eta_{Qi} \quad (39)$$

in which $\eta_{Qi} > 0$ is an arbitrarily small parameter. h_{Qi} can be any smooth function so that

$$h_{Qi} \geq \|\Lambda_{\dot{\mathbf{p}}_{id}} \phi_{\chi_i}^T \tilde{\vartheta}_{\alpha_i}\| + \|\Lambda_{\mathbf{V}_i}^{-1} \tilde{\theta}_5\| + d_{QiM} + \Lambda_{\mathbf{V}_i}^{-1} \delta_{Qi}. \quad (40)$$

Using (36) and (38), the resulting error dynamics of \mathbf{z}_{pi} can be written as

$$\begin{aligned} \Lambda_{\theta_{\beta_i}} \dot{\mathbf{z}}_{pi} = & -\Lambda_{k_{Qi}} \mathbf{z}_{pi} - \mathcal{F}_i \Lambda_{\mathbf{A}_i} \mathbf{J}_h^T \mathbf{z}_2 \\ & + \Lambda_{\mathbf{V}_i}^{-1} \mathbf{Q}_{ids2} - \tilde{\mathbf{d}}_{Qi} + \tilde{\mathbf{d}}_{Qi}^*. \end{aligned} \quad (41)$$

E. Pressure Controller for Rod End Chamber

The error dynamics of \mathbf{z}_{po} is expressed as

$$\begin{aligned} \Lambda_{\theta_{\beta_o}} \dot{\mathbf{z}}_{po} = & \Lambda_{\mathbf{V}_o}^{-1} \left(\Lambda_{\mathbf{A}_o} \mathbf{J}_h \dot{\mathbf{q}} - \mathbf{Q}_o + \theta_6 + \tilde{\Delta}_{Qi} \right) - \Lambda_{\theta_{\beta_o}} \dot{\mathbf{p}}_{od}. \end{aligned} \quad (42)$$

Similar to \mathbf{Q}_{id} , \mathbf{Q}_{od} is designed as

$$\begin{aligned} \mathbf{Q}_{od} &= \mathbf{Q}_{oda1} + \mathbf{Q}_{ods1} + \mathbf{Q}_{oda2} + \mathbf{Q}_{ods2} + \Upsilon_{Qo} \\ \mathbf{Q}_{oda1} &= \Lambda_{\mathbf{A}_o} \mathbf{J}_h \dot{\mathbf{q}} + \hat{\theta}_6 - \Lambda_{\mathbf{V}_o} \Lambda_{\dot{\mathbf{p}}_{od}} \phi_{\chi_o}^T \hat{\vartheta}_{\alpha_o} \\ \mathbf{Q}_{oda2} &= \Lambda_{\mathbf{V}_o} \hat{\mathbf{d}}_{Qo}, \quad \dot{\hat{\mathbf{d}}}_{Qo} = \text{Proj}_{\hat{\mathbf{d}}}(\Lambda_{\gamma_{Qo}} \mathcal{H}_{Qo} \mathbf{z}_{po}) \\ \mathbf{Q}_{ods1} &= \Lambda_{\mathbf{V}_o} \Lambda_{k_{Qo}} \mathbf{z}_{po}, \quad \Upsilon_{Qo} = -\Lambda_{\mathbf{V}_o} \mathcal{F}_o \Lambda_{\mathbf{A}_o} \mathbf{J}_h^T \mathbf{z}_2 \end{aligned} \quad (43)$$

in which $\Lambda_{k_{Qo}}$ and $\Lambda_{\gamma_{Qo}}$ are s.p.d. gain matrixes. $\mathcal{H}_{Qo} = \mathcal{H}(\hat{\mathbf{d}}_{Qo}, \mathbf{z}_{po}, \Lambda_{\theta_{\beta_o}}^{-1})$. \mathcal{F}_o is designed as $\mathcal{F}_o = \mathcal{F}(\mathbf{z}_{po}, \Lambda_{\mathbf{A}_o} \mathbf{J}_h^T \mathbf{z}_2, -\bar{\theta}_{\beta_o})$. $\|\hat{\mathbf{d}}_{Qo}\| \leq d_{QoM}$, with d_{QoM} being a preset bound. \mathbf{d}_{Qo} represents the static component of the residual nonlinearities, which is defined as

$$\mathbf{d}_{Qo} + \tilde{\mathbf{d}}_{Qo}^* \triangleq \Lambda_{\mathbf{V}_o}^{-1} \left(-\tilde{\theta}_6 + \tilde{\Delta}_{Qi} \right) + \Lambda_{\dot{\mathbf{p}}_{od}} \phi_{\chi_o}^T \tilde{\vartheta}_{\alpha_o} \quad (44)$$

where $\tilde{\mathbf{d}}_{Qo}^*$ denotes the high-frequency component.

$\mathbf{Q}_{ods2} = \eta_{Qo}^{-1} h_{Qo}^2 \Lambda_{\mathbf{V}_o} \mathbf{z}_{po} / 4$ is designed to satisfy the following two conditions:

$$\begin{aligned} 1) \quad & \mathbf{z}_{po}^T \Lambda_{\theta_{\beta_o}}^{-1} \Lambda_{\mathbf{V}_o}^{-1} \mathbf{Q}_{ods2} \geq 0 \\ 2) \quad & \mathbf{z}_{po}^T \Lambda_{\theta_{\beta_o}}^{-1} \left(-\Lambda_{\mathbf{V}_o}^{-1} \mathbf{Q}_{ods2} - \tilde{\mathbf{d}}_{Qo} + \tilde{\mathbf{d}}_{Qo}^* \right) \leq \underline{\theta}_{\beta_o} \eta_{Qo} \end{aligned} \quad (45)$$

in which $\eta_{Qo} > 0$ is an arbitrarily small parameter. h_{Qo} is a smooth function that satisfies

$$h_{Qo} \geq \|\Lambda_{\dot{\mathbf{p}}_{od}} \phi_{\chi_o}^T \tilde{\vartheta}_{\alpha_o}\| + \|\Lambda_{\mathbf{V}_o}^{-1} \tilde{\theta}_6\| + d_{QoM} + \Lambda_{\mathbf{V}_o}^{-1} \delta_{Qo}. \quad (46)$$

The resulting error dynamics of \mathbf{z}_{pi} can be written as

$$\begin{aligned} \Lambda_{\theta_{\beta_o}} \dot{\mathbf{z}}_{po} = & -\Lambda_{k_{Qo}} \mathbf{z}_{po} + \mathcal{F}_o \Lambda_{\mathbf{A}_o} \mathbf{J}_h^T \mathbf{z}_2 \\ & - \Lambda_{\mathbf{V}_o}^{-1} \mathbf{Q}_{ods2} - \tilde{\mathbf{d}}_{Qo} + \tilde{\mathbf{d}}_{Qo}^*. \end{aligned} \quad (47)$$

Finally, the control command of the valve \mathbf{u}_{vi} and \mathbf{u}_{vo} can be synthesized by the valve flow mappings in (5) as

$$\mathbf{u}_{vi} = \Lambda_{\mathbf{h}_i}^{-1} \Lambda_{\mathbf{k}_{qi}}^{-1} \mathbf{Q}_i, \quad \mathbf{u}_{vo} = \Lambda_{\mathbf{h}_o}^{-1} \Lambda_{\mathbf{k}_{qo}}^{-1} \mathbf{Q}_o. \quad (48)$$

F. X-Swapping-Based Online Parameter Estimation

If the nonlinear uncertainties within the dynamics in (15) are assumed to be zero after a finite time, i.e., assuming $\tilde{\Delta}_F =$

$\tilde{\Delta}_{Qi} = \tilde{\Delta}_{Qo} = 0$, the system dynamics for parameter estimation can be rewritten as

$$\begin{aligned} \phi_F^T \Theta_F &= \boldsymbol{\tau} - \mathbf{M} \ddot{\mathbf{q}} - \mathbf{C} \dot{\mathbf{q}} - \mathbf{G} \\ \Lambda_{\dot{\mathbf{p}}_i} \phi_{\chi_i}^T \vartheta_{\alpha_i} - \Lambda_{\mathbf{V}_i}^{-1} \theta_5 &= -\Lambda_{\mathbf{V}_i}^{-1} \Lambda_{\mathbf{A}_i} \mathbf{J}_h \dot{\mathbf{q}} + \Lambda_{\mathbf{V}_i}^{-1} \mathbf{Q}_i \\ \Lambda_{\dot{\mathbf{p}}_o} \phi_{\chi_o}^T \vartheta_{\alpha_o} - \Lambda_{\mathbf{V}_o}^{-1} \theta_6 &= \Lambda_{\mathbf{V}_o}^{-1} \Lambda_{\mathbf{A}_o} \mathbf{J}_h \dot{\mathbf{q}} - \Lambda_{\mathbf{V}_o}^{-1} \mathbf{Q}_o \end{aligned} \quad (49)$$

in which $\Theta_F, \Theta_{Qi} = [\vartheta_{\alpha_i}^T, \theta_5^T]^T$, and $\Theta_{Qo} = [\vartheta_{\alpha_o}^T, \theta_6^T]^T$ are parameters to be estimated. Define the following regressors:

$$\varphi_F^T = \mathbf{M} \dot{\mathbf{q}}, \quad \varphi_{\varepsilon_i}^T = [\Lambda_{\varepsilon_{\bullet 0}}, \dots, \Lambda_{\varepsilon_{\bullet 3}}] \quad (50)$$

where $\varepsilon_{\bullet 0} = \mathbf{p}_\bullet$, $\varepsilon_{\bullet 1} = p_{\text{atm}} \ln(\mathbf{p}_\bullet)$, $\varepsilon_{\bullet 2} = -p_{\text{atm}}^2 \mathbf{p}_\bullet^{-1}$, and $\varepsilon_{\bullet 3} = -\frac{1}{2} p_{\text{atm}}^3 \Lambda_{\mathbf{p}_\bullet^{-1}} \mathbf{p}_\bullet^{-1}$ (with $\bullet \in \{i, o\}$). The differentiates of φ_F^T and $\varphi_{\varepsilon_i}^T$ are able to be written as

$$\begin{aligned} \frac{d}{dt} (\varphi_F^T) &= \mathbf{M} \ddot{\mathbf{q}} + \mathbf{C} \dot{\mathbf{q}} + \mathbf{G}^T \dot{\mathbf{q}} \\ \frac{d}{dt} (\varphi_{\varepsilon_i}^T) &= \Lambda_{\dot{\mathbf{p}}_{\bullet d}} \phi_{\chi_\bullet}^T. \end{aligned} \quad (51)$$

Then, the dynamics (49) can be rewritten as

$$\begin{aligned} \phi_F^T \Theta_F &= u_{F1} + \dot{u}_{F2} \\ \dot{\varphi}_{\varepsilon_i}^T \vartheta_{\alpha_i} - \Lambda_{\mathbf{V}_i}^{-1} \theta_5 &= u_{Qi} \\ \dot{\varphi}_{\varepsilon_o}^T \vartheta_{\alpha_o} - \Lambda_{\mathbf{V}_o}^{-1} \theta_6 &= u_{Qo} \end{aligned} \quad (52)$$

with $u_{F1} = \boldsymbol{\tau} + \mathbf{C}^T \dot{\mathbf{q}} - \mathbf{G}$, $u_{F2} = -\varphi_F^T$, $u_{Qi} = -\Lambda_{\mathbf{V}_i}^{-1} \Lambda_{\mathbf{A}_i} \mathbf{J}_h \dot{\mathbf{q}} + \Lambda_{\mathbf{V}_i}^{-1} \mathbf{Q}_i$, and $u_{Qo} = \Lambda_{\mathbf{V}_o}^{-1} \Lambda_{\mathbf{A}_o} \mathbf{J}_h \dot{\mathbf{q}} - \Lambda_{\mathbf{V}_o}^{-1} \mathbf{Q}_o$.

The first-order filters for acquiring states is designed as

$$\dot{\xi}_\bullet = -\lambda_\bullet \xi_\bullet + u_\bullet, \quad \dot{\psi}_\bullet = -\lambda_\bullet \psi_\bullet + \mathcal{T}_\bullet \quad (53)$$

in which λ_\bullet represents the break frequency of the first-order filters (with $\bullet \in \{F1, F2, Qi, Qo\}$). And \mathcal{T}_\bullet is defined as

$$\begin{aligned} \mathcal{T}_{F1}^T &= \mathcal{T}_{F2}^T = [\Lambda_{\mathbf{q}}, \Lambda_{\mathbf{S}_f}, \Lambda_{\mathbf{S}_f} \Lambda_{\mathbf{e}_f}, -\mathbf{I}_n] \\ \mathcal{T}_{Qi}^T &= [-\lambda_i \varphi_{\varepsilon_i}^T, -\Lambda_{\mathbf{V}_i}^{-1}] \\ \mathcal{T}_{Qo}^T &= [-\lambda_o \varphi_{\varepsilon_o}^T, -\Lambda_{\mathbf{V}_o}^{-1}]. \end{aligned} \quad (54)$$

Let $\lambda_{F1} = \lambda_{F2} = \lambda_F$. Then, define variables as $y_F = \xi_{F1} - \lambda_F \xi_{F2} + u_{F2}$, $y_{Qi} = \xi_{Qi}$, and $y_{Qo} = \xi_{Qo}$, whose estimations \check{y}_\bullet (with $\bullet \in \{F, Qi, Qo\}$) can be given as

$$\check{y}_\bullet = -\Phi_\bullet^T \Theta_\bullet \quad (55)$$

in which $\Phi_F^T = -\mathcal{T}_F^T$, $\Phi_{Qi}^T = \Psi_{Qi}^T - \mathcal{T}_{Qi}^T$, and $\Phi_{Qo}^T = \Psi_{Qo}^T - \mathcal{T}_{Qo}^T$, with $\Psi_{Qi}^T \triangleq [-\varphi_{\varepsilon_i}^T, \mathbf{0}_{n \times n}]$ and $\Psi_{Qo}^T \triangleq [-\varphi_{\varepsilon_o}^T, \mathbf{0}_{n \times n}]$.

Define the discrepancies $\dot{\tilde{y}}_\bullet = \check{y}_\bullet - y_\bullet$. Then, differentiate \tilde{y}_\bullet , one can get $\dot{\tilde{y}}_\bullet = -\lambda_\bullet \tilde{y}_\bullet$, which means $\tilde{y}_\bullet = 0$ can always be guaranteed if the initial conditions of the filters defined in (53) are chosen properly to satisfy $\tilde{y}_\bullet(0) = 0$. Therefore, $y_\bullet = \check{y}_\bullet \forall t$. Define $\hat{y}_\bullet = -\Phi_\bullet^T \hat{\Theta}_\bullet$ represents the prediction of y_\bullet . The prediction errors ϵ_\bullet can be given as

$$\epsilon_\bullet = \hat{y}_\bullet - y_\bullet = -\Phi_\bullet^T \tilde{\Theta}_\bullet. \quad (56)$$

Thus, the static parametric models which are linear with respect to the parameter estimation errors $\hat{\Theta}_F, \hat{\Theta}_{Qi}$ and $\hat{\Theta}_{Qo}$ have been obtained successfully for estimation. The adaptive function in

(17) is chosen as $\nu_{\bullet} = \Phi_{\bullet}\epsilon_{\bullet}$. Then, the recursive ridge regression estimation algorithm can be used for online estimation, where Γ_{\bullet} is defined as

$$\dot{\Gamma}_{\bullet} = \begin{cases} \iota_{\bullet}\Gamma_{\bullet} - \Gamma_{\bullet}\Phi_{\bullet}\Phi_{\bullet}^T\Gamma_{\bullet}, & \bar{\lambda}_{\Gamma_{\bullet}} \leq \rho_{\bullet M} \\ 0, & \text{otherwise} \end{cases} \quad (57)$$

with ι_{\bullet} being the forgetting factor.

Remark 3.2: Traditional adaptive methods are often challenging to apply to (49) due to the coupling between unmeasurable derivative terms (\dot{q}_i , \dot{p}_i , and \dot{p}_o) and unknown dynamic parameters Θ . To address this, a method similar to pre-integration, as shown in (51), was used to construct an intermediate variable in (50), which contains only measurable states. Furthermore, the real-time numerical results of the coupling term were directly derived from the intermediate variables using the X-swapping algorithm, as given in (53)–(56), while maintaining the same phase lag, thereby yielding the prediction errors ϵ_{\bullet} for the parameter. Then, the online adaptive method is not limited to approaches such as the least-squares method and the gradient descent method.

G. Theoretical Results

Lemma 3.1: Define $f_{\mathcal{F}} = x^T(\mathcal{Q}\mathcal{F} - \mathbf{I})y$ with $\mathcal{Q} \in \mathbb{R}^{n \times n}$ being any s.p.d. matrix, $x \in \mathbb{R}^n$, and $y \in \mathbb{R}^n$. Positive and negative $f_{\mathcal{F}}$ are both feasible to be achieved by the design of \mathcal{F} as follows:

$$\mathcal{F}(x, y, \underline{\lambda}_{\mathcal{Q}}) = \frac{|n_x^T n_y|}{\underline{\lambda}_{\mathcal{Q}}} n_x n_y^T \Rightarrow f_{\mathcal{F}} \geq 0 \forall x, y \quad (58)$$

where n_x and n_y represent the unit vector of x and y , respectively. Besides, if $\mathcal{F} = \mathcal{F}(x, y, -\underline{\lambda}_{\mathcal{Q}})$, $f_{\mathcal{F}} \leq 0 \forall x, y$. The proof is given in Appendix A. ■

The following theoretical results about the proposed system control design can be obtained.

Theorem 3.1: (Boundedness) Considering the parameter estimates updated by (17) and the motion control law, the system controller with \mathbf{u}_{vi} and \mathbf{u}_{vo} as the input guarantees that all signals are bounded. Furthermore, the positive-definite function V_s defined by

$$V_s = \frac{1}{2}\mathbf{z}_2^T \mathbf{M} \mathbf{z}_2 + \frac{1}{2}\mathbf{z}_{pi}^T \mathbf{z}_{pi} + \frac{1}{2}\mathbf{z}_{po}^T \mathbf{z}_{po} \quad (59)$$

is bounded above by

$$V_s(t) \leq \exp(-\lambda_s t)V_s(0) + \frac{\eta_s}{\lambda_s}[1 - \exp(-\lambda_s t)] \quad (60)$$

with $\lambda_s = \min\{2k_F/\bar{\lambda}_M, 2\bar{\theta}_{\beta i}k_{Qi}, 2\bar{\theta}_{\beta o}k_{Qo}\}$ and $\eta_s = \eta_F + \underline{\theta}_{\beta i}\eta_{Qi} + \underline{\theta}_{\beta o}\eta_{Qo}$. The proof is given in Appendix B. ■

Theorem 3.2: (Asymptotic Tracking) Consider the control law (25), (36), and (43) with the adaptation law (17), applied to the hydraulic manipulator with dynamics described by (15). If after a finite time t_f , $\tilde{\Delta}_F = \tilde{\Delta}_{Qi} = \tilde{\Delta}_{Qo} = 0 \forall t \geq t_f$, when the PE condition is satisfied

$$\exists T, t_f, \varepsilon_d > 0 \text{ s.t. } \int_t^{t+T} \Phi \Phi^T d\tau \geq \varepsilon_d \mathbf{I} \forall t \geq t_f \quad (61)$$

in addition to the results outlined in *Theorem 3.1*, the parameter estimates $\hat{\Theta}$ asymptotically converge to true values and the

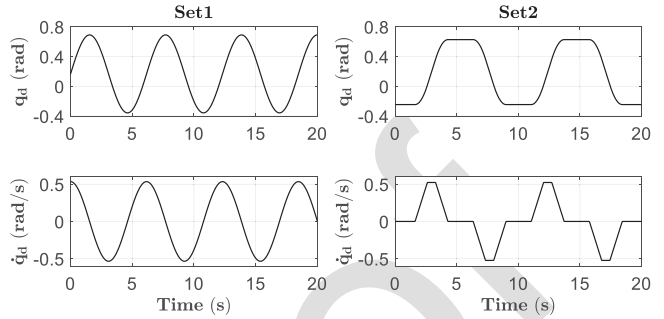


Fig. 3. Reference trajectories in experiment Set1 and Set2.

asymptotic tracking is achieved, i.e., the tracking errors $\mathbf{z}_1 \rightarrow 0$ as $t \rightarrow \infty$. The proof is given in Appendix C. ■

IV. COMPARATIVE EXPERIMENTS AND ANALYSIS

A. Experiment Setup

The proposed control method is applied to a hydraulic manipulator for testing, as shown in Fig. 1. The links 2, 3, and 4 are always coplanar because the link offsets are zeros, and this plane is positioned by the vertical revolution of joint 1. Each joint is independently driven by a hydraulic cylinder, which converts the linear motion of the cylinder into rotational motion at the joint. Flow rates for the two chambers of the hydraulic cylinder are independently regulated by a three-position four-way proportional valve. Pressure feedback is provided by GEFTRAN KS series pressure transmitters with a precision of 0.5%, while joint position sensing is achieved using POSITAL IXARC series absolute encoders, offering a 16-bit single-turn resolution. The following three methods were compared:

- 1) **C1:** The proposed controller in this study. The control law could be represented by (25), (36), and (43), where the parameters were specified as $\Lambda_{k_1} = \text{diag}([80, 80])$, $\Lambda_{k_F} = \text{diag}([27, 58])$, $\Lambda_{k_{Qi}} = \text{diag}([35, 33])$, $\Lambda_{k_{Qo}} = \text{diag}([45, 25])$, $\Lambda_{\gamma_F} = \text{diag}([180, 500])$, and $\Lambda_{\gamma_{Qi}} = \Lambda_{\gamma_{Qo}} = \text{diag}([1, 5]) \times 10^{-6}$.
- 2) **C2:** A controller similar to C1, but lacking online parameter estimation for $\vartheta_{\beta \bullet}$, i.e., $\vartheta_{\beta \bullet}(t) \equiv \vartheta_{\beta \bullet}(0)$.
- 3) **C3:** The effective bulk modulus is treated as a lumped parameter for both estimation and compensation, consistent with most existing studies [28], [29]. Specifically, in (13), $\vartheta_{\beta \bullet} = \alpha_{\bullet 0}$ is the parameter to be estimated while $\alpha_{\bullet j} \equiv 0$ (with $\bullet \in \{i, o\}$, $j \in \{1, 2, 3\}$), with all other variables remaining consistent with C1.

The aforementioned controllers were first compared in joint space to evaluate the control systems, particularly in terms of frequency response, transient behavior, and smooth tracking performance, with the reference trajectories shown in Fig. 3.

- 1) **Set1:** Sine curve tracking experiment. The desired trajectory was set as $q_d(t) = 0.52 \sin(0.325\pi t) + 0.17 \text{ rad}$.
- 2) **Set2:** Point-to-point S-curve tracking experiment, including acceleration, constant speed, and deceleration.

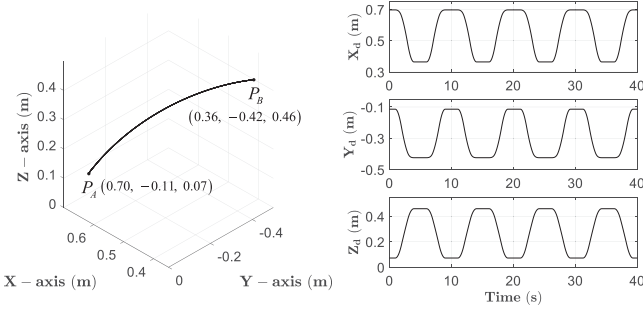


Fig. 4. Desired path and the corresponding reference trajectory for each axis used in Set3.

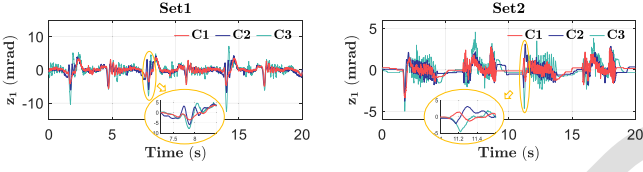


Fig. 5. Comparison of tracking errors in Set1 and Set2.

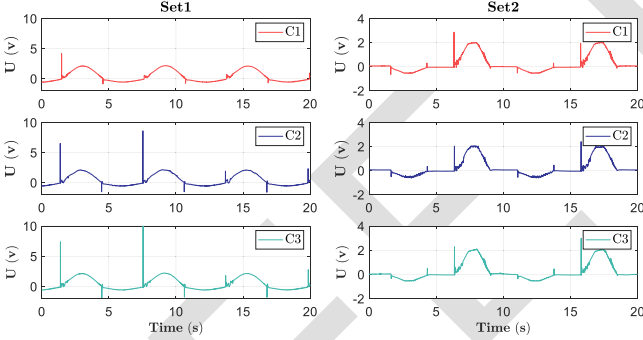


Fig. 6. Control signals under different control strategies.

The S-curve was from -0.25 to 0.63 rad, with the maximum angular velocity $\dot{q}_{d\max} = \pi/6$ rad \cdot s $^{-1}$ and the maximum angular acceleration $\ddot{q}_{d\max} = \pi/6$ rad \cdot s $^{-2}$.

In addition, a reference trajectory was set in Cartesian space, as shown in Fig. 4.

3) **Set3:** Multi-DoF trajectory tracking experiment. A preset endpoint of the hydraulic manipulator was required to reciprocate between P_A and P_B , with the global coordinate system defined in Fig. 1. During this process, the reference trajectories in joint space were calculated using inverse kinematics and then controlled by C1–C3.

The selected performance indicators are as follows: the root mean square error $e_{R\bullet} = \sqrt{\frac{1}{T} \int_0^T |\bullet|^2 dt}$, the peak error $e_{M\bullet} = \max\{|\bullet|\}$, and the normalizing performance indicator $\rho_e = e_M / |\dot{q}|_{\max}$ [1].

B. Experiment Results and Discussion

The tracking results for Set1 and Set2 are presented in Fig. 5, with $1 \text{ mrad} = 10^{-3} \text{ rad}$. Fig. 6 shows the corresponding

TABLE I
NUMERICAL COMPARISON OF TRACKING RESULTS

	e_{Rz1} (mrad)	e_{Mz1} (mrad)	ρ_e (s)	$e_{Rz_{pi}}$ (MPa)	$e_{Rz_{po}}$ (MPa)	$e_{Mz_{pi}}$ (MPa)	$e_{Mz_{po}}$ (MPa)
Set1	C1	1.25	5.65	10.64	0.23	0.19	1.04
	C2	1.38	6.79	12.80	0.26	0.23	2.77
	C3	1.96	12.58	23.70	0.30	0.24	2.15
Set2	C1	0.64	3.35	6.40	0.18	0.20	1.23
	C2	0.73	3.77	7.19	0.20	0.24	1.25
	C3	1.00	4.98	9.52	0.29	0.27	1.26
							2.06

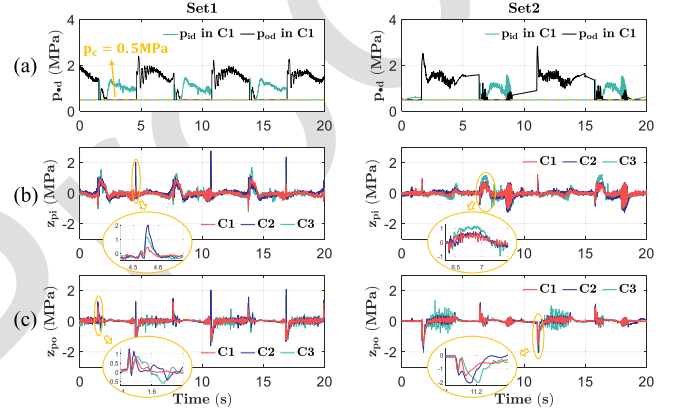


Fig. 7. Reference pressure trajectories in C1 and the comparison of pressure tracking error in experiment Set1 and Set2.

control signals under different control strategies. The associated performance indicators are provided in Table I. During the transition phase of start-stop motion, rapid pressure changes lead to significant fluctuations in error, indicating that the actual effective bulk modulus has undergone substantial changes that cannot be ignored. Notably, the tracking performance of C1 and C2 significantly exceeds that of C3, despite C3 being at the threshold of extreme performance, as indicated by substantial oscillations in its control error. These results suggest that the control gain using the lumped modeling method has reached its limit, indicating the nonlinear relationship between the effective bulk modulus and the pressure cannot be treated as a constant under low-pressure conditions. The effective bulk modulus model developed in this paper accurately captures the system's dynamic behavior and effectively enhances tracking accuracy. In addition, C1 demonstrates superior performance compared to C2. The online learning of ϑ_{β} allows C1 to exhibit greater adaptability to changes in operating conditions, such as oil temperature or entrained air content.

Fig. 7(a) presents the reference pressure trajectories in C1, with the desired low pressure $p_c = 0.5$ MPa in (33). The method proposed in Section III-C significantly reduces the pressure supply demand of the chamber while ensuring that the net moment τ meets predetermined requirements, thereby establishing a foundation for the subsequent reduction of throttling losses. Building on the reference pressure, Fig. 7(b) and (c) illustrates the control effects of pressure. The performance indicators for pressure control are provided in Table I. Both C1 and C2 exhibit more

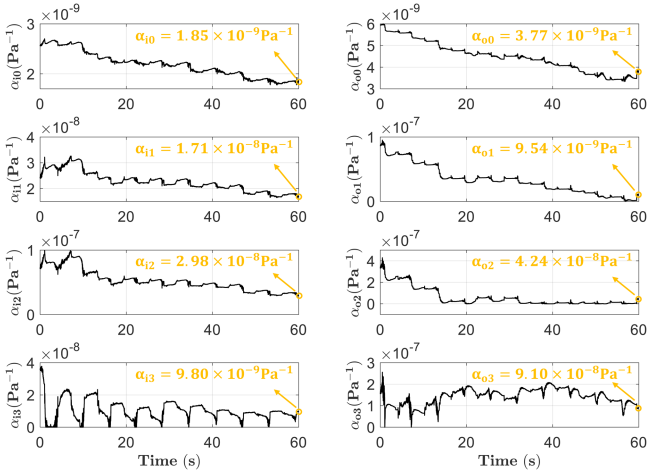
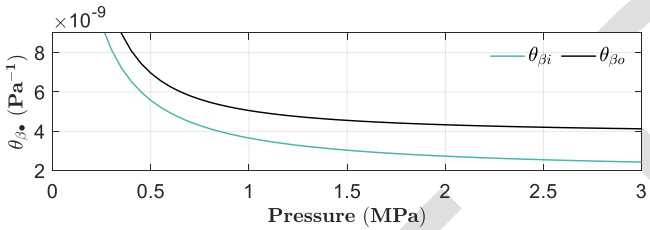
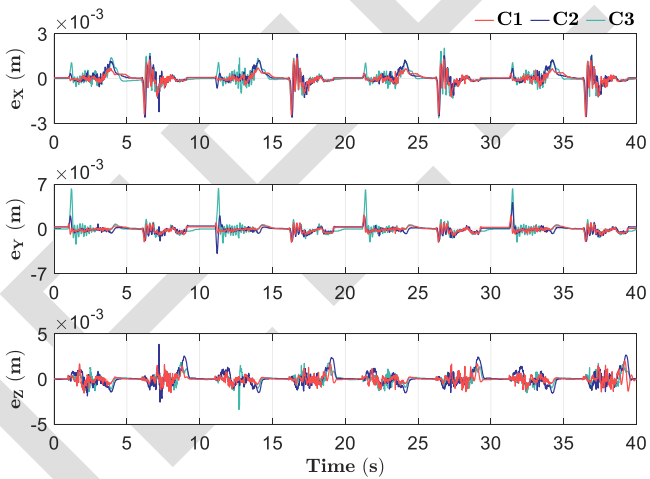
Fig. 8. Estimation results of θ_α by C1 in Set1.Fig. 9. Fitting result of θ_{β_o} with respect to pressure by C1 in Set1.

Fig. 10. Tracking errors of each dimension in Cartesian space in Set3.

534 accurate and stable pressure tracking performance, whereas C3
535 is more susceptible to significant pressure oscillations.

536 The estimation results of ϑ_{α_i} and ϑ_{α_o} by C1 in Set1 are
537 given in Fig. 8. The parameters of both chambers exhibit a
538 certain convergence effect, indicating that the proposed model
539 accurately fits the real effective bulk modulus model. By substi-
540 tuting the final convergence value from Fig. 8 into (13), and the
541 fitting result of θ_{β_o} with respect to chamber pressure is shown
542 in Fig. 9. The proposed improved model has consistent results

543 with the tangent bulk modulus model and the IFAS model,
544 demonstrating the accuracy and effectiveness of the proposed
545 model in describing actual systems.

546 Fig. 10 presents the multijoint control results for Set3. C1
547 exhibits superior tracking performance across all dimensions,
548 particularly along the Y-axis. This suggests that, compared to
549 other global nonlinearities in hydraulic manipulators, such as
550 joint coupling and gravity, the nonlinear effect of the effective
551 bulk modulus is significant and cannot be overlooked.

V. CONCLUSION

552 In this study, a control-oriented model for the effective bulk
553 modulus is developed that is both feasible for control design
554 and accurately reflects its nonlinear relationship with work-
555 ing pressure. A model-based adaptive robust motion controller
556 is then synthesized for the multi-DOF hydraulic manipulator
557 equipped with independent metering units. The primary pa-
558 rameters of the manipulator, including those in the proposed
559 bulk modulus model, can be updated online through an es-
560 pecially designed X-swapping scheme. The experiment results
561 demonstrate that the proposed method significantly improves
562 motion control accuracy while maintaining system pressure at
563 a low level. Moreover, the method exhibits good convergence
564 properties, and the final fitting results show a high degree
565 of consistency with the theoretical model. Notably, accurately
566 modeling the effective bulk modulus and compensating for its
567 nonlinear behavior in real time, it has great potential for reducing
568 throttling losses that typically occur when adjusting pressure in
569 conventional hydraulic systems. This capability is particularly
570 important for applications such as mobile robotics, industrial
571 automation, and precision actuation systems, where minimizing
572 energy consumption and enhancing system efficiency are es-
573 sential. In future research, we will focus on exploring energy-saving
574 control methods for hydraulic manipulators that balance motion
575 performance and energy efficiency, while further mitigating the
576 impact of disturbances, such as load variations and temperature
577 changes.

APPENDIX A PROOF OF LEMMA 3.1

579 If either x or y is a zero vector, $f_Y = 0$ is always satisfied.
580 The following discussion considers the case where both x and
581 y are nonzero vectors.

582 Define $\mathcal{P} = \mathcal{Q} - \underline{\lambda}_{\mathcal{Q}} \mathbf{I}$, which is a positive semidefinite matrix,
583 i.e., $x^T \mathcal{P} x \geq 0 \forall x$. Thus, one can obtain

$$x^T \mathcal{Q} x \geq \underline{\lambda}_{\mathcal{Q}} x^T x \quad \forall x. \quad (\text{A.1})$$

585 When $\mathcal{F} = \mathcal{F}(x, y, \underline{\lambda}_{\mathcal{Q}})$, noting $n_x = x / \sqrt{x^T x}$ and $n_y =$
586 $y / \sqrt{y^T y}$, f_Y can be scaled as

$$\begin{aligned} f_Y &= \frac{|x^T y|}{\underline{\lambda}_{\mathcal{Q}} x^T x y^T y} (x^T \mathcal{Q} x) y^T y - x^T y \\ &\geq \frac{|x^T y|}{\underline{\lambda}_{\mathcal{Q}} x^T x y^T y} (\underline{\lambda}_{\mathcal{Q}} x^T x) y^T y - x^T y \\ &\geq 0 \quad \forall x, y. \end{aligned} \quad (\text{A.2})$$

587 Correspondingly, when $\mathcal{F} = \mathcal{F}(x, y, -\underline{\lambda}_Q)$, the sign of f_Y
 588 changes as

$$\begin{aligned} f_Y &= \frac{|x^T y|}{-\underline{\lambda}_Q x^T y y^T y} (x^T Q x) y^T y - x^T y \\ &\leq \frac{|x^T y|}{-\underline{\lambda}_Q x^T y y^T y} (\underline{\lambda}_Q x^T x) y^T y - x^T y \\ &\leq 0 \forall x, y. \end{aligned} \quad (\text{A.3})$$

589 Therefore, both positive and negative values of f_Y are achievable
 590 by the design of \mathcal{F} . \square

APPENDIX B PROOF OF THEOREM 3.1

591 Define the Lyapunov function as

$$V_s = \frac{1}{2} \mathbf{z}_2^T \mathbf{M} \mathbf{z}_2 + \frac{1}{2} \mathbf{z}_{pi}^T \mathbf{z}_{pi} + \frac{1}{2} \mathbf{z}_{po}^T \mathbf{z}_{po}. \quad (\text{B.1})$$

593 Combining *Property 2.2*, (41), and (47), the derivative of (B.1)
 594 can be written as

$$\begin{aligned} \dot{V}_s &= \mathbf{z}_2^T (\mathbf{M} \dot{\mathbf{z}}_2 + \mathbf{C} \mathbf{z}_2) + \mathbf{z}_{pi}^T \dot{\mathbf{z}}_{pi} + \mathbf{z}_{po}^T \dot{\mathbf{z}}_{po} \\ &= -\mathbf{z}_2^T \Lambda_{k_F} \mathbf{z}_2 + \Upsilon_V + \mathbf{z}_2^T \left(\boldsymbol{\tau}_{ds2} - \tilde{\mathbf{d}}_F + \tilde{\mathbf{d}}_F^* \right) \\ &\quad - \mathbf{z}_{pi}^T \Lambda_{\theta_{\beta_i}}^{-1} \Lambda_{k_{Qi}} \mathbf{z}_{pi} - \mathbf{z}_{po}^T \Lambda_{\theta_{\beta_o}}^{-1} \Lambda_{k_{Qo}} \mathbf{z}_{po} \\ &\quad + \mathbf{z}_{pi}^T \Lambda_{\theta_{\beta_i}}^{-1} \left(\Lambda_{\mathbf{V}_i}^{-1} \mathbf{Q}_{ids2} - \tilde{\mathbf{d}}_{Qi} + \tilde{\mathbf{d}}_{Qi}^* \right) \\ &\quad + \mathbf{z}_{po}^T \Lambda_{\theta_{\beta_o}}^{-1} \left(-\Lambda_{\mathbf{V}_o}^{-1} \mathbf{Q}_{ods2} - \tilde{\mathbf{d}}_{Qo} + \tilde{\mathbf{d}}_{Qo}^* \right) \end{aligned} \quad (\text{B.2})$$

595 where $\Upsilon_V = \mathbf{z}_2^T \mathbf{z}_3 + \mathbf{z}_{pi}^T \Lambda_{\theta_{\beta_i}}^{-1} \Lambda_{\mathbf{V}_i}^{-1} \Upsilon_{Qi} - \mathbf{z}_{po}^T \Lambda_{\theta_{\beta_o}}^{-1} \Lambda_{\mathbf{V}_o}^{-1} \Upsilon_{Qo}$.
 596 Noting *Lemma 3.1* and referring back to \mathbf{z}_3 in (32), $\tilde{\Upsilon}_{Qi}$ in (36)
 597 and Υ_{Qo} in (43), Υ_V can be scaled to

$$\begin{aligned} \Upsilon_V &= \mathbf{z}_2^T \mathbf{J}_h (\Lambda_{\mathbf{A}_i} \mathbf{z}_{pi} - \Lambda_{\mathbf{A}_o} \mathbf{z}_{po}) \\ &\quad - \mathbf{z}_{pi}^T \Lambda_{\theta_{\beta_i}}^{-1} \mathcal{F}_i \Lambda_{\mathbf{A}_i} \mathbf{J}_h^T \mathbf{z}_2 + \mathbf{z}_{po}^T \Lambda_{\theta_{\beta_o}}^{-1} \mathcal{F}_o \Lambda_{\mathbf{A}_o} \mathbf{J}_h^T \mathbf{z}_2 \\ &= -\mathbf{z}_{pi}^T \left(\Lambda_{\theta_{\beta_i}}^{-1} \mathcal{F}_i - \mathbf{I} \right) \Lambda_{\mathbf{A}_i} \mathbf{J}_h^T \mathbf{z}_2 \\ &\quad + \mathbf{z}_{po}^T \left(\Lambda_{\theta_{\beta_o}}^{-1} \mathcal{F}_o - \mathbf{I} \right) \Lambda_{\mathbf{A}_o} \mathbf{J}_h^T \mathbf{z}_2 \\ &\leq 0. \end{aligned} \quad (\text{B.3})$$

598 According to *Property 2.1* as well as the conditions (28)-2),
 599 (39)-2), and (45)-2), \dot{V}_s can be further converted as

$$\begin{aligned} \dot{V}_s &\leq -\mathbf{z}_2^T \Lambda_{k_F} \mathbf{z}_2 - \mathbf{z}_{pi}^T \Lambda_{\theta_{\beta_i}}^{-1} \Lambda_{k_{Qi}} \mathbf{z}_{pi} \\ &\quad - \mathbf{z}_{po}^T \Lambda_{\theta_{\beta_o}}^{-1} \Lambda_{k_{Qo}} \mathbf{z}_{po} + \eta_F + \underline{\theta}_{\beta_i} \eta_{Qi} + \underline{\theta}_{\beta_o} \eta_{Qo} \\ &\leq -\underline{k}_F \mathbf{z}_2^T \mathbf{z}_2 - \bar{\theta}_{\beta_i} \underline{k}_{Qi} \mathbf{z}_{pi}^T \mathbf{z}_{pi} - \bar{\theta}_{\beta_o} \underline{k}_{Qo} \mathbf{z}_{po}^T \mathbf{z}_{po} + \eta_s \\ &\leq -\lambda_s V_s + \eta_s \end{aligned} \quad (\text{B.4})$$

600 which leads to (60) by comparison Lemma and the boundedness
 601 of all the close-loop system signals is guaranteed. \square

APPENDIX C PROOF OF THEOREM 3.2

602 Referring back to (22), one can obtain

$$\begin{aligned} f_d &\triangleq \hat{\mathbf{d}}_F^T [\Lambda_{\gamma_F}^{-1} \text{Proj}_{\hat{\mathbf{d}}}(\Lambda_{\gamma_F} \mathcal{H}_F \mathbf{z}_2) - \mathbf{z}_2] \\ &\quad + \hat{\mathbf{d}}_{Qi}^T [\Lambda_{\gamma_{Qi}}^{-1} \text{Proj}_{\hat{\mathbf{d}}}(\Lambda_{\gamma_{Qi}} \mathcal{H}_{Qi} \mathbf{z}_{pi}) - \Lambda_{\theta_{\beta_i}}^{-1} \mathbf{z}_{pi}] \\ &\quad + \hat{\mathbf{d}}_{Qo}^T [\Lambda_{\gamma_{Qo}}^{-1} \text{Proj}_{\hat{\mathbf{d}}}(\Lambda_{\gamma_{Qo}} \mathcal{H}_{Qo} \mathbf{z}_{po}) - \Lambda_{\theta_{\beta_o}}^{-1} \mathbf{z}_{po}] \\ &\leq 0. \end{aligned} \quad (\text{C.1})$$

603 Define the Lyapunov function as

$$\begin{aligned} V_a &= V_s + \frac{1}{2} \hat{\mathbf{d}}_F^T \Lambda_{\gamma_F}^{-1} \hat{\mathbf{d}}_F + \frac{1}{2} \hat{\mathbf{d}}_{Qi}^T \Lambda_{\gamma_{Qi}}^{-1} \hat{\mathbf{d}}_{Qi} \\ &\quad + \frac{1}{2} \hat{\mathbf{d}}_{Qo}^T \Lambda_{\gamma_{Qo}}^{-1} \hat{\mathbf{d}}_{Qo}. \end{aligned} \quad (\text{C.2})$$

604 If PE condition in (61) is satisfied, the parameters can be estimated to the true values, i.e., $\dot{\Theta}_\bullet \rightarrow 0$ as $t \rightarrow \infty$ and $\dot{\Theta}_\bullet \in \mathcal{L}_2^{l_{\Theta_\bullet}}[0, \infty)$ (with $\bullet \in \{F, Qi, Qo\}$). Noting $\tilde{\Delta}_F = \tilde{\Delta}_{Qi} = \tilde{\Delta}_{Qo} = 0$, from (28)-1), (39)-1), (45)-1), and (B.3), the derivative of (C.2) can be written as

$$\begin{aligned} \dot{V}_a &= \dot{V}_s + \hat{\mathbf{d}}_F^T \Lambda_{\gamma_F}^{-1} \dot{\hat{\mathbf{d}}}_F + \hat{\mathbf{d}}_{Qi}^T \Lambda_{\gamma_{Qi}}^{-1} \dot{\hat{\mathbf{d}}}_{Qi} + \hat{\mathbf{d}}_{Qo}^T \Lambda_{\gamma_{Qo}}^{-1} \dot{\hat{\mathbf{d}}}_{Qo} \\ &= -\mathbf{z}_2^T \Lambda_{k_F} \mathbf{z}_2 - \mathbf{z}_{pi}^T \Lambda_{\theta_{\beta_i}}^{-1} \Lambda_{k_{Qi}} \mathbf{z}_{pi} \\ &\quad - \mathbf{z}_{po}^T \Lambda_{\theta_{\beta_o}}^{-1} \Lambda_{k_{Qo}} \mathbf{z}_{po} + \Upsilon_V + f_d + \tilde{f}_\theta + \mathbf{z}_2^T \boldsymbol{\tau}_{ds2} \\ &\quad + \mathbf{z}_{pi}^T \Lambda_{\theta_{\beta_i}}^{-1} \Lambda_{\mathbf{V}_i}^{-1} \mathbf{Q}_{ids2} - \mathbf{z}_{po}^T \Lambda_{\theta_{\beta_o}}^{-1} \Lambda_{\mathbf{V}_o}^{-1} \mathbf{Q}_{ods2} \\ &\leq -\mathbf{z}_2^T \Lambda_{k_F} \mathbf{z}_2 - \mathbf{z}_{pi}^T \Lambda_{\theta_{\beta_i}}^{-1} \Lambda_{k_{Qi}} \mathbf{z}_{pi} \\ &\quad - \mathbf{z}_{po}^T \Lambda_{\theta_{\beta_o}}^{-1} \Lambda_{k_{Qo}} \mathbf{z}_{po} + \tilde{f}_\theta \end{aligned} \quad (\text{C.3})$$

605 where $\tilde{f}_\theta \triangleq \mathbf{z}_2^T Y_F^T \tilde{\Theta}_F + \mathbf{z}_{pi}^T Y_{Qi}^T \tilde{\Theta}_{Qi} + \mathbf{z}_{po}^T Y_{Qo}^T \tilde{\Theta}_{Qo}$, with

$$\begin{aligned} Y_F^T &\triangleq \phi_F^T \\ Y_{Qi}^T &\triangleq \left[\Lambda_{\theta_{\beta_i}}^{-1} \Lambda_{\dot{\mathbf{p}}_{id}} \phi_{\chi_i}^T, -\Lambda_{\theta_{\beta_i}}^{-1} \Lambda_{\mathbf{V}_i}^{-1} \right] \\ Y_{Qo}^T &\triangleq \left[\Lambda_{\theta_{\beta_o}}^{-1} \Lambda_{\dot{\mathbf{p}}_{od}} \phi_{\chi_o}^T, -\Lambda_{\theta_{\beta_o}}^{-1} \Lambda_{\mathbf{V}_o}^{-1} \right]. \end{aligned} \quad (\text{C.4})$$

606 Therefore, $\dot{V}_a(t) \leq \dot{V}_a(0) \forall t \geq t_f$. Since ϕ_\bullet^T is uniformly bounded, $Y_\bullet^T \tilde{\Theta}_\bullet \in \mathcal{L}_2^n[0, \infty)$ (with $\bullet \in \{F, Qi, Qo\}$). By integrating both side of (C.3), it follows that $\mathbf{z}_2, \mathbf{z}_{pi}, \mathbf{z}_{po} \in \mathcal{L}_2^n[0, \infty)$. As a result, the asymptotic tracking can be obtained by applying Barbalat's lemma. \square

REFERENCES

- [1] J. Mattila, J. Koivumäki, D. G. Caldwell, and C. Semini, "A survey on control of hydraulic robotic manipulators with projection to future trends," *IEEE/ASME Trans. Mechatron.*, vol. 22, no. 2, pp. 669–680, Apr. 2017.
- [2] Z. Yao, F. Xu, G.-P. Jiang, and J. Yao, "Data-driven control of hydraulic manipulators by reinforcement learning," *IEEE/ASME Trans. Mechatron.*, vol. 29, no. 4, pp. 2673–2684, Aug. 2024.
- [3] J. Shen, J. Zhang, H. Zong, M. Cheng, and B. Xu, "Hierarchical decoupling controller with cylinder separated model of hydraulic manipulators for contact force/motion control," *IEEE/ASME Trans. Mechatron.*, vol. 28, no. 2, pp. 1081–1092, Apr. 2023.

- [4] W. Sun and Y. Yuan, "Passivity based hierarchical multi-task tracking control for redundant manipulators with uncertainties," *Automatica*, vol. 155, 2023, Art. no. 111159.
- [5] F. Huang, X. Yang, D. Mei, and Z. Chen, "Unified contact model and hybrid motion/force control for teleoperated manipulation in unknown environments," *IEEE/ASME Trans. Mechatron.*, vol. 30, no. 2, pp. 921–932, Apr. 2025.
- [6] J. Koivumäki and J. Mattila, "Stability-guaranteed impedance control of hydraulic robotic manipulators," *IEEE/ASME Trans. Mechatron.*, vol. 22, no. 2, pp. 601–612, Apr. 2017.
- [7] J. Mi, J. Yao, and W. Deng, "Adaptive rise control of winding tension with active disturbance rejection," *Chin. J. Mech. Eng.*, vol. 37, no. 1, 2024, Art. no. 52111159.
- [8] W. Deng, H. Zhou, J. Zhou, and J. Yao, "Neural network-based adaptive asymptotic prescribed performance tracking control of hydraulic manipulators," *IEEE Trans. Syst., Man, Cybern. Syst.*, vol. 53, no. 1, pp. 285–295, Jan. 2023.
- [9] Z. Chen, S. Zhou, C. Shen, L. Lyu, J. Zhang, and B. Yao, "Observer-based adaptive robust precision motion control of a multi-joint hydraulic manipulator," *IEEE/CAA J. Automatica Sinica*, vol. 11, no. 5, pp. 1213–1226, May 2024.
- [10] Z. Chen et al., "Motion control of independent metering electro-hydraulic system based on chamber pressure planning without mode switch," *J. Mech. Eng.*, vol. 60, pp. 302–312, 2024.
- [11] T. Lin, Y. Lin, H. Ren, H. Chen, Z. Li, and Q. Chen, "A double variable control load sensing system for electric hydraulic excavator," *Energy*, vol. 223, 2021, Art. no. 119999.
- [12] M. Cheng, B. Sun, R. Ding, and B. Xu, "A multi-mode electronic load sensing control scheme with power limitation and pressure cut-off for mobile machinery," *Chin. J. Mech. Eng.*, vol. 36, no. 1, 2023, Art. no. 29.
- [13] Y. Xia et al., "Advanced motion control of hydraulic manipulator with precise compensation of dynamic friction," *IEEE Trans. Ind. Inform.*, vol. 20, no. 7, pp. 9375–9384, Jul. 2024.
- [14] Y. Yuan and W. Sun, "An integrated kinematic calibration and dynamic identification method with only static measurements for serial robot," *IEEE/ASME Trans. Mechatron.*, vol. 28, no. 5, pp. 2762–2773, Oct. 2023.
- [15] S. Zhou, Y. Xia, M. Qi, D. Mei, and Z. Chen, "Transformed workspace adaptive mapping based master-slave operation control for hydraulic manipulator," *IEEE Trans. Ind. Electron.*, early access, Jan. 28, 2025, doi: [10.1109/TIE.2024.3525099](https://doi.org/10.1109/TIE.2024.3525099).
- [16] J. Zhang, F. Zhang, M. Cheng, R. Ding, B. Xu, and H. Zong, "Parameter identification of hydraulic manipulators considering physical feasibility and control stability," *IEEE Trans. Ind. Electron.*, vol. 71, no. 1, pp. 718–728, Jan. 2024.
- [17] L. Wang, W. J. Book, and J. D. Huggins, "Application of singular perturbation theory to hydraulic pump controlled systems," *IEEE/ASME Trans. Mechatron.*, vol. 17, no. 2, pp. 251–259, Apr. 2012.
- [18] S. Zhang, T. Minav, M. Pietola, H. Kauranne, and J. Kajaste, "The effects of control methods on energy efficiency and position tracking of an electro-hydraulic excavator equipped with zonal hydraulics," *Autom. Construction*, vol. 100, pp. 129–144, 2019.
- [19] J. Wang, G. Gong, and H. Yang, "Control of bulk modulus of oil in hydraulic systems," in *Proc. IEEE/ASME Int. Conf. Adv. Intell. Mechatron.*, 2008, pp. 1390–1395.
- [20] H. Yang, B. Feng, and G. Gong, "Measurement of effective fluid bulk modulus in hydraulic system," *J. Dyn. Syst., Meas., Control*, vol. 133, no. 6, 2011, Art. no. 061021.
- [21] H. B. Murrenhoff, "Grundlagen der fluidtechnik-teil 1: Hydraulik," 2011.
- [22] S. Kim and H. Murrenhoff, "Measurement of effective bulk modulus for hydraulic oil at low pressure," *J. Fluids Eng.*, vol. 134, 2012, Art. no. 021201.
- [23] S. Shi, Z. He, D. Zeng, P. Huang, and G. Jin, "Identification and modeling of a servo pump-controlled hydraulic system," *IEEE/ASME Trans. Mechatron.*, early access, Oct. 4, 2024, doi: [10.1109/TMECH.2024.3454518](https://doi.org/10.1109/TMECH.2024.3454518).
- [24] J. Schwarz and B. Lohmann, "Robust identification and control of mobile hydraulic systems using a decentralized valve structure," *Control Eng. Pract.*, vol. 151, 2024, Art. no. 106030.
- [25] J. Liu et al., "Motion control of electro-hydrostatic actuators with modeling and compensation of nonlinear bulk modulus," *IEEE Trans. Ind. Electron.*, vol. 72, no. 6, pp. 6185–6193, Jun. 2025.
- [26] D. T. Liem, "Trajectory control of a hydraulic system using intelligent control approach based on adaptive prediction model," *IFAC J. Syst. Control*, vol. 26, 2023, Art. no. 100228.
- [27] P. Righettini, R. Strada, S. Valilou, and E. KhademOlama, "Nonlinear model of a servo-hydraulic shaking table with dynamic model of effective bulk modulus," *Mech. Syst. Signal Process.*, vol. 110, pp. 248–259, 2018.
- [28] W. Shen and J. Wang, "An integral terminal sliding mode control scheme for speed control system using a double-variable hydraulic transformer," *ISA Trans.*, vol. 124, pp. 386–394, 2022.
- [29] Z. Chen, B. Helian, Y. Zhou, and M. Geimer, "An integrated trajectory planning and motion control strategy of a variable rotational speed pump-controlled electro-hydraulic actuator," *IEEE/ASME Trans. Mechatron.*, vol. 28, no. 1, pp. 588–597, Feb. 2023.
- [30] H. Ding, Y. Li, Q. Zhu, and J. Su, "Position servo with variable speed pump-controlled cylinder: Design, modelling and experimental investigation," *Int. J. Hydromechatronics*, vol. 7, no. 2, pp. 155–175, 2024.
- [31] Y. Sun, Y. Wan, H. Ma, and X. Liang, "Compensation control of hydraulic manipulator under pressure shock disturbance," *Nonlinear Dyn.*, vol. 111, no. 12, pp. 11153–11169, 2023.
- [32] J. Koivumäki, W.-H. Zhu, and J. Mattila, "Energy-efficient and high-precision control of hydraulic robots," *Control Eng. Pract.*, vol. 85, pp. 176–193, 2019.
- [33] Y. Zhou, R. Ding, M. Cheng, L. Liao, Z. Chen, and B. Yao, "Precision motion control of independent metering hydraulic swing system with large inertia loads: A case study on a rotary drilling rig," *IEEE Trans. Ind. Electron.*, early access, Mar. 21, 2025, doi: [10.1109/TIE.2025.3549091](https://doi.org/10.1109/TIE.2025.3549091).
- [34] R. Ding et al., "A review of independent metering control system for mobile machinery," *Int. J. Hydromechatronics*, vol. 8, no. 5, pp. 1–39, 2025.
- [35] L. Lyu, Z. Chen, and B. Yao, "Parallel-connected pump-valves coordinated electro-hydraulic system: Comparative study and motion control," *J. Mech. Eng.*, vol. 58, pp. 136–151, 2022.
- [36] R. Ding, M. Cheng, L. Jiang, and G. Hu, "Active fault-tolerant control for electro-hydraulic systems with an independent metering valve against valve faults," *IEEE Trans. Ind. Electron.*, vol. 68, no. 8, pp. 7221–7232, Aug. 2021.
- [37] G. Stojanoski, G. Rath, and M. Gimpel, "The effects of bulk modulus on the dynamics of controlled independent metering system," in *Proc. 16th Scand. Int. Conf. Fluid Power*, 2019.
- [38] Y. Gao, Y. Shen, T. Xu, W. Zhang, and L. Güvenç, "Oscillatory yaw motion control for hydraulic power steering articulated vehicles considering the influence of varying bulk modulus," *IEEE Trans. Control Syst. Technol.*, vol. 27, no. 3, pp. 1284–1292, May 2019.



Yangxiu Xia received the B.Eng. degree in ocean engineering and technology from Zhejiang University, Hangzhou, China, in 2022. He is currently working toward the Ph.D. degree in ocean technology and engineering with the Ocean College, Zhejiang University, Zhoushan, China.



Jiajia Liu received the B.Eng. degree in marine engineering from the Wuhan University of Technology, Wuhan, China, in 2018, and the M.Eng. degree in marine engineering from the Huazhong University of Science and Technology, Wuhan, in 2021. He is currently working toward the Ph. D. degree in electronic information with the Ocean College, Zhejiang University.

759
760
761
762
763
764
765
766
767



Litong Lyu received the B.Eng. and Ph.D. degrees in mechatronics engineering from Zhejiang University, Hangzhou, China, in 2015 and 2020, respectively.

Since 2020, he has been with the School of Mechanical Engineering, Shijiazhuang Tiedao University, Hebei, China, where he is currently an Associate Professor.

768
769
770
771
772
773
774



Manzhi Qi received the B.Eng. degree in ocean engineering and technology from Zhejiang University, Hangzhou, China, in 2024. He is currently working toward the Ph.D. degree in ocean technology and engineering with the Ocean College, Zhejiang University, Zhoushan, China.



Shizhao Zhou received the B.Eng. and Ph.D. degrees from Zhejiang University, Hangzhou, China, in 2018 and 2024, respectively.

Since 2024, he has been with the School of Mechanical Engineering and Automation, Fuzhou University, Fuzhou, China, where he is currently an Associate Professor. His research interests include advanced control of mechatronic hydraulic systems especially hydraulic manipulators.

775
776
777 Q7
778
779
780
781
782
783
784
785
786
787
788
789
790
791
792
793
794
795
796
797
798
799
800
801



Zheng Chen (Senior Member, IEEE) received the B.Eng. and Ph.D. degrees in mechatronic control engineering from Zhejiang University, Hangzhou, China, in 2007 and 2012, respectively.

From 2013 to 2015, he was a Postdoctoral Researcher with the Department of Mechanical Engineering, Dalhousie University, Halifax, NS, Canada. Since 2015, he has been an Associated Professor with the Ocean College, Zhejiang University, Hangzhou. His research interests mainly focus on advanced control of robotic and mechatronic systems (e.g., nonlinear adaptive robust control, motion control, trajectory planning, telerobotics, exoskeleton, mobile manipulator, precision mechatronic systems, and underwater robots).

786
787
788
789
790
791
792
793
794
795
796
797
798
799
800
801

GENERAL INSTRUCTION

- **Authors:** Please check and confirm whether the name of the corresponding author is correct as set.
- **Authors:** Carefully check the page proofs (and coordinate with all authors); additional changes or updates WILL NOT be accepted after the article is published online/print in its final form. Please check author names and affiliations, funding, as well as the overall article for any errors prior to sending in your author proof corrections.
- **Authors:** We cannot accept new source files as corrections for your article. If possible, please annotate the PDF proof we have sent you with your corrections and upload it via the Author Gateway. Alternatively, you may send us your corrections in list format. You may also upload revised graphics via the Author Gateway.

QUERIES

- Q1. Author: Please confirm or add details for any funding or financial support for the research of this article.
- Q2. Author: Please check and confirm whether the author affiliations in the first footnote are correct as set.
- Q3. Author: Please provide the expansions for IFAS, if applicable.
- Q4. Author: Please update Refs. [15], [24], and [33], if already published.
- Q5. Author: Please provide the complete bibliographic details for Ref. [21].
- Q6. Author: Please provide the page range for Ref. [36].
- Q7. Author: Please provide the subjects in which the author Shizhao Zhou received his respective degrees.

Control-Oriented Modeling of Effective Bulk Modulus and Online Compensation for Hydraulic Manipulator Motion Control

Yangxiu Xia^{1D}, Jiajia Liu^{1D}, Litong Lyu^{1D}, Manzhi Qi^{1D}, Shizhao Zhou^{1D},
and Zheng Chen^{1D}, Senior Member, IEEE

Abstract—Model-based control methods have been acknowledged as powerful solutions for hydraulic manipulators through compensating nonlinear dynamics. Hydraulic oil, as the working medium for energy transfer, significantly affects the system's rigidity and control performance. In most studies, the effective bulk modulus of oil is either treated as a constant or estimated as an unknown parameter. However, it is closely related to working pressure and can vary several times under different pressures. Although several theoretical models for the effective bulk modulus exist, their complexity and dependence on specific measurement equipment limit models' application in hydraulic manipulator control. In this study, a control-oriented model for the effective bulk modulus is developed, balancing the feasibility of control design and the accuracy of the model description. A model-based controller is then synthesized for a multi-degree-of-freedom hydraulic manipulator. Through an especially designed X-swapping scheme, the primary parameters of the manipulator, including those in the bulk modulus model, can be updated online without additional hardware dependencies. Theoretical analysis and experiment results demonstrate that the method improves the dynamic performance of hydraulic manipulators under varying pressures. Notably, this represents the first instance where a hydraulic manipulator controller accounts for the nonlinear characteristics of the effective bulk modulus.

Index Terms—Effective bulk modulus, hydraulic manipulator, motion control, parameter estimation, X-swapping.

I. INTRODUCTION

HYDRAULIC manipulators are widely used in applications including construction, underwater operations, and various other scenarios [1], [2]. With the trends toward automation and intelligence, closed-loop control of the hydraulic manipulators becomes increasingly important, no matter the machine is controlled through human-aided teleoperation or fully automated processes [3], [4], [5]. To achieve desired control performance, model-based control methods, such as virtual decomposition control [6], robust integral of the sign of the error [7], [8], and adaptive robust control (ARC) [9], [10], have been acknowledged as powerful solutions. And there have been numerous research achievements in modeling and compensating for factors such as payload inertia [11], [12], dynamic friction force/torque [13], and contacting force [3]. The essence of such model-based control method lies on precise model compensation of the nonlinear dynamics of the hydraulic manipulator, which means that more precise model compensation leads to enhanced control performance [14], [15].

The bulk modulus of hydraulic oil, as the primary working medium for energy transfer in hydraulic manipulators, determines the system's rigidity and is a key parameter influencing its dynamic performance [16]. The bulk modulus of pure oil is very large, making it approximately incompressible in most hydraulic transmission systems. However, due to entrained insoluble air in oil and the radial deformation of hydraulic hoses, the characterization of the effective bulk modulus is quite complicated and strongly nonlinear. Changes in working pressure can cause its value to vary by several times [17], [18], significantly affecting the efficiency and operational stability of hydraulic manipulators.

Therefore, numerous studies have focused on the measurement and theoretical modeling of the effective bulk modulus. Yang et al. [19], [20] derived a tangent bulk modulus model for oil with entrapped air and developed a measurement device to validate the model's accuracy. Murrenhoff et al. [21], [22] proposed the IFAS model, accounting for factors such as low pressures, varying temperature, and entrained air content, and

Q1 Received 26 November 2024; revised 11 April 2025; accepted 25 May 2025. Recommended by Technical Editor S. Jeong and Senior Editor H. Fujimoto. This work was supported in part by the Zhejiang Provincial Natural Science Foundation of China under Grant LR23E050001; in part by the Science and Technology Project of Hebei Education Department under Grant BJ2025200; in part by the Youth Talent Program Supported by China Railway Society; and in part by the National Natural Science Foundation of China under Grant 52105065. (Corresponding author: Zheng Chen.)

Q2 Yangxiu Xia, Jiajia Liu, Manzhi Qi, and Zheng Chen are with the State Key Laboratory of Ocean Sensing, Zhejiang University, Hangzhou 310058, China, and also with Ocean College, Zhejiang University, Zhoushan 316021, China (e-mail: yx.xia@zju.edu.cn; jiajia_liu@zju.edu.cn; manzhi.q@zju.edu.cn; zheng_chen@zju.edu.cn).

Litong Lyu is with the School of Mechanical Engineering, Shijiazhuang Tiedao University, Shijiazhuang 050043, China (e-mail: litong_lyu@stdt.edu.cn).

Shizhao Zhou is with the School of Mechanical Engineering and Automation, Fuzhou University, Fuzhou 350108, China (e-mail: zhoushizhao@zju.edu.cn).

Color versions of one or more figures in this article are available at <https://doi.org/10.1109/TMECH.2025.3583563>.

Digital Object Identifier 10.1109/TMECH.2025.3583563

verified the consistency of the model using three different methods (mass change, volume change, and soundspeed methods). With advances in measurement technology, subsequent studies have further validated the effectiveness of these two models through experimentation and demonstrated a strong relationship between the effective bulk modulus and working pressure [23], [24]. Particularly at low pressure, the effective bulk modulus of elasticity is significantly lower than at high pressure, indicating that the rigidity of the hydraulic system undergoes substantial changes with pressure variations [25], [26].

However, the mathematical formulation of the effective bulk modulus model is complex, and some states cannot be obtained in real time, making it challenging to apply in real-time control of hydraulic manipulators. Specifically, the acquisition of internal states (such as air content and the polytropic constant) in these models relies on specialized measurement equipment [27], which complicates the deployment of hydraulic systems in practice. Moreover, with continuous operation, parameters such as air content and temperature change in real time, resulting in offline results that cannot be directly applied to online pressure control. In addition, such a complex model significantly increases both the design and computational complexity of the controller. Consequently, there is limited research effectively applying these models to control. This also explains why most current research on hydraulic control either regards it as a known parameter or approaches it as an unknown lumped parameter for online estimation [28], [29], [30].

The actuators of hydraulic manipulators frequently undergo stop-and-go situations and the pressure changes quickly [31]. Considering the nonlinear characteristics of the effective bulk modulus will improve the control performance of the hydraulic manipulator, especially when there are rapid changes in working pressure. On one hand, this can improve control performance by enhancing the accuracy of feedforward model compensation. On the other hand, in most model-based control methods, the effective bulk modulus serves as a parameter in the feedback control law. Accurately accounting for its variations is crucial for tuning feedback gains, optimizing control, and other related tasks. In addition, the use of independent metering systems allows for individual adjustment of cylinder pressure in each chamber, enabling functions such as energy conservation [32], [33], [34]. The pressure within each chamber may vary significantly, leading to distinct effective bulk modulus values. Therefore, the primary challenge lies in the mathematical formulation used to capture this relationship, which must not only accurately reflect the underlying mechanism of the effective bulk modulus but also account for the feasibility of control design and enable online adaptation of key parameters whenever possible.

In this study, a control-oriented effective bulk modulus compensation method is proposed, which balances the feasibility of control design and the accuracy of the model description. The contributions of this study can be summarized as follows:

1) A control-oriented model for the effective bulk modulus is developed, which is feasible for model compensation and accurately reflects its nonlinear relationship with working pressure.

2) A model-based adaptive robust motion controller is synthesized for the multi-degree-of-freedom (DOF) hydraulic manipulator. Through an especially designed X-swapping

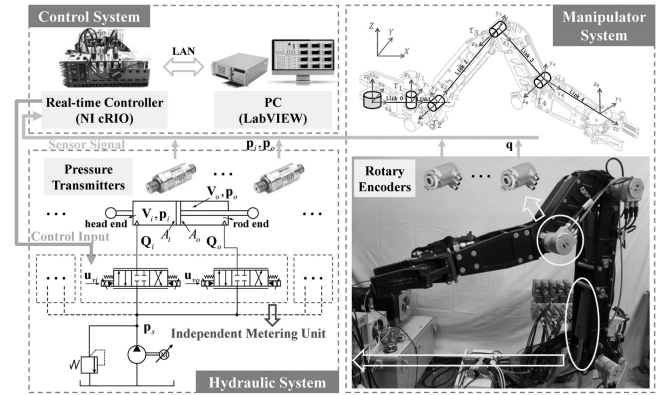


Fig. 1. Schematic diagram of a general hydraulic manipulator.

scheme, the primary parameters of the hydraulic manipulator, including those in the proposed bulk modulus model, can be updated online without additional sensors or other hardware dependencies.

3) The performance is evaluated both theoretically and through comparative experiments. The results demonstrate that the proposed method effectively enhances the dynamic performance of hydraulic manipulators across different pressure conditions.

II. PROBLEM STATEMENT AND PRELIMINARIES

A. Modeling of Hydraulic Manipulator

Consider an n -DOF hydraulic manipulator (as shown in Fig. 1), where each hydraulic cylinder is controlled by an independent metering unit [35], [36]. The rigid body dynamics can be represented as

$$\mathbf{M}(\mathbf{q})\ddot{\mathbf{q}} + \mathbf{C}(\mathbf{q}, \dot{\mathbf{q}})\dot{\mathbf{q}} + \mathbf{G}(\mathbf{q}) = \boldsymbol{\tau} - \mathbf{f}_F + \Delta_F \quad (1)$$

where $\mathbf{q} \in \mathbb{R}^n$, $\dot{\mathbf{q}} \in \mathbb{R}^n$, and $\ddot{\mathbf{q}} \in \mathbb{R}^n$ denote the joint angle position, velocity, and acceleration, respectively. The mass matrix $\mathbf{M}(\mathbf{q}) \in \mathbb{R}^{n \times n}$, the Coriolis and centrifugal matrix $\mathbf{C}(\mathbf{q}, \dot{\mathbf{q}}) \in \mathbb{R}^{n \times n}$, and the vector of gravity $\mathbf{G}(\mathbf{q}) \in \mathbb{R}^n$ are defined accordingly. $\Delta_F \in \mathbb{R}^n$ represents the lumped uncertain nonlinearities, including external interference and other hard-to model terms. $\mathbf{f}_F \in \mathbb{R}^n$ is modeled as Stribeck friction

$$\mathbf{f}_F = \Lambda_{\dot{\mathbf{q}}} \mathbf{f}_v + \Lambda_{\mathbf{S}_f} (\mathbf{f}_c + \Lambda_{\mathbf{e}_f} \mathbf{f}_s) \quad (2)$$

with $\mathbf{f}_c \in \mathbb{R}^n$, $(\mathbf{f}_c + \mathbf{f}_s) \in \mathbb{R}^n$, and $\mathbf{f}_v \in \mathbb{R}^n$ representing the coefficients of the Coulomb friction, the static friction, and the viscous friction, respectively. $\Lambda_{\bullet} = \text{diag}(\bullet)$ represents the vector \bullet expanded into a diagonal matrix. $\mathbf{e}_f = e^{-(\dot{\mathbf{q}}/\dot{q}_s)^2}$, where \dot{q}_s is the Stribeck velocity threshold. $\mathbf{S}_f = \tanh(k_f \dot{\mathbf{q}})$ serves as an approximation of the sign function, with k_f chosen to be sufficiently large.

The net moment vector $\boldsymbol{\tau} \in \mathbb{R}^n$ in (1) is defined as

$$\boldsymbol{\tau} = \mathbf{J}_h(\mathbf{q}) (\Lambda_{\mathbf{A}_i} \mathbf{p}_i - \Lambda_{\mathbf{A}_o} \mathbf{p}_o) \quad (3)$$

in which $\mathbf{J}_h(\mathbf{q}) \in \mathbb{R}^{n \times n}$ is the nonsingular joint Jacobian matrix. $\mathbf{A}_i \in \mathbb{R}^n$ and $\mathbf{A}_o \in \mathbb{R}^n$ denote the piston areas at each chambers. $\mathbf{p}_i \in \mathbb{R}^n$ and $\mathbf{p}_o \in \mathbb{R}^n$ are the chamber pressure of

164 each cylinder, whose dynamics can be further expressed as

$$\begin{aligned} \Lambda_{\mathbf{V}_i} \Lambda_{\beta_{ei}^{-1}} \dot{\mathbf{p}}_i &= -\Lambda_{\mathbf{A}_i} \mathbf{J}_h \dot{\mathbf{q}} + \mathbf{Q}_i + \Delta_{Qi} \\ \Lambda_{\mathbf{V}_o} \Lambda_{\beta_{eo}^{-1}} \dot{\mathbf{p}}_o &= \Lambda_{\mathbf{A}_o} \mathbf{J}_h \dot{\mathbf{q}} - \mathbf{Q}_o + \Delta_{Qo} \end{aligned} \quad (4)$$

165 where $\mathbf{V}_i \in \mathbb{R}^n$ and $\mathbf{V}_o \in \mathbb{R}^n$ are the total compressible volumes. $\Delta_{Qi} \in \mathbb{R}^n$ and $\Delta_{Qo} \in \mathbb{R}^n$ denote the modeling errors, 166 including flow leakages and valve flow mapping errors. β_{ei} and 167 β_{eo} represent the effective bulk modulus, which will be further 168 explained later.

170 $\mathbf{Q}_i \in \mathbb{R}^n$ and $\mathbf{Q}_o \in \mathbb{R}^n$ in (4) are the supplied flow rates, 171 which can be derived from the valve flow mappings

$$\mathbf{Q}_i = \Lambda_{\mathbf{k}_{qi}} \Lambda_{\mathbf{h}_i} \mathbf{u}_{vi}, \quad \mathbf{Q}_o = \Lambda_{\mathbf{k}_{qo}} \Lambda_{\mathbf{h}_o} \mathbf{u}_{vo} \quad (5)$$

172 in which $\mathbf{k}_{qi} \in \mathbb{R}^n$ and $\mathbf{k}_{qo} \in \mathbb{R}^n$ denote the valves' flow gain 173 coefficient. $\mathbf{u}_{vi} \in \mathbb{R}^n$ and $\mathbf{u}_{vo} \in \mathbb{R}^n$ are the control commands 174 for each valve. $\mathbf{h}_i \in \mathbb{R}^n$ and $\mathbf{h}_o \in \mathbb{R}^n$ are defined as

$$\begin{aligned} \mathbf{h}_i &= \Lambda_S(\mathbf{u}_{vi}) \sqrt{\mathbf{p}_s - \mathbf{p}_i} + \Lambda_{S(-\mathbf{u}_{vi})} \sqrt{\mathbf{p}_i - \mathbf{p}_r} \\ \mathbf{h}_o &= \Lambda_S(\mathbf{u}_{vo}) \sqrt{\mathbf{p}_o - \mathbf{p}_r} + \Lambda_{S(-\mathbf{u}_{vo})} \sqrt{\mathbf{p}_s - \mathbf{p}_o} \end{aligned} \quad (6)$$

175 with \mathbf{p}_s and \mathbf{p}_r being the supply pressure of the pump 176 and the tank reference pressure, respectively. $S(\bullet) = [S_1(\bullet_1), \dots, S_n(\bullet_n)]^T$ is an elementwise selective function, 177 whose m th element is defined as

$$S_m(\bullet_m) = \begin{cases} 1, & \bullet_m > 0 \\ 0, & \bullet_m \leq 0. \end{cases} \quad (7)$$

179 The following notations are used throughout this article: $\hat{\mathbf{x}} = 180 \hat{\mathbf{x}} - \mathbf{x}$ denotes the estimation error, with $\hat{\mathbf{x}}$ being the estimate of 181 vector \mathbf{x} . $\lambda_{\mathbf{X}} = \min(\text{eig}(\mathbf{X}))$ and $\bar{\lambda}_{\mathbf{X}} = \max(\text{eig}(\mathbf{X}))$ mean 182 the minimum and maximum eigenvalues of matrix \mathbf{X} .

183 *Property 2.1:* The inertia matrix $\mathbf{M}(\mathbf{q})$ is a symmetric positive definite (s.p.d.) matrix, and satisfies

$$\underline{\lambda}_{\mathbf{M}} \|x\|^2 \leq x^T \mathbf{M}(\mathbf{q}) x \leq \bar{\lambda}_{\mathbf{M}} \|x\| \quad \forall x \in \mathbb{R}^n. \quad (8)$$

185 *Property 2.2:* $\dot{\mathbf{M}}(\mathbf{q}) - 2\mathbf{C}(\mathbf{q}, \dot{\mathbf{q}})$ is a skew-symmetric matrix, i.e.,

$$x^T [\dot{\mathbf{M}}(\mathbf{q}) - 2\mathbf{C}(\mathbf{q}, \dot{\mathbf{q}})] x = 0 \quad \forall x \in \mathbb{R}^n. \quad (9)$$

187 B. Modeling of Effective Bulk Modulus

188 As discussed in the introduction, almost all existing studies 189 focusing on hydraulic control systems treated the effective bulk 190 modulus as a known parameter or as an unknown lumped parameter 191 to be estimated online [28], [29]. However, hydraulic oil, 192 as the primary working medium for energy transfer, determines 193 the system's rigidity and is a key parameter influencing control 194 performance [37]. To figure out the real characteristic of the 195 effective bulk modulus, some studies tried to derive theoretical 196 models through some specific experiments aided by additional 197 measuring equipment. Two representative studies have 198 constructed the tangent bulk modulus model and the IFAS model, 199 respectively, which are outlined as follows:

200 1) tangent bulk modulus model [19], [38]:

$$\beta_e = \frac{(V_{a0} - V'_a) \chi^{1/\kappa} + V_{f0} e^{-\varsigma}}{(V_{a0} - V'_a) \kappa^{-1} p_{atm}^{-1} \chi^{\frac{\kappa+1}{\kappa}} + V_{f0} \beta_0^{-1} e^{-\varsigma}}. \quad (10)$$

201 2) IFAS model [21], [22]:

$$\beta_e = \frac{\varpi \chi^{1/\kappa} + (1 - \varpi) (1 + m\varsigma)^{-1/m}}{\varpi (\kappa p_{atm})^{-1} \chi^{\frac{\kappa+1}{\kappa}} + (1 - \varpi) \beta_0^{-1} (1 + m\varsigma)^{\frac{m-1}{m}}}. \quad (11)$$

202 With $\varsigma = (p_{abs} - p_{atm})/\beta_0$ and $\chi = p_{atm}/p_{abs}$. p_{abs} and p_{atm} 203 are the absolute pressure and the atmospheric pressure, respectively. ϖ means the entrained air content and m is the 204 pressure-related term in the bulk modulus of oil. κ represents 205 the polytropic constant of air, ranging from 1.0 to 1.4. β_0 and 206 V_{f0} are the bulk modulus and the volume of pure oil. V_{a0} and 207 V'_a denote the total volume of bubbles at atmosphere and the 208 dissolved volume of air when pressure changes from p_{atm} to p . 209 It is worth noting that $\gamma_b \leq 2\%$ is typically observed in general 210 hydraulic systems [22], where $\gamma_b = (V_{a0} - V'_a)/V_{f0}$.

211 While models mentioned previously have demonstrated good 212 agreement with experimental results, they are not suitable for 213 use in controllers for model compensation. This limitation 214 arises from their noninvertible structures, which prevent the 215 construction of a model compensation law, and the requirement 216 for specific measurements of internal states. Therefore, in this 217 study, we try to develop a control-oriented model based on these 218 theoretical models. According to (10) and (11), considering the 219 fact that $\beta_0 \gg (p_{abs} - p_{atm})$ and $\chi^{-1/\kappa} \gg \gamma_b$, the reciprocal of 220 the effective bulk modulus $\beta_{e\bullet}$ (with $\bullet \in \{i, o\}$) can be modeled 221 as

$$\beta_{e\bullet}^{-1} = \beta_0^{-1} + \gamma_b \kappa^{-1} p_{atm}^{-1} (\chi_{\bullet})^{\frac{\kappa+1}{\kappa}} \quad (12)$$

223 where $\chi_{\bullet} = p_{atm} \mathbf{p}_{\bullet}^{-1}$ with \mathbf{p}_{\bullet} being the elementwise reciprocal 224 of \mathbf{p}_{\bullet} . Then, to address the unmeasurable state γ_b and polytropic 225 constant κ , a third-order polynomial expansion is utilized as an 226 approximation, which is depicted by

$$\beta_{e\bullet}^{-1} = \theta_{\beta\bullet} + R_n(\chi_{\bullet}), \quad \theta_{\beta\bullet} \triangleq \phi_{\chi_{\bullet}}^T \vartheta_{\alpha\bullet} \quad (13)$$

227 with $\phi_{\chi_{\bullet}}^T = [\Lambda_{\chi_{\bullet}}^0, \dots, \Lambda_{\chi_{\bullet}}^3]$. $\vartheta_{\alpha\bullet} = [\alpha_{\bullet,0}^T, \dots, \alpha_{\bullet,3}^T]^T \in \mathbb{R}^{4n}$ is the 228 internal parameter set to be estimated later, where $\alpha_{\bullet,0}$ corresponds 229 to the bulk modulus of pure oil. $\alpha_{\bullet,1}$, $\alpha_{\bullet,2}$, and $\alpha_{\bullet,3}$ reflects 230 the influence of entrained air content and temperature on the 231 effective bulk modulus together. $R_n(\chi_{\bullet})$ represents the Peano 232 remainder. The proposed model for the effective bulk modulus 233 in (13) is constructed by simplification of the theoretical models 234 considering practical conditions. This model adopts a parametric 235 polynomial structure that is invertible, enabling its use for model 236 compensation with only pressure measurements required. The 237 process of utilizing the model for compensation and updating 238 the parameters online will be detailed in Section III-F.

239 C. Model Parameterization

240 The uncertain nonlinearities in (1), (4), and (13) can be split 241 into the nominal value $\Delta_{\bullet,n}$ with slow variation and the bounded

deviation value $\tilde{\Delta}_\bullet$, which are given by

$$\begin{aligned}\Delta_{Fn} + \tilde{\Delta}_F &\triangleq \Delta_F \\ \Delta_{Qin} + \tilde{\Delta}_{Qi} &\triangleq \Delta_{Qi} - \Lambda_{Vi} \Lambda_{\dot{p}_i} R_n(\chi_i) \\ \Delta_{Qon} + \tilde{\Delta}_{Qo} &\triangleq \Delta_{Qo} - \Lambda_{Vo} \Lambda_{\dot{p}_o} R_n(\chi_o)\end{aligned}\quad (14)$$

Define $\theta_1 = \mathbf{f}_v$, $\theta_2 = \mathbf{f}_c$, $\theta_3 = \mathbf{f}_s$, $\theta_4 = \Delta_{Fn}$, $\theta_5 = \Delta_{Qin}$, $\theta_6 = \Delta_{Qon}$. The sets of the parameters to be estimated online are grouped as $\Theta_F = [\theta_1^T, \theta_2^T, \theta_3^T, \theta_4^T]^T$, $\Theta_{Qi} = [\vartheta_{\alpha_i}^T, \theta_5^T]^T$, and $\Theta_{Qo} = [\vartheta_{\alpha_o}^T, \theta_6^T]^T$. Referring back to (13), the dynamics model can be parameterized as

$$\begin{aligned}M\ddot{\mathbf{q}} + C\dot{\mathbf{q}} + G &= \tau - \phi_F^T \Theta_F + \tilde{\Delta}_F \\ \Lambda_{V_i} \Lambda_{\theta_{\beta_i}} \dot{p}_i &= -\Lambda_{A_i} \mathbf{J}_h \dot{\mathbf{q}} + \mathbf{Q}_i + \theta_5 + \tilde{\Delta}_{Qi} \\ \Lambda_{V_o} \Lambda_{\theta_{\beta_o}} \dot{p}_o &= \Lambda_{A_o} \mathbf{J}_h \dot{\mathbf{q}} - \mathbf{Q}_o + \theta_6 + \tilde{\Delta}_{Qo}\end{aligned}\quad (15)$$

with $\phi_F^T = [\Lambda_{\dot{\mathbf{q}}}, \Lambda_{S_f}, \Lambda_{S_f} \Lambda_{E_f}, -\mathbf{I}_n]$.

Assumption 2.1: The bounds of parametric uncertainties and uncertain nonlinearities are known, i.e.,

$$\begin{aligned}\Theta_F &\in \Omega_{\Theta_F}, \Theta_{Qi} \in \Omega_{\Theta_{Qi}}, \Theta_{Qo} \in \Omega_{\Theta_{Qo}} \\ \|\tilde{\Delta}_F\| &\leq \delta_F, \|\tilde{\Delta}_{Qi}\| \leq \delta_{Qi}, \|\tilde{\Delta}_{Qo}\| \leq \delta_{Qo}\end{aligned}\quad (16)$$

where $\Omega_\bullet \triangleq \{\bullet : \bullet_{\min} \preceq \bullet \preceq \bullet_{\max}\}$. δ_F , δ_{Qi} , δ_{Qo} , \bullet_{\min} , and \bullet_{\max} are known scalars (with $\bullet \in \{\Theta_F, \Theta_{Qi}, \Theta_{Qo}\}$). Especially, $\bar{\theta}_{\beta_i}$ and $\underline{\theta}_{\beta_o}$ represent the known upper and lower bounds of θ_{β_i} (with $\bullet \in \{i, o\}$), respectively.

D. Control Objective

The task for the controller is to generate the control commands \mathbf{u}_{vi} and \mathbf{u}_{vo} for the valves such that the joint angles $\mathbf{q}(t)$ track a set of desired trajectories $\mathbf{q}_d(t) \in \mathbb{R}^n$ as closely as possible, which are assumed to be known, bounded, and at least third-order differentiable. In addition, since the independent metering configuration is used to control the hydraulic manipulator [35], [36], the flexibility should be handled properly to keep the cylinder working pressure at a low level.

I2. CONTROL DESIGN

The control framework is illustrated in Fig. 2. Through the reference pressure generation module, one chamber is required to maintain low pressure, while the other generates the necessary net moment. What is more, to address nonlinear variations in effective elastic modulus under low pressure, an X-swapping-based online parameter estimation method is proposed.

A. Projection Type Adaptation Law With Rate Limits

The parameter estimation $\hat{\Theta}$ will be updated by the structure

$$\dot{\hat{\Theta}} = \text{sat}_{\dot{\hat{\Theta}}_M}(\text{Proj}_{\hat{\Theta}}(\Gamma\nu)) \quad (17)$$

in which $\dot{\hat{\Theta}}_M$ is a preset rate limit, and Γ is any continuously differentiable s.p.d. matrix. ν is an adaptation function to be synthesized later. For any ν , the properties $\hat{\Theta} \in \Omega_\Theta$ and $\|\dot{\hat{\Theta}}\| \leq \dot{\hat{\Theta}}_M$ will always be satisfied.

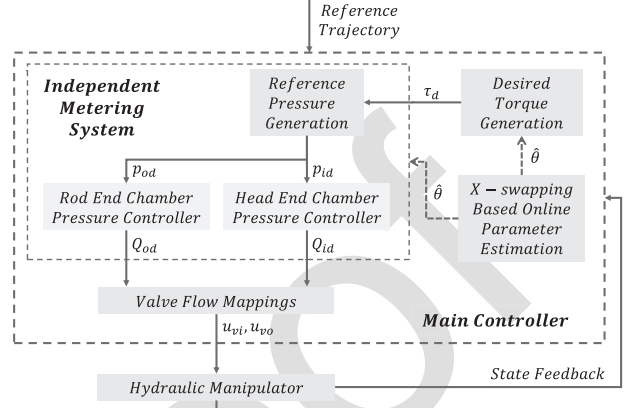


Fig. 2. Overall control framework.

The saturation function $\text{sat}_{\dot{\hat{\Theta}}_M}(\bullet)$ is expressed as

$$\text{sat}_{\dot{\hat{\Theta}}_M}(\bullet) = \begin{cases} \frac{\dot{\hat{\Theta}}_M}{\|\bullet\|} \bullet, & \|\bullet\| > \dot{\hat{\Theta}}_M \\ \bullet, & \text{otherwise.} \end{cases} \quad (18)$$

The projection-type adaptation law for $\hat{\Theta}$ is defined as

$$\text{Proj}_{\hat{\Theta}}(\bullet) = \begin{cases} \bullet - \Gamma \frac{n_{\hat{\Theta}} n_{\hat{\Theta}}^T}{n_{\hat{\Theta}}^T \Gamma n_{\hat{\Theta}}} \bullet, & \hat{\Theta} \in \partial\Omega_\Theta \text{ and } n_{\hat{\Theta}}^T \bullet > 0 \\ \bullet, & \text{otherwise} \end{cases} \quad (19)$$

where $\partial\Omega_\Theta$ represents the boundary of Ω_Θ . $n_{\hat{\Theta}}$ denotes the outward unit normal vector at $\hat{\Theta} \in \partial\Omega_\Theta$.

In addition, an gradient descent-based projection-type adaptation law for $\hat{\mathbf{d}} \in \mathbb{R}^n$ is defined as

$$\dot{\hat{\mathbf{d}}} = \text{Proj}_{\hat{\mathbf{d}}}(\Gamma \mathcal{H} \nu) \quad (20)$$

in which $\text{Proj}_{\hat{\mathbf{d}}}(\bullet) = [\text{Proj}_{\hat{d}_1}(\bullet_1), \dots, \text{Proj}_{\hat{d}_n}(\bullet_n)]^T$ is an elementwise operations projection function, whose m th element is designed as

$$\text{Proj}_{\hat{d}_m}(\bullet_m) = \begin{cases} 0, & |\hat{d}_m| = d_M \text{ and } \hat{d}_m \nu_m > 0 \\ \bullet_m, & \text{otherwise} \end{cases} \quad (21)$$

with d_M being a preset bound.

$\mathcal{H}(\hat{\mathbf{d}}, \nu, \mathcal{Q}) = \text{diag}([h_1, \dots, h_n])$ in (20) is a diagonal matrix, where $h_m = -\bar{\lambda}_{\mathcal{Q}} \text{sgn}(\hat{d}_m \nu_m)$ is a possible choice, such that (20) satisfies the following properties:

$$(P1) \|\dot{\hat{\mathbf{d}}}\| \leq d_M \quad \forall t$$

$$(P2) \hat{\mathbf{d}}^T [\Gamma^{-1} \text{Proj}_{\hat{\mathbf{d}}}(\Gamma \mathcal{H} \nu) - \mathcal{Q} \nu] \leq 0 \quad \forall \nu \quad (22)$$

in which $\mathcal{Q} \in \mathbb{R}^{n \times n}$ is any positive definite diagonal matrix and $\text{sgn}(\bullet)$ denotes the sign function.

B. Desired Torque Generation

Let $\mathbf{z}_1 = \mathbf{q} - \mathbf{q}_d$ denote the angle tracking error, a switching function can be defined as

$$\mathbf{z}_2 = \dot{\mathbf{z}}_1 + \Lambda_{k_1} \mathbf{z}_1 = \dot{\mathbf{q}} - \dot{\mathbf{q}}_{eq}, \dot{\mathbf{q}}_{eq} \triangleq \dot{\mathbf{q}}_d - \Lambda_{k_1} \mathbf{z}_1 \quad (23)$$

with $k_1 = [k_{11}, \dots, k_{1n}]^T$ being a positive constant gain vector. It can be obtained that $\mathcal{L}[\mathbf{z}_2] = \Lambda_{G(s)}\mathcal{L}[\mathbf{z}_1]$ and $G(s) = [1/(s+k_{11}), \dots, 1/(s+k_{1n})]^T$, where $\mathcal{L}[\bullet]$ means the Laplace transform of \bullet . Therefore, as long as the $\mathbf{z}_2 \rightarrow 0$, the tracking error \mathbf{z}_1 will be very small or converge to zero.

Differentiating (23) and noting (15), it has

$$\begin{aligned} \mathbf{M}\dot{\mathbf{z}}_2 + \mathbf{C}\mathbf{z}_2 &= \boldsymbol{\tau}_d - \phi_F^T \boldsymbol{\Theta}_F - \mathbf{G} + \mathbf{z}_3 \\ &\quad + \tilde{\Delta}_F - (\mathbf{M}\ddot{\mathbf{q}}_{eq} + \mathbf{C}\dot{\mathbf{q}}_{eq}) \end{aligned} \quad (24)$$

in which $\mathbf{z}_3 = \boldsymbol{\tau} - \boldsymbol{\tau}_d$. $\boldsymbol{\tau}_d$ denotes the desired torque, which is designed as

$$\begin{aligned} \boldsymbol{\tau}_d &= \boldsymbol{\tau}_{da1} + \boldsymbol{\tau}_{ds1} + \boldsymbol{\tau}_{da2} + \boldsymbol{\tau}_{ds2} \\ \boldsymbol{\tau}_{da1} &= \phi_F^T \hat{\boldsymbol{\Theta}}_F + \mathbf{M}\ddot{\mathbf{q}}_{eq} + \mathbf{C}\dot{\mathbf{q}}_{eq} + \mathbf{G} \\ \boldsymbol{\tau}_{ds1} &= -\Lambda_{k_F} \mathbf{z}_2 \end{aligned} \quad (25)$$

with Λ_{k_F} being a s.p.d. gain matrix. The details about $\boldsymbol{\tau}_{da2}$ and $\boldsymbol{\tau}_{ds2}$ will be given later.

By substituting (25) into (24), all parameter estimation discrepancies $\tilde{\boldsymbol{\Theta}}_F$ and uncertain nonlinearities $\tilde{\Delta}_F$ can be lumped into

$$\mathbf{d}_F + \tilde{\mathbf{d}}_F^* \triangleq \phi_F^T \tilde{\boldsymbol{\Theta}}_F + \tilde{\Delta}_F \quad (26)$$

where \mathbf{d}_F and $\tilde{\mathbf{d}}_F^*$ denote the static component and the high-frequency component, respectively.

Then, $\boldsymbol{\tau}_{da2}$ in (25) is designed to compensate \mathbf{d}_F as

$$\boldsymbol{\tau}_{da2} = -\hat{\mathbf{d}}_F, \quad \dot{\hat{\mathbf{d}}}_F = \text{Proj}_{\hat{\mathbf{d}}}(\Lambda_{\gamma_F} \mathcal{H}_F \mathbf{z}_2), \quad \|\hat{\mathbf{d}}_F\| \leq d_{FM} \quad (27)$$

with $\mathcal{H}_F = \mathcal{H}(\hat{\mathbf{d}}_F, \mathbf{z}_2, \mathbf{I})$. Λ_{γ_F} is a s.p.d. matrix and d_{FM} is a preset bound.

Select $\boldsymbol{\tau}_{ds2} = -\eta_F^{-1} h_F^2 \mathbf{z}_2 / 4$ to ensure that the following two conditions are met:

$$\begin{aligned} 1) \quad &\mathbf{z}_2^T \boldsymbol{\tau}_{ds2} \leq 0 \\ 2) \quad &\mathbf{z}_2^T (\boldsymbol{\tau}_{ds2} - \tilde{\mathbf{d}}_F + \tilde{\mathbf{d}}_F^*) \leq \eta_F \end{aligned} \quad (28)$$

in which $\eta_F > 0$ is an arbitrarily small parameter and h_F can be any smooth function so that

$$h_F \geq \|\phi_F^T \tilde{\boldsymbol{\Theta}}_F\| + d_{FM} + \delta_F. \quad (29)$$

Using (25) and (27), the resulting error dynamics of \mathbf{z}_2 can be written as

$$\mathbf{M}\dot{\mathbf{z}}_2 + \mathbf{C}\mathbf{z}_2 = -\Lambda_{k_F} \mathbf{z}_2 + \mathbf{z}_3 + \boldsymbol{\tau}_{ds2} - \tilde{\mathbf{d}}_F + \tilde{\mathbf{d}}_F^*. \quad (30)$$

C. Generation of Reference Pressure for Each Chamber

Define the reference pressure trajectories for both chambers as \mathbf{p}_{id} and \mathbf{p}_{od} , which will be given later and must satisfy the following conditions:

$$\mathbf{J}_h (\Lambda_{\mathbf{A}_i} \mathbf{p}_{id} - \Lambda_{\mathbf{A}_o} \mathbf{p}_{od}) = \boldsymbol{\tau}_d. \quad (31)$$

By defining the pressure tracking errors as $\mathbf{z}_{pi} = \mathbf{p}_i - \mathbf{p}_{id}$ and $\mathbf{z}_{po} = \mathbf{p}_o - \mathbf{p}_{od}$, \mathbf{z}_3 in (30) can be expressed further as

$$\mathbf{z}_3 = \mathbf{J}_h (\Lambda_{\mathbf{A}_i} \mathbf{z}_{pi} - \Lambda_{\mathbf{A}_o} \mathbf{z}_{po}). \quad (32)$$

Referring back to (7), \mathbf{p}_{od} for the rod end chamber is designed as

$$\mathbf{p}_{od} = \Lambda_{S(\xi_{po})} \mathbf{p}_c + \Lambda_{S(-\xi_{po})} \Lambda_{\mathbf{A}_o}^{-1} (\Lambda_{\mathbf{A}_i} \mathbf{p}_c - \mathbf{J}_h^{-1} \boldsymbol{\tau}_d) \quad (33)$$

with $\xi_{po} = \Lambda_{\mathbf{A}_i}^{-1} (\Lambda_{\mathbf{A}_o} \mathbf{p}_c + \mathbf{J}_h^{-1} \boldsymbol{\tau}_d) - \mathbf{p}_c$. \mathbf{p}_c represents the desired low pressure, while avoiding occasional pressure fluctuations that could cause the local pressure to drop below the air separation pressure, potentially leading to cavitation.

Then, \mathbf{p}_{id} for the head end chamber can be integrated as

$$\mathbf{p}_{id} = \Lambda_{\mathbf{A}_i}^{-1} (\Lambda_{\mathbf{A}_o} \mathbf{p}_{od} + \mathbf{J}_h^{-1} \boldsymbol{\tau}_d). \quad (34)$$

Remark 3.1: The independent metering unit shown in Fig. 1 enables numerous reference pressure configurations that satisfy (29). According to (31) and (32), the reference pressure in both chambers will not fall below the preset pressure \mathbf{p}_c , while at least one chamber reaches \mathbf{p}_c , thereby minimizing the overall working pressure. In addition, the proposed generation method ensures that the desired torque $\boldsymbol{\tau}_d$ remains unchanged, thus maintaining the required high-precision motion control performance.

D. Pressure Controller for Head End Chamber

The error dynamics of \mathbf{z}_{pi} is expressed as

$$\Lambda_{\theta_{\beta_i}} \dot{\mathbf{z}}_{pi} = \Lambda_{\mathbf{V}_i}^{-1} (\mathbf{Q}_i - \Lambda_{\mathbf{A}_i} \mathbf{J}_h \dot{\mathbf{q}} + \theta_5 + \tilde{\Delta}_{Qi}) - \Lambda_{\theta_{\beta_i}} \dot{\mathbf{p}}_{id}. \quad (35)$$

Given the sufficiently high bandwidth of the control valve, the dynamics of the valve spool motion can be neglected [10], allowing the assumption $\mathbf{Q}_i = \mathbf{Q}_{id}$. Referring back to (13) and noting $\Lambda_{\theta_{\beta_i}} \dot{\mathbf{p}}_{id} = \Lambda_{\dot{\mathbf{p}}_{id}} \phi_{\chi_i}^T \dot{\vartheta}_{\alpha_i}$, \mathbf{Q}_{id} can be designed as

$$\begin{aligned} \mathbf{Q}_{id} &= \mathbf{Q}_{ida1} + \mathbf{Q}_{ids1} + \mathbf{Q}_{ida2} + \mathbf{Q}_{ids2} + \Upsilon_{Qi} \\ \mathbf{Q}_{ida1} &= \Lambda_{\mathbf{A}_i} \mathbf{J}_h \dot{\mathbf{q}} - \hat{\theta}_5 + \Lambda_{\mathbf{V}_i} \Lambda_{\dot{\mathbf{p}}_{id}} \phi_{\chi_i}^T \dot{\vartheta}_{\alpha_i} \\ \mathbf{Q}_{ids1} &= -\Lambda_{\mathbf{V}_i} \Lambda_{k_{Qi}} \mathbf{z}_{pi}, \quad \Upsilon_{Qi} = -\Lambda_{\mathbf{V}_i} \mathcal{F}_i \Lambda_{\mathbf{A}_i} \mathbf{J}_h^T \mathbf{z}_2 \end{aligned} \quad (36)$$

with $\Lambda_{k_{Qi}}$ being an s.p.d. gain matrix. \mathcal{F}_i is designed as $\mathcal{F}_i = \mathcal{F}(\mathbf{z}_{pi}, \Lambda_{\mathbf{A}_i} \mathbf{J}_h^T \mathbf{z}_2, \bar{\theta}_{\beta_i})$, where the specific definition and property of \mathcal{F} will be demonstrated in the *Lemma 3.1*. Substituting (36) into (35), all uncertainties can be lumped into

$$\mathbf{d}_{Qi} + \tilde{\mathbf{d}}_{Qi}^* \triangleq \Lambda_{\mathbf{V}_i}^{-1} (-\hat{\theta}_5 + \tilde{\Delta}_{Qi}) + \Lambda_{\dot{\mathbf{p}}_{id}} \phi_{\chi_i}^T \tilde{\vartheta}_{\alpha_i} \quad (37)$$

where \mathbf{d}_{Qi} and $\tilde{\mathbf{d}}_{Qi}^*$ denote the static component and the high-frequency component, respectively.

Then, \mathbf{Q}_{ida2} in (36) is designed as

$$\mathbf{Q}_{ida2} = -\Lambda_{\mathbf{V}_i} \hat{\mathbf{d}}_{Qi}, \quad \dot{\hat{\mathbf{d}}}_{Qi} = \text{Proj}_{\hat{\mathbf{d}}}(\Lambda_{\gamma_{Qi}} \mathcal{H}_{Qi} \mathbf{z}_{pi}) \quad (38)$$

with $\mathcal{H}_{Qi} = \mathcal{H}(\hat{\mathbf{d}}_{Qi}, \mathbf{z}_{pi}, \Lambda_{\theta_{\beta_i}}^{-1})$. $\Lambda_{\gamma_{Qi}}$ is a s.p.d. matrix and $\|\hat{\mathbf{d}}_{Qi}\| \leq d_{QiM}$, where d_{QiM} being a preset bound.

Select $\mathbf{Q}_{ids2} = -\eta_{Qi}^{-1} h_{Qi}^2 \Lambda_{\mathbf{V}_i} \mathbf{z}_{pi} / 4$ to ensure that the following two conditions are met:

$$1) \quad \mathbf{z}_{pi}^T \Lambda_{\theta_{\beta_i}}^{-1} \Lambda_{\mathbf{V}_i}^{-1} \mathbf{Q}_{ids2} \leq 0$$

$$2) \quad \mathbf{z}_{pi}^T \Lambda_{\theta_{\beta_i}}^{-1} (\Lambda_{\mathbf{V}_i}^{-1} \mathbf{Q}_{ids2} - \tilde{\mathbf{d}}_{Qi} + \tilde{\mathbf{d}}_{Qi}^*) \leq \underline{\theta}_{\beta_i} \eta_{Qi} \quad (39)$$

in which $\eta_{Qi} > 0$ is an arbitrarily small parameter. h_{Qi} can be any smooth function so that

$$h_{Qi} \geq \|\Lambda_{\dot{\mathbf{p}}_{id}} \phi_{\chi_i}^T \tilde{\vartheta}_{\alpha_i}\| + \|\Lambda_{\mathbf{V}_i}^{-1} \tilde{\theta}_5\| + d_{QiM} + \Lambda_{\mathbf{V}_i}^{-1} \delta_{Qi}. \quad (40)$$

Using (36) and (38), the resulting error dynamics of \mathbf{z}_{pi} can be written as

$$\begin{aligned} \Lambda_{\theta_{\beta_i}} \dot{\mathbf{z}}_{pi} = & -\Lambda_{k_{Qi}} \mathbf{z}_{pi} - \mathcal{F}_i \Lambda_{\mathbf{A}_i} \mathbf{J}_h^T \mathbf{z}_2 \\ & + \Lambda_{\mathbf{V}_i}^{-1} \mathbf{Q}_{ids2} - \tilde{\mathbf{d}}_{Qi} + \tilde{\mathbf{d}}_{Qi}^*. \end{aligned} \quad (41)$$

E. Pressure Controller for Rod End Chamber

The error dynamics of \mathbf{z}_{po} is expressed as

$$\Lambda_{\theta_{\beta_o}} \dot{\mathbf{z}}_{po} = \Lambda_{\mathbf{V}_o}^{-1} \left(\Lambda_{\mathbf{A}_o} \mathbf{J}_h \dot{\mathbf{q}} - \mathbf{Q}_o + \theta_6 + \tilde{\Delta}_{Qi} \right) - \Lambda_{\theta_{\beta_o}} \dot{\mathbf{p}}_{od}. \quad (42)$$

Similar to \mathbf{Q}_{id} , \mathbf{Q}_{od} is designed as

$$\begin{aligned} \mathbf{Q}_{od} &= \mathbf{Q}_{oda1} + \mathbf{Q}_{ods1} + \mathbf{Q}_{oda2} + \mathbf{Q}_{ods2} + \Upsilon_{Qo} \\ \mathbf{Q}_{oda1} &= \Lambda_{\mathbf{A}_o} \mathbf{J}_h \dot{\mathbf{q}} + \hat{\theta}_6 - \Lambda_{\mathbf{V}_o} \Lambda_{\dot{\mathbf{p}}_{od}} \phi_{\chi_o}^T \hat{\vartheta}_{\alpha_o} \\ \mathbf{Q}_{oda2} &= \Lambda_{\mathbf{V}_o} \hat{\mathbf{d}}_{Qo}, \quad \dot{\hat{\mathbf{d}}}_{Qo} = \text{Proj}_{\hat{\mathbf{d}}}(\Lambda_{\gamma_{Qo}} \mathcal{H}_{Qo} \mathbf{z}_{po}) \\ \mathbf{Q}_{ods1} &= \Lambda_{\mathbf{V}_o} \Lambda_{k_{Qo}} \mathbf{z}_{po}, \quad \Upsilon_{Qo} = -\Lambda_{\mathbf{V}_o} \mathcal{F}_o \Lambda_{\mathbf{A}_o} \mathbf{J}_h^T \mathbf{z}_2 \end{aligned} \quad (43)$$

in which $\Lambda_{k_{Qo}}$ and $\Lambda_{\gamma_{Qo}}$ are s.p.d. gain matrixes. $\mathcal{H}_{Qo} = \mathcal{H}(\hat{\mathbf{d}}_{Qo}, \mathbf{z}_{po}, \Lambda_{\theta_{\beta_o}}^{-1})$. \mathcal{F}_o is designed as $\mathcal{F}_o = \mathcal{F}(\mathbf{z}_{po}, \Lambda_{\mathbf{A}_o} \mathbf{J}_h^T \mathbf{z}_2, -\bar{\theta}_{\beta_o})$. $\|\hat{\mathbf{d}}_{Qo}\| \leq d_{QoM}$, with d_{QoM} being a preset bound. \mathbf{d}_{Qo} represents the static component of the residual nonlinearities, which is defined as

$$\mathbf{d}_{Qo} + \tilde{\mathbf{d}}_{Qo}^* \triangleq \Lambda_{\mathbf{V}_o}^{-1} \left(-\tilde{\theta}_6 + \tilde{\Delta}_{Qi} \right) + \Lambda_{\dot{\mathbf{p}}_{od}} \phi_{\chi_o}^T \tilde{\vartheta}_{\alpha_o} \quad (44)$$

where $\tilde{\mathbf{d}}_{Qo}^*$ denotes the high-frequency component.

$\mathbf{Q}_{ods2} = \eta_{Qo}^{-1} h_{Qo}^2 \Lambda_{\mathbf{V}_o} \mathbf{z}_{po} / 4$ is designed to satisfy the following two conditions:

$$\begin{aligned} 1) \quad &\mathbf{z}_{po}^T \Lambda_{\theta_{\beta_o}}^{-1} \Lambda_{\mathbf{V}_o}^{-1} \mathbf{Q}_{ods2} \geq 0 \\ 2) \quad &\mathbf{z}_{po}^T \Lambda_{\theta_{\beta_o}}^{-1} \left(-\Lambda_{\mathbf{V}_o}^{-1} \mathbf{Q}_{ods2} - \tilde{\mathbf{d}}_{Qo} + \tilde{\mathbf{d}}_{Qo}^* \right) \leq \underline{\theta}_{\beta_o} \eta_{Qo} \end{aligned} \quad (45)$$

in which $\eta_{Qo} > 0$ is an arbitrarily small parameter. h_{Qo} is a smooth function that satisfies

$$h_{Qo} \geq \|\Lambda_{\dot{\mathbf{p}}_{od}} \phi_{\chi_o}^T \tilde{\vartheta}_{\alpha_o}\| + \|\Lambda_{\mathbf{V}_o}^{-1} \tilde{\theta}_6\| + d_{QoM} + \Lambda_{\mathbf{V}_o}^{-1} \delta_{Qo}. \quad (46)$$

The resulting error dynamics of \mathbf{z}_{pi} can be written as

$$\begin{aligned} \Lambda_{\theta_{\beta_o}} \dot{\mathbf{z}}_{po} = & -\Lambda_{k_{Qo}} \mathbf{z}_{po} + \mathcal{F}_o \Lambda_{\mathbf{A}_o} \mathbf{J}_h^T \mathbf{z}_2 \\ & - \Lambda_{\mathbf{V}_o}^{-1} \mathbf{Q}_{ods2} - \tilde{\mathbf{d}}_{Qo} + \tilde{\mathbf{d}}_{Qo}^*. \end{aligned} \quad (47)$$

Finally, the control command of the valve \mathbf{u}_{vi} and \mathbf{u}_{vo} can be synthesized by the valve flow mappings in (5) as

$$\mathbf{u}_{vi} = \Lambda_{\mathbf{h}_i}^{-1} \Lambda_{\mathbf{k}_{qi}}^{-1} \mathbf{Q}_i, \quad \mathbf{u}_{vo} = \Lambda_{\mathbf{h}_o}^{-1} \Lambda_{\mathbf{k}_{qo}}^{-1} \mathbf{Q}_o. \quad (48)$$

F. X-Swapping-Based Online Parameter Estimation

If the nonlinear uncertainties within the dynamics in (15) are assumed to be zero after a finite time, i.e., assuming $\tilde{\Delta}_F =$

$\tilde{\Delta}_{Qi} = \tilde{\Delta}_{Qo} = 0$, the system dynamics for parameter estimation can be rewritten as

$$\begin{aligned} \phi_F^T \Theta_F &= \boldsymbol{\tau} - \mathbf{M} \ddot{\mathbf{q}} - \mathbf{C} \dot{\mathbf{q}} - \mathbf{G} \\ \Lambda_{\dot{\mathbf{p}}_i} \phi_{\chi_i}^T \vartheta_{\alpha_i} - \Lambda_{\mathbf{V}_i}^{-1} \theta_5 &= -\Lambda_{\mathbf{V}_i}^{-1} \Lambda_{\mathbf{A}_i} \mathbf{J}_h \dot{\mathbf{q}} + \Lambda_{\mathbf{V}_i}^{-1} \mathbf{Q}_i \\ \Lambda_{\dot{\mathbf{p}}_o} \phi_{\chi_o}^T \vartheta_{\alpha_o} - \Lambda_{\mathbf{V}_o}^{-1} \theta_6 &= \Lambda_{\mathbf{V}_o}^{-1} \Lambda_{\mathbf{A}_o} \mathbf{J}_h \dot{\mathbf{q}} - \Lambda_{\mathbf{V}_o}^{-1} \mathbf{Q}_o \end{aligned} \quad (49)$$

in which $\Theta_F, \Theta_{Qi} = [\vartheta_{\alpha_i}^T, \theta_5^T]^T$, and $\Theta_{Qo} = [\vartheta_{\alpha_o}^T, \theta_6^T]^T$ are parameters to be estimated. Define the following regressors:

$$\varphi_F^T = \mathbf{M} \dot{\mathbf{q}}, \quad \varphi_{\varepsilon_{\bullet}}^T = [\Lambda_{\varepsilon_{\bullet 0}}, \dots, \Lambda_{\varepsilon_{\bullet 3}}] \quad (50)$$

where $\varepsilon_{\bullet 0} = \mathbf{p}_{\bullet}$, $\varepsilon_{\bullet 1} = p_{\text{atm}} \ln(\mathbf{p}_{\bullet})$, $\varepsilon_{\bullet 2} = -p_{\text{atm}}^2 \mathbf{p}_{\bullet}^{-1}$, and $\varepsilon_{\bullet 3} = -\frac{1}{2} p_{\text{atm}}^3 \Lambda_{\mathbf{p}_{\bullet}^{-1}} \mathbf{p}_{\bullet}^{-1}$ (with $\bullet \in \{i, o\}$). The differentiates of φ_F^T and $\varphi_{\varepsilon_{\bullet}}^T$ are able to be written as

$$\begin{aligned} \frac{d}{dt} (\varphi_F^T) &= \mathbf{M} \ddot{\mathbf{q}} + \mathbf{C} \dot{\mathbf{q}} + \mathbf{G} \\ \frac{d}{dt} (\varphi_{\varepsilon_{\bullet}}^T) &= \Lambda_{\dot{\mathbf{p}}_{\bullet d}} \phi_{\chi_{\bullet}}^T. \end{aligned} \quad (51)$$

Then, the dynamics (49) can be rewritten as

$$\begin{aligned} \phi_F^T \Theta_F &= u_{F1} + \dot{u}_{F2} \\ \dot{\varphi}_{\varepsilon_i}^T \vartheta_{\alpha_i} - \Lambda_{\mathbf{V}_i}^{-1} \theta_5 &= u_{Qi} \\ \dot{\varphi}_{\varepsilon_o}^T \vartheta_{\alpha_o} - \Lambda_{\mathbf{V}_o}^{-1} \theta_6 &= u_{Qo} \end{aligned} \quad (52)$$

with $u_{F1} = \boldsymbol{\tau} + \mathbf{C}^T \dot{\mathbf{q}} - \mathbf{G}$, $u_{F2} = -\varphi_F^T$, $u_{Qi} = -\Lambda_{\mathbf{V}_i}^{-1} \Lambda_{\mathbf{A}_i} \mathbf{J}_h \dot{\mathbf{q}} + \Lambda_{\mathbf{V}_i}^{-1} \mathbf{Q}_i$, and $u_{Qo} = \Lambda_{\mathbf{V}_o}^{-1} \Lambda_{\mathbf{A}_o} \mathbf{J}_h \dot{\mathbf{q}} - \Lambda_{\mathbf{V}_o}^{-1} \mathbf{Q}_o$.

The first-order filters for acquiring states is designed as

$$\dot{\xi}_{\bullet} = -\lambda_{\bullet} \xi_{\bullet} + u_{\bullet}, \quad \dot{\psi}_{\bullet} = -\lambda_{\bullet} \psi_{\bullet} + \mathcal{T}_{\bullet} \quad (53)$$

in which λ_{\bullet} represents the break frequency of the first-order filters (with $\bullet \in \{F1, F2, Qi, Qo\}$). And \mathcal{T}_{\bullet} is defined as

$$\begin{aligned} \mathcal{T}_{F1}^T &= \mathcal{T}_{F2}^T = [\Lambda_{\mathbf{q}}, \Lambda_{\mathbf{S}_f}, \Lambda_{\mathbf{S}_f} \Lambda_{\mathbf{e}_f}, -\mathbf{I}_n] \\ \mathcal{T}_{Qi}^T &= [-\lambda_i \varphi_{\varepsilon_i}^T, -\Lambda_{\mathbf{V}_i}^{-1}] \\ \mathcal{T}_{Qo}^T &= [-\lambda_o \varphi_{\varepsilon_o}^T, -\Lambda_{\mathbf{V}_o}^{-1}]. \end{aligned} \quad (54)$$

Let $\lambda_{F1} = \lambda_{F2} = \lambda_F$. Then, define variables as $y_F = \xi_{F1} - \lambda_F \xi_{F2} + u_{F2}$, $y_{Qi} = \xi_{Qi}$, and $y_{Qo} = \xi_{Qo}$, whose estimations \tilde{y}_{\bullet} (with $\bullet \in \{F, Qi, Qo\}$) can be given as

$$\tilde{y}_{\bullet} = -\Phi_{\bullet}^T \Theta_{\bullet} \quad (55)$$

in which $\Phi_F^T = -\mathcal{T}_F^T$, $\Phi_{Qi}^T = \Psi_{Qi}^T - \mathcal{T}_{Qi}^T$, and $\Phi_{Qo}^T = \Psi_{Qo}^T - \mathcal{T}_{Qo}^T$, with $\Psi_{Qi}^T \triangleq [-\varphi_{\varepsilon_i}^T, \mathbf{0}_{n \times n}]$ and $\Psi_{Qo}^T \triangleq [-\varphi_{\varepsilon_o}^T, \mathbf{0}_{n \times n}]$.

Define the discrepancies $\tilde{y}_{\bullet} = \tilde{y}_{\bullet} - y_{\bullet}$. Then, differentiate \tilde{y}_{\bullet} , one can get $\dot{\tilde{y}}_{\bullet} = -\lambda_{\bullet} \tilde{y}_{\bullet}$, which means $\tilde{y}_{\bullet} = 0$ can always be guaranteed if the initial conditions of the filters defined in (53) are chosen properly to satisfy $\tilde{y}_{\bullet}(0) = 0$. Therefore, $y_{\bullet} = \tilde{y}_{\bullet} \forall t$. Define $\hat{y}_{\bullet} = -\Phi_{\bullet}^T \hat{\Theta}_{\bullet}$. $\hat{\Theta}_{\bullet}$ represents the prediction of y_{\bullet} . The prediction errors ϵ_{\bullet} can be given as

$$\epsilon_{\bullet} = \hat{y}_{\bullet} - y_{\bullet} = -\Phi_{\bullet}^T \tilde{\Theta}_{\bullet}. \quad (56)$$

Thus, the static parametric models which are linear with respect to the parameter estimation errors $\hat{\Theta}_F, \hat{\Theta}_{Qi}$ and $\hat{\Theta}_{Qo}$ have been obtained successfully for estimation. The adaptive function in

(17) is chosen as $\nu_{\bullet} = \Phi_{\bullet}\epsilon_{\bullet}$. Then, the recursive ridge regression estimation algorithm can be used for online estimation, where Γ_{\bullet} is defined as

$$\dot{\Gamma}_{\bullet} = \begin{cases} \iota_{\bullet}\Gamma_{\bullet} - \Gamma_{\bullet}\Phi_{\bullet}\Phi_{\bullet}^T\Gamma_{\bullet}, & \bar{\lambda}_{\Gamma_{\bullet}} \leq \rho_{\bullet M} \\ 0, & \text{otherwise} \end{cases} \quad (57)$$

with ι_{\bullet} being the forgetting factor.

Remark 3.2: Traditional adaptive methods are often challenging to apply to (49) due to the coupling between unmeasurable derivative terms (\dot{q}_i , \dot{p}_i , and \dot{p}_o) and unknown dynamic parameters Θ . To address this, a method similar to pre-integration, as shown in (51), was used to construct an intermediate variable in (50), which contains only measurable states. Furthermore, the real-time numerical results of the coupling term were directly derived from the intermediate variables using the X-swapping algorithm, as given in (53)–(56), while maintaining the same phase lag, thereby yielding the prediction errors ϵ_{\bullet} for the parameter. Then, the online adaptive method is not limited to approaches such as the least-squares method and the gradient descent method.

G. Theoretical Results

Lemma 3.1: Define $f_{\mathcal{F}} = x^T(\mathcal{Q}\mathcal{F} - \mathbf{I})y$ with $\mathcal{Q} \in \mathbb{R}^{n \times n}$ being any s.p.d. matrix, $x \in \mathbb{R}^n$, and $y \in \mathbb{R}^n$. Positive and negative $f_{\mathcal{F}}$ are both feasible to be achieved by the design of \mathcal{F} as follows:

$$\mathcal{F}(x, y, \underline{\lambda}_{\mathcal{Q}}) = \frac{|n_x^T n_y|}{\underline{\lambda}_{\mathcal{Q}}} n_x n_y^T \Rightarrow f_{\mathcal{F}} \geq 0 \forall x, y \quad (58)$$

where n_x and n_y represent the unit vector of x and y , respectively. Besides, if $\mathcal{F} = \mathcal{F}(x, y, -\underline{\lambda}_{\mathcal{Q}})$, $f_{\mathcal{F}} \leq 0 \forall x, y$. The proof is given in Appendix A. ■

The following theoretical results about the proposed system control design can be obtained.

Theorem 3.1: (Boundedness) Considering the parameter estimates updated by (17) and the motion control law, the system controller with \mathbf{u}_{vi} and \mathbf{u}_{vo} as the input guarantees that all signals are bounded. Furthermore, the positive-definite function V_s defined by

$$V_s = \frac{1}{2}\mathbf{z}_2^T \mathbf{M} \mathbf{z}_2 + \frac{1}{2}\mathbf{z}_{pi}^T \mathbf{z}_{pi} + \frac{1}{2}\mathbf{z}_{po}^T \mathbf{z}_{po} \quad (59)$$

is bounded above by

$$V_s(t) \leq \exp(-\lambda_s t)V_s(0) + \frac{\eta_s}{\lambda_s}[1 - \exp(-\lambda_s t)] \quad (60)$$

with $\lambda_s = \min\{2k_F/\bar{\lambda}_M, 2\bar{\theta}_{\beta i}k_{Qi}, 2\bar{\theta}_{\beta o}k_{Qo}\}$ and $\eta_s = \eta_F + \underline{\theta}_{\beta i}\eta_{Qi} + \underline{\theta}_{\beta o}\eta_{Qo}$. The proof is given in Appendix B. ■

Theorem 3.2: (Asymptotic Tracking) Consider the control law (25), (36), and (43) with the adaptation law (17), applied to the hydraulic manipulator with dynamics described by (15). If after a finite time t_f , $\tilde{\Delta}_F = \tilde{\Delta}_{Qi} = \tilde{\Delta}_{Qo} = 0 \forall t \geq t_f$, when the PE condition is satisfied

$$\exists T, t_f, \varepsilon_d > 0 \text{ s.t. } \int_t^{t+T} \Phi \Phi^T d\tau \geq \varepsilon_d \mathbf{I} \forall t \geq t_f \quad (61)$$

in addition to the results outlined in *Theorem 3.1*, the parameter estimates $\hat{\Theta}$ asymptotically converge to true values and the

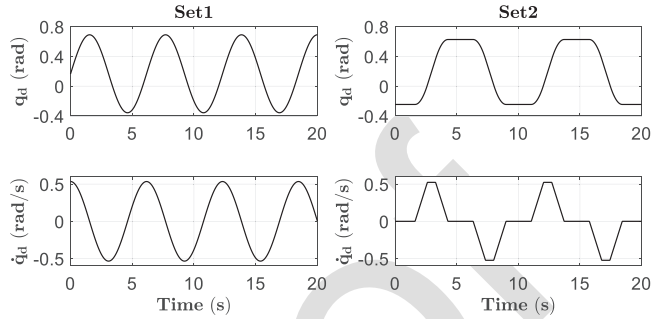


Fig. 3. Reference trajectories in experiment Set1 and Set2.

asymptotic tracking is achieved, i.e., the tracking errors $\mathbf{z}_1 \rightarrow 0$ as $t \rightarrow \infty$. The proof is given in Appendix C. ■

IV. COMPARATIVE EXPERIMENTS AND ANALYSIS

A. Experiment Setup

The proposed control method is applied to a hydraulic manipulator for testing, as shown in Fig. 1. The links 2, 3, and 4 are always coplanar because the link offsets are zeros, and this plane is positioned by the vertical revolution of joint 1. Each joint is independently driven by a hydraulic cylinder, which converts the linear motion of the cylinder into rotational motion at the joint. Flow rates for the two chambers of the hydraulic cylinder are independently regulated by a three-position four-way proportional valve. Pressure feedback is provided by GEFTRAN KS series pressure transmitters with a precision of 0.5%, while joint position sensing is achieved using POSITAL IXARC series absolute encoders, offering a 16-bit single-turn resolution. The following three methods were compared:

- 1) **C1:** The proposed controller in this study. The control law could be represented by (25), (36), and (43), where the parameters were specified as $\Lambda_{k_1} = \text{diag}([80, 80])$, $\Lambda_{k_F} = \text{diag}([27, 58])$, $\Lambda_{k_{Qi}} = \text{diag}([35, 33])$, $\Lambda_{k_{Qo}} = \text{diag}([45, 25])$, $\Lambda_{\gamma_F} = \text{diag}([180, 500])$, and $\Lambda_{\gamma_{Qi}} = \Lambda_{\gamma_{Qo}} = \text{diag}([1, 5]) \times 10^{-6}$.
- 2) **C2:** A controller similar to C1, but lacking online parameter estimation for $\vartheta_{\beta \bullet}$, i.e., $\vartheta_{\beta \bullet}(t) \equiv \vartheta_{\beta \bullet}(0)$.
- 3) **C3:** The effective bulk modulus is treated as a lumped parameter for both estimation and compensation, consistent with most existing studies [28], [29]. Specifically, in (13), $\vartheta_{\beta \bullet} = \alpha_{\bullet 0}$ is the parameter to be estimated while $\alpha_{\bullet j} \equiv 0$ (with $\bullet \in \{i, o\}$, $j \in \{1, 2, 3\}$), with all other variables remaining consistent with C1.

The aforementioned controllers were first compared in joint space to evaluate the control systems, particularly in terms of frequency response, transient behavior, and smooth tracking performance, with the reference trajectories shown in Fig. 3.

- 1) **Set1:** Sine curve tracking experiment. The desired trajectory was set as $q_d(t) = 0.52 \sin(0.325\pi t) + 0.17 \text{ rad}$.
- 2) **Set2:** Point-to-point S-curve tracking experiment, including acceleration, constant speed, and deceleration.

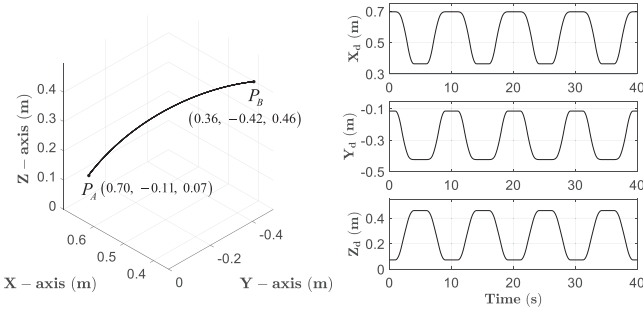


Fig. 4. Desired path and the corresponding reference trajectory for each axis used in Set3.

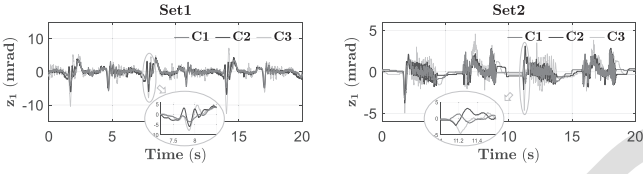


Fig. 5. Comparison of tracking errors in Set1 and Set2.

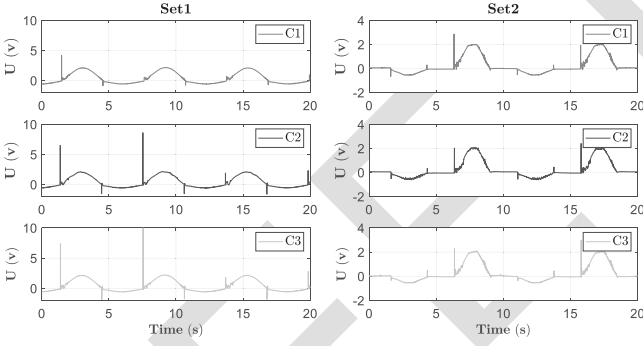


Fig. 6. Control signals under different control strategies.

The S-curve was from -0.25 to 0.63 rad, with the maximum angular velocity $\dot{q}_{d\max} = \pi/6$ rad \cdot s $^{-1}$ and the maximum angular acceleration $\ddot{q}_{d\max} = \pi/6$ rad \cdot s $^{-2}$.

In addition, a reference trajectory was set in Cartesian space, as shown in Fig. 4.

3) **Set3:** Multi-DoF trajectory tracking experiment. A preset endpoint of the hydraulic manipulator was required to reciprocate between P_A and P_B , with the global coordinate system defined in Fig. 1. During this process, the reference trajectories in joint space were calculated using inverse kinematics and then controlled by C1–C3.

The selected performance indicators are as follows: the root mean square error $e_{R\bullet} = \sqrt{\frac{1}{T} \int_0^T |\bullet|^2 dt}$, the peak error $e_{M\bullet} = \max\{|\bullet|\}$, and the normalizing performance indicator $\rho_e = e_M / |\dot{q}|_{\max}$ [1].

B. Experiment Results and Discussion

The tracking results for Set1 and Set2 are presented in Fig. 5, with $1 \text{ mrad} = 10^{-3} \text{ rad}$. Fig. 6 shows the corresponding

TABLE I
NUMERICAL COMPARISON OF TRACKING RESULTS

	e_{Rz1} (mrad)	e_{Mz1} (mrad)	ρ_e (s)	$e_{Rz_{pi}}$ (MPa)	$e_{Rz_{po}}$ (MPa)	$e_{Mz_{pi}}$ (MPa)	$e_{Mz_{po}}$ (MPa)
Set1	C1	1.25	5.65	10.64	0.23	0.19	1.04
	C2	1.38	6.79	12.80	0.26	0.23	2.77
	C3	1.96	12.58	23.70	0.30	0.24	2.15
Set2	C1	0.64	3.35	6.40	0.18	0.20	1.23
	C2	0.73	3.77	7.19	0.20	0.24	1.25
	C3	1.00	4.98	9.52	0.29	0.27	2.06

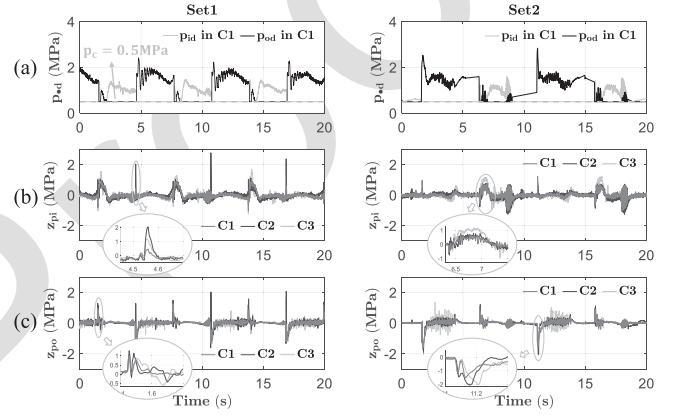


Fig. 7. Reference pressure trajectories in C1 and the comparison of pressure tracking error in experiment Set1 and Set2.

control signals under different control strategies. The associated performance indicators are provided in Table I. During the transition phase of start-stop motion, rapid pressure changes lead to significant fluctuations in error, indicating that the actual effective bulk modulus has undergone substantial changes that cannot be ignored. Notably, the tracking performance of C1 and C2 significantly exceeds that of C3, despite C3 being at the threshold of extreme performance, as indicated by substantial oscillations in its control error. These results suggest that the control gain using the lumped modeling method has reached its limit, indicating the nonlinear relationship between the effective bulk modulus and the pressure cannot be treated as a constant under low-pressure conditions. The effective bulk modulus model developed in this paper accurately captures the system's dynamic behavior and effectively enhances tracking accuracy. In addition, C1 demonstrates superior performance compared to C2. The online learning of ϑ_{β} allows C1 to exhibit greater adaptability to changes in operating conditions, such as oil temperature or entrained air content.

Fig. 7(a) presents the reference pressure trajectories in C1, with the desired low pressure $p_c = 0.5$ MPa in (33). The method proposed in Section III-C significantly reduces the pressure supply demand of the chamber while ensuring that the net moment τ meets predetermined requirements, thereby establishing a foundation for the subsequent reduction of throttling losses. Building on the reference pressure, Fig. 7(b) and (c) illustrates the control effects of pressure. The performance indicators for pressure control are provided in Table I. Both C1 and C2 exhibit more

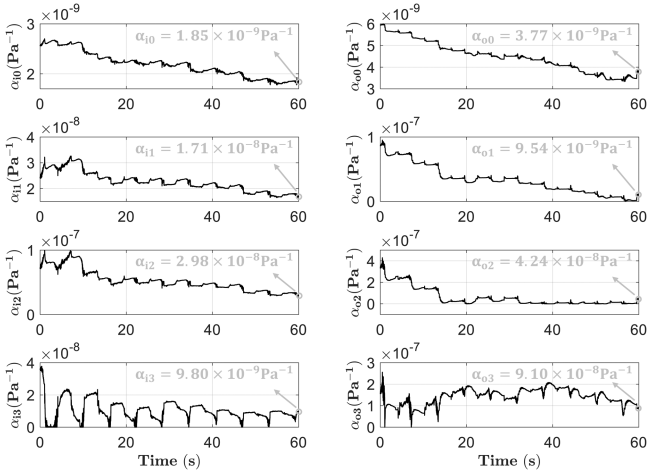
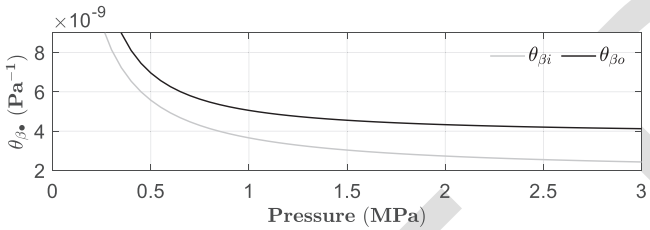
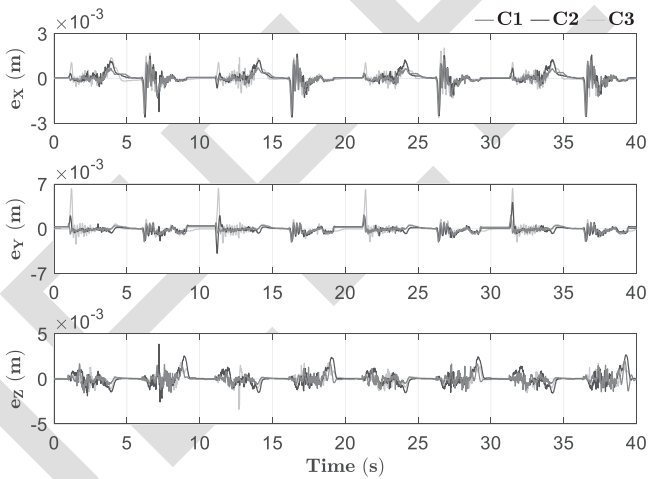
Fig. 8. Estimation results of θ_α by C1 in Set1.Fig. 9. Fitting result of $\theta_{\beta\bullet}$ with respect to pressure by C1 in Set1.

Fig. 10. Tracking errors of each dimension in Cartesian space in Set3.

534 accurate and stable pressure tracking performance, whereas C3
535 is more susceptible to significant pressure oscillations.

536 The estimation results of ϑ_{α_i} and ϑ_{α_o} by C1 in Set1 are
537 given in Fig. 8. The parameters of both chambers exhibit a
538 certain convergence effect, indicating that the proposed model
539 accurately fits the real effective bulk modulus model. By substi-
540 tuting the final convergence value from Fig. 8 into (13), and the
541 fitting result of $\theta_{\beta\bullet}$ with respect to chamber pressure is shown
542 in Fig. 9. The proposed improved model has consistent results

543 with the tangent bulk modulus model and the IFAS model,
544 demonstrating the accuracy and effectiveness of the proposed
545 model in describing actual systems.

546 Fig. 10 presents the multijoint control results for Set3. C1
547 exhibits superior tracking performance across all dimensions,
548 particularly along the Y-axis. This suggests that, compared to
549 other global nonlinearities in hydraulic manipulators, such as
550 joint coupling and gravity, the nonlinear effect of the effective
551 bulk modulus is significant and cannot be overlooked.

V. CONCLUSION

552 In this study, a control-oriented model for the effective bulk
553 modulus is developed that is both feasible for control design
554 and accurately reflects its nonlinear relationship with work-
555 ing pressure. A model-based adaptive robust motion controller
556 is then synthesized for the multi-DOF hydraulic manipulator
557 equipped with independent metering units. The primary pa-
558 rameters of the manipulator, including those in the proposed
559 bulk modulus model, can be updated online through an es-
560 pecially designed X-swapping scheme. The experiment results
561 demonstrate that the proposed method significantly improves
562 motion control accuracy while maintaining system pressure at
563 a low level. Moreover, the method exhibits good convergence
564 properties, and the final fitting results show a high degree
565 of consistency with the theoretical model. Notably, accurately
566 modeling the effective bulk modulus and compensating for its
567 nonlinear behavior in real time, it has great potential for reducing
568 throttling losses that typically occur when adjusting pressure in
569 conventional hydraulic systems. This capability is particularly
570 important for applications such as mobile robotics, industrial
571 automation, and precision actuation systems, where minimizing
572 energy consumption and enhancing system efficiency are es-
573 sential. In future research, we will focus on exploring energy-saving
574 control methods for hydraulic manipulators that balance motion
575 performance and energy efficiency, while further mitigating the
576 impact of disturbances, such as load variations and temperature
577 changes.

APPENDIX A PROOF OF LEMMA 3.1

579 If either x or y is a zero vector, $f_Y = 0$ is always satisfied.
580 The following discussion considers the case where both x and
581 y are nonzero vectors.

582 Define $\mathcal{P} = \mathcal{Q} - \underline{\lambda}_{\mathcal{Q}} \mathbf{I}$, which is a positive semidefinite matrix,
583 i.e., $x^T \mathcal{P} x \geq 0 \forall x$. Thus, one can obtain

$$x^T \mathcal{Q} x \geq \underline{\lambda}_{\mathcal{Q}} x^T x \quad \forall x. \quad (\text{A.1})$$

585 When $\mathcal{F} = \mathcal{F}(x, y, \underline{\lambda}_{\mathcal{Q}})$, noting $n_x = x / \sqrt{x^T x}$ and $n_y =$
586 $y / \sqrt{y^T y}$, f_Y can be scaled as

$$\begin{aligned} f_Y &= \frac{|x^T y|}{\underline{\lambda}_{\mathcal{Q}} x^T x y^T y} (x^T \mathcal{Q} x) y^T y - x^T y \\ &\geq \frac{|x^T y|}{\underline{\lambda}_{\mathcal{Q}} x^T x y^T y} (\underline{\lambda}_{\mathcal{Q}} x^T x) y^T y - x^T y \\ &\geq 0 \quad \forall x, y. \end{aligned} \quad (\text{A.2})$$

587 Correspondingly, when $\mathcal{F} = \mathcal{F}(x, y, -\underline{\lambda}_{\mathcal{Q}})$, the sign of f_{Υ}
 588 changes as

$$\begin{aligned} f_{\Upsilon} &= \frac{|x^T y|}{-\underline{\lambda}_{\mathcal{Q}} x^T x y^T y} (x^T Q x) y^T y - x^T y \\ &\leq \frac{|x^T y|}{-\underline{\lambda}_{\mathcal{Q}} x^T x y^T y} (\underline{\lambda}_{\mathcal{Q}} x^T x) y^T y - x^T y \\ &\leq 0 \forall x, y. \end{aligned} \quad (\text{A.3})$$

589 Therefore, both positive and negative values of f_{Υ} are achievable
 590 by the design of \mathcal{F} . \square

APPENDIX B PROOF OF THEOREM 3.1

591 Define the Lyapunov function as

$$V_s = \frac{1}{2} \mathbf{z}_2^T \mathbf{M} \mathbf{z}_2 + \frac{1}{2} \mathbf{z}_{pi}^T \mathbf{z}_{pi} + \frac{1}{2} \mathbf{z}_{po}^T \mathbf{z}_{po}. \quad (\text{B.1})$$

593 Combining *Property 2.2*, (41), and (47), the derivative of (B.1)
 594 can be written as

$$\begin{aligned} \dot{V}_s &= \mathbf{z}_2^T (\mathbf{M} \dot{\mathbf{z}}_2 + \mathbf{C} \mathbf{z}_2) + \mathbf{z}_{pi}^T \dot{\mathbf{z}}_{pi} + \mathbf{z}_{po}^T \dot{\mathbf{z}}_{po} \\ &= -\mathbf{z}_2^T \Lambda_{k_F} \mathbf{z}_2 + \Upsilon_V + \mathbf{z}_2^T \left(\boldsymbol{\tau}_{ds2} - \tilde{\mathbf{d}}_F + \tilde{\mathbf{d}}_F^* \right) \\ &\quad - \mathbf{z}_{pi}^T \Lambda_{\theta_{\beta_i}}^{-1} \Lambda_{k_{Qi}} \mathbf{z}_{pi} - \mathbf{z}_{po}^T \Lambda_{\theta_{\beta_o}}^{-1} \Lambda_{k_{Qo}} \mathbf{z}_{po} \\ &\quad + \mathbf{z}_{pi}^T \Lambda_{\theta_{\beta_i}}^{-1} \left(\Lambda_{\mathbf{V}_i}^{-1} \mathbf{Q}_{ids2} - \tilde{\mathbf{d}}_{Qi} + \tilde{\mathbf{d}}_{Qi}^* \right) \\ &\quad + \mathbf{z}_{po}^T \Lambda_{\theta_{\beta_o}}^{-1} \left(-\Lambda_{\mathbf{V}_o}^{-1} \mathbf{Q}_{ods2} - \tilde{\mathbf{d}}_{Qo} + \tilde{\mathbf{d}}_{Qo}^* \right) \end{aligned} \quad (\text{B.2})$$

595 where $\Upsilon_V = \mathbf{z}_2^T \mathbf{z}_3 + \mathbf{z}_{pi}^T \Lambda_{\theta_{\beta_i}}^{-1} \Lambda_{\mathbf{V}_i}^{-1} \Upsilon_{Qi} - \mathbf{z}_{po}^T \Lambda_{\theta_{\beta_o}}^{-1} \Lambda_{\mathbf{V}_o}^{-1} \Upsilon_{Qo}$.
 596 Noting *Lemma 3.1* and referring back to \mathbf{z}_3 in (32), $\tilde{\Upsilon}_{Qi}$ in (36)
 597 and Υ_{Qo} in (43), Υ_V can be scaled to

$$\begin{aligned} \Upsilon_V &= \mathbf{z}_2^T \mathbf{J}_h (\Lambda_{\mathbf{A}_i} \mathbf{z}_{pi} - \Lambda_{\mathbf{A}_o} \mathbf{z}_{po}) \\ &\quad - \mathbf{z}_{pi}^T \Lambda_{\theta_{\beta_i}}^{-1} \mathcal{F}_i \Lambda_{\mathbf{A}_i} \mathbf{J}_h^T \mathbf{z}_2 + \mathbf{z}_{po}^T \Lambda_{\theta_{\beta_o}}^{-1} \mathcal{F}_o \Lambda_{\mathbf{A}_o} \mathbf{J}_h^T \mathbf{z}_2 \\ &= -\mathbf{z}_{pi}^T \left(\Lambda_{\theta_{\beta_i}}^{-1} \mathcal{F}_i - \mathbf{I} \right) \Lambda_{\mathbf{A}_i} \mathbf{J}_h^T \mathbf{z}_2 \\ &\quad + \mathbf{z}_{po}^T \left(\Lambda_{\theta_{\beta_o}}^{-1} \mathcal{F}_o - \mathbf{I} \right) \Lambda_{\mathbf{A}_o} \mathbf{J}_h^T \mathbf{z}_2 \\ &\leq 0. \end{aligned} \quad (\text{B.3})$$

598 According to *Property 2.1* as well as the conditions (28)-2),
 599 (39)-2), and (45)-2), \dot{V}_s can be further converted as

$$\begin{aligned} \dot{V}_s &\leq -\mathbf{z}_2^T \Lambda_{k_F} \mathbf{z}_2 - \mathbf{z}_{pi}^T \Lambda_{\theta_{\beta_i}}^{-1} \Lambda_{k_{Qi}} \mathbf{z}_{pi} \\ &\quad - \mathbf{z}_{po}^T \Lambda_{\theta_{\beta_o}}^{-1} \Lambda_{k_{Qo}} \mathbf{z}_{po} + \eta_F + \underline{\theta}_{\beta_i} \eta_{Qi} + \underline{\theta}_{\beta_o} \eta_{Qo} \\ &\leq -\underline{k}_F \mathbf{z}_2^T \mathbf{z}_2 - \bar{\theta}_{\beta_i} \underline{k}_{Qi} \mathbf{z}_{pi}^T \mathbf{z}_{pi} - \bar{\theta}_{\beta_o} \underline{k}_{Qo} \mathbf{z}_{po}^T \mathbf{z}_{po} + \eta_s \\ &\leq -\lambda_s V_s + \eta_s \end{aligned} \quad (\text{B.4})$$

600 which leads to (60) by comparison Lemma and the boundedness
 601 of all the close-loop system signals is guaranteed. \square

APPENDIX C PROOF OF THEOREM 3.2

Referring back to (22), one can obtain

$$\begin{aligned} f_{\mathbf{d}} &\triangleq \hat{\mathbf{d}}_F^T [\Lambda_{\gamma_F}^{-1} \text{Proj}_{\hat{\mathbf{d}}}(\Lambda_{\gamma_F} \mathcal{H}_F \mathbf{z}_2) - \mathbf{z}_2] \\ &\quad + \hat{\mathbf{d}}_{Qi}^T [\Lambda_{\gamma_{Qi}}^{-1} \text{Proj}_{\hat{\mathbf{d}}}(\Lambda_{\gamma_{Qi}} \mathcal{H}_{Qi} \mathbf{z}_{pi}) - \Lambda_{\theta_{\beta_i}}^{-1} \mathbf{z}_{pi}] \\ &\quad + \hat{\mathbf{d}}_{Qo}^T [\Lambda_{\gamma_{Qo}}^{-1} \text{Proj}_{\hat{\mathbf{d}}}(\Lambda_{\gamma_{Qo}} \mathcal{H}_{Qo} \mathbf{z}_{po}) - \Lambda_{\theta_{\beta_o}}^{-1} \mathbf{z}_{po}] \\ &\leq 0. \end{aligned} \quad (\text{C.1})$$

Define the Lyapunov function as

$$\begin{aligned} V_a &= V_s + \frac{1}{2} \hat{\mathbf{d}}_F^T \Lambda_{\gamma_F}^{-1} \hat{\mathbf{d}}_F + \frac{1}{2} \hat{\mathbf{d}}_{Qi}^T \Lambda_{\gamma_{Qi}}^{-1} \hat{\mathbf{d}}_{Qi} \\ &\quad + \frac{1}{2} \hat{\mathbf{d}}_{Qo}^T \Lambda_{\gamma_{Qo}}^{-1} \hat{\mathbf{d}}_{Qo}. \end{aligned} \quad (\text{C.2})$$

If PE condition in (61) is satisfied, the parameters can be estimated to the true values, i.e., $\tilde{\Theta}_{\bullet} \rightarrow 0$ as $t \rightarrow \infty$ and $\tilde{\Theta}_{\bullet} \in \mathcal{L}_2^{l_{\Theta_{\bullet}}} [0, \infty)$ (with $\bullet \in \{F, Qi, Qo\}$). Noting $\tilde{\Delta}_F = \tilde{\Delta}_{Qi} = \tilde{\Delta}_{Qo} = 0$, from (28)-1), (39)-1), (45)-1), and (B.3), the derivative of (C.2) can be written as

$$\begin{aligned} \dot{V}_a &= \dot{V}_s + \hat{\mathbf{d}}_F^T \Lambda_{\gamma_F}^{-1} \dot{\hat{\mathbf{d}}}_F + \hat{\mathbf{d}}_{Qi}^T \Lambda_{\gamma_{Qi}}^{-1} \dot{\hat{\mathbf{d}}}_{Qi} + \hat{\mathbf{d}}_{Qo}^T \Lambda_{\gamma_{Qo}}^{-1} \dot{\hat{\mathbf{d}}}_{Qo} \\ &= -\mathbf{z}_2^T \Lambda_{k_F} \mathbf{z}_2 - \mathbf{z}_{pi}^T \Lambda_{\theta_{\beta_i}}^{-1} \Lambda_{k_{Qi}} \mathbf{z}_{pi} \\ &\quad - \mathbf{z}_{po}^T \Lambda_{\theta_{\beta_o}}^{-1} \Lambda_{k_{Qo}} \mathbf{z}_{po} + \Upsilon_V + f_{\mathbf{d}} + \tilde{f}_{\theta} + \mathbf{z}_2^T \boldsymbol{\tau}_{ds2} \\ &\quad + \mathbf{z}_{pi}^T \Lambda_{\theta_{\beta_i}}^{-1} \Lambda_{\mathbf{V}_i}^{-1} \mathbf{Q}_{ids2} - \mathbf{z}_{po}^T \Lambda_{\theta_{\beta_o}}^{-1} \Lambda_{\mathbf{V}_o}^{-1} \mathbf{Q}_{ods2} \\ &\leq -\mathbf{z}_2^T \Lambda_{k_F} \mathbf{z}_2 - \mathbf{z}_{pi}^T \Lambda_{\theta_{\beta_i}}^{-1} \Lambda_{k_{Qi}} \mathbf{z}_{pi} \\ &\quad - \mathbf{z}_{po}^T \Lambda_{\theta_{\beta_o}}^{-1} \Lambda_{k_{Qo}} \mathbf{z}_{po} + \tilde{f}_{\theta} \end{aligned} \quad (\text{C.3})$$

where $\tilde{f}_{\theta} \triangleq \mathbf{z}_2^T Y_F^T \tilde{\Theta}_F + \mathbf{z}_{pi}^T Y_{Qi}^T \tilde{\Theta}_{Qi} + \mathbf{z}_{po}^T Y_{Qo}^T \tilde{\Theta}_{Qo}$, with

$$\begin{aligned} Y_F^T &\triangleq \phi_F^T \\ Y_{Qi}^T &\triangleq \left[\Lambda_{\theta_{\beta_i}}^{-1} \Lambda_{\dot{\mathbf{p}}_{id}} \phi_{\chi_i}^T, -\Lambda_{\theta_{\beta_i}}^{-1} \Lambda_{\mathbf{V}_i}^{-1} \right] \\ Y_{Qo}^T &\triangleq \left[\Lambda_{\theta_{\beta_o}}^{-1} \Lambda_{\dot{\mathbf{p}}_{od}} \phi_{\chi_o}^T, -\Lambda_{\theta_{\beta_o}}^{-1} \Lambda_{\mathbf{V}_o}^{-1} \right]. \end{aligned} \quad (\text{C.4})$$

Therefore, $\dot{V}_a(t) \leq \dot{V}_a(0) \forall t \geq t_f$. Since ϕ_{\bullet}^T is uniformly bounded, $Y_{\bullet}^T \tilde{\Theta}_{\bullet} \in \mathcal{L}_2^n [0, \infty)$ (with $\bullet \in \{F, Qi, Qo\}$). By integrating both side of (C.3), it follows that $\mathbf{z}_2, \mathbf{z}_{pi}, \mathbf{z}_{po} \in \mathcal{L}_2^n [0, \infty)$. As a result, the asymptotic tracking can be obtained by applying Barbalat's lemma. \square

REFERENCES

- [1] J. Mattila, J. Koivumäki, D. G. Caldwell, and C. Semini, "A survey on control of hydraulic robotic manipulators with projection to future trends," *IEEE/ASME Trans. Mechatron.*, vol. 22, no. 2, pp. 669–680, Apr. 2017.
- [2] Z. Yao, F. Xu, G.-P. Jiang, and J. Yao, "Data-driven control of hydraulic manipulators by reinforcement learning," *IEEE/ASME Trans. Mechatron.*, vol. 29, no. 4, pp. 2673–2684, Aug. 2024.
- [3] J. Shen, J. Zhang, H. Zong, M. Cheng, and B. Xu, "Hierarchical decoupling controller with cylinder separated model of hydraulic manipulators for contact force/motion control," *IEEE/ASME Trans. Mechatron.*, vol. 28, no. 2, pp. 1081–1092, Apr. 2023.

- [4] W. Sun and Y. Yuan, "Passivity based hierarchical multi-task tracking control for redundant manipulators with uncertainties," *Automatica*, vol. 155, 2023, Art. no. 111159.
- [5] F. Huang, X. Yang, D. Mei, and Z. Chen, "Unified contact model and hybrid motion/force control for teleoperated manipulation in unknown environments," *IEEE/ASME Trans. Mechatron.*, vol. 30, no. 2, pp. 921–932, Apr. 2025.
- [6] J. Koivumäki and J. Mattila, "Stability-guaranteed impedance control of hydraulic robotic manipulators," *IEEE/ASME Trans. Mechatron.*, vol. 22, no. 2, pp. 601–612, Apr. 2017.
- [7] J. Mi, J. Yao, and W. Deng, "Adaptive rise control of winding tension with active disturbance rejection," *Chin. J. Mech. Eng.*, vol. 37, no. 1, 2024, Art. no. 52111159.
- [8] W. Deng, H. Zhou, J. Zhou, and J. Yao, "Neural network-based adaptive asymptotic prescribed performance tracking control of hydraulic manipulators," *IEEE Trans. Syst., Man, Cybern. Syst.*, vol. 53, no. 1, pp. 285–295, Jan. 2023.
- [9] Z. Chen, S. Zhou, C. Shen, L. Lyu, J. Zhang, and B. Yao, "Observer-based adaptive robust precision motion control of a multi-joint hydraulic manipulator," *IEEE/CAA J. Automatica Sinica*, vol. 11, no. 5, pp. 1213–1226, May 2024.
- [10] Z. Chen et al., "Motion control of independent metering electro-hydraulic system based on chamber pressure planning without mode switch," *J. Mech. Eng.*, vol. 60, pp. 302–312, 2024.
- [11] T. Lin, Y. Lin, H. Ren, H. Chen, Z. Li, and Q. Chen, "A double variable control load sensing system for electric hydraulic excavator," *Energy*, vol. 223, 2021, Art. no. 119999.
- [12] M. Cheng, B. Sun, R. Ding, and B. Xu, "A multi-mode electronic load sensing control scheme with power limitation and pressure cut-off for mobile machinery," *Chin. J. Mech. Eng.*, vol. 36, no. 1, 2023, Art. no. 29.
- [13] Y. Xia et al., "Advanced motion control of hydraulic manipulator with precise compensation of dynamic friction," *IEEE Trans. Ind. Inform.*, vol. 20, no. 7, pp. 9375–9384, Jul. 2024.
- [14] Y. Yuan and W. Sun, "An integrated kinematic calibration and dynamic identification method with only static measurements for serial robot," *IEEE/ASME Trans. Mechatron.*, vol. 28, no. 5, pp. 2762–2773, Oct. 2023.
- [15] S. Zhou, Y. Xia, M. Qi, D. Mei, and Z. Chen, "Transformed workspace adaptive mapping based master-slave operation control for hydraulic manipulator," *IEEE Trans. Ind. Electron.*, early access, Jan. 28, 2025, doi: 10.1109/TIE.2024.3525099.
- [16] J. Zhang, F. Zhang, M. Cheng, R. Ding, B. Xu, and H. Zong, "Parameter identification of hydraulic manipulators considering physical feasibility and control stability," *IEEE Trans. Ind. Electron.*, vol. 71, no. 1, pp. 718–728, Jan. 2024.
- [17] L. Wang, W. J. Book, and J. D. Huggins, "Application of singular perturbation theory to hydraulic pump controlled systems," *IEEE/ASME Trans. Mechatron.*, vol. 17, no. 2, pp. 251–259, Apr. 2012.
- [18] S. Zhang, T. Minav, M. Pietola, H. Kauranne, and J. Kajaste, "The effects of control methods on energy efficiency and position tracking of an electro-hydraulic excavator equipped with zonal hydraulics," *Autom. Construction*, vol. 100, pp. 129–144, 2019.
- [19] J. Wang, G. Gong, and H. Yang, "Control of bulk modulus of oil in hydraulic systems," in *Proc. IEEE/ASME Int. Conf. Adv. Intell. Mechatron.*, 2008, pp. 1390–1395.
- [20] H. Yang, B. Feng, and G. Gong, "Measurement of effective fluid bulk modulus in hydraulic system," *J. Dyn. Syst., Meas., Control*, vol. 133, no. 6, 2011, Art. no. 061021.
- [21] H. B. Murrenhoff, "Grundlagen der fluidtechnik-teil 1: Hydraulik," 2011.
- [22] S. Kim and H. Murrenhoff, "Measurement of effective bulk modulus for hydraulic oil at low pressure," *J. Fluids Eng.*, vol. 134, 2012, Art. no. 021201.
- [23] S. Shi, Z. He, D. Zeng, P. Huang, and G. Jin, "Identification and modeling of a servo pump-controlled hydraulic system," *IEEE/ASME Trans. Mechatron.*, early access, Oct. 4, 2024, doi: 10.1109/TMECH.2024.3454518.
- [24] J. Schwarz and B. Lohmann, "Robust identification and control of mobile hydraulic systems using a decentralized valve structure," *Control Eng. Pract.*, vol. 151, 2024, Art. no. 106030.
- [25] J. Liu et al., "Motion control of electro-hydrostatic actuators with modeling and compensation of nonlinear bulk modulus," *IEEE Trans. Ind. Electron.*, vol. 72, no. 6, pp. 6185–6193, Jun. 2025.
- [26] D. T. Liem, "Trajectory control of a hydraulic system using intelligent control approach based on adaptive prediction model," *IFAC J. Syst. Control*, vol. 26, 2023, Art. no. 100228.
- [27] P. Righettini, R. Strada, S. Valilou, and E. KhademOlama, "Nonlinear model of a servo-hydraulic shaking table with dynamic model of effective bulk modulus," *Mech. Syst. Signal Process.*, vol. 110, pp. 248–259, 2018.
- [28] W. Shen and J. Wang, "An integral terminal sliding mode control scheme for speed control system using a double-variable hydraulic transformer," *ISA Trans.*, vol. 124, pp. 386–394, 2022.
- [29] Z. Chen, B. Helian, Y. Zhou, and M. Geimer, "An integrated trajectory planning and motion control strategy of a variable rotational speed pump-controlled electro-hydraulic actuator," *IEEE/ASME Trans. Mechatron.*, vol. 28, no. 1, pp. 588–597, Feb. 2023.
- [30] H. Ding, Y. Li, Q. Zhu, and J. Su, "Position servo with variable speed pump-controlled cylinder: Design, modelling and experimental investigation," *Int. J. Hydromechatronics*, vol. 7, no. 2, pp. 155–175, 2024.
- [31] Y. Sun, Y. Wan, H. Ma, and X. Liang, "Compensation control of hydraulic manipulator under pressure shock disturbance," *Nonlinear Dyn.*, vol. 111, no. 12, pp. 11153–11169, 2023.
- [32] J. Koivumäki, W.-H. Zhu, and J. Mattila, "Energy-efficient and high-precision control of hydraulic robots," *Control Eng. Pract.*, vol. 85, pp. 176–193, 2019.
- [33] Y. Zhou, R. Ding, M. Cheng, L. Liao, Z. Chen, and B. Yao, "Precision motion control of independent metering hydraulic swing system with large inertia loads: A case study on a rotary drilling rig," *IEEE Trans. Ind. Electron.*, early access, Mar. 21, 2025, doi: 10.1109/TIE.2025.3549091.
- [34] R. Ding et al., "A review of independent metering control system for mobile machinery," *Int. J. Hydromechatronics*, vol. 8, no. 5, pp. 1–39, 2025.
- [35] L. Lyu, Z. Chen, and B. Yao, "Parallel-connected pump-valves coordinated electro-hydraulic system: Comparative study and motion control," *J. Mech. Eng.*, vol. 58, pp. 136–151, 2022.
- [36] R. Ding, M. Cheng, L. Jiang, and G. Hu, "Active fault-tolerant control for electro-hydraulic systems with an independent metering valve against valve faults," *IEEE Trans. Ind. Electron.*, vol. 68, no. 8, pp. 7221–7232, Aug. 2021.
- [37] G. Stojanoski, G. Rath, and M. Gimpel, "The effects of bulk modulus on the dynamics of controlled independent metering system," in *Proc. 16th Scand. Int. Conf. Fluid Power*, 2019.
- [38] Y. Gao, Y. Shen, T. Xu, W. Zhang, and L. Güvenç, "Oscillatory yaw motion control for hydraulic power steering articulated vehicles considering the influence of varying bulk modulus," *IEEE Trans. Control Syst. Technol.*, vol. 27, no. 3, pp. 1284–1292, May 2019.



Yangxiu Xia received the B.Eng. degree in ocean engineering and technology from Zhejiang University, Hangzhou, China, in 2022. He is currently working toward the Ph.D. degree in ocean technology and engineering with the Ocean College, Zhejiang University, Zhoushan, China.



Jiajia Liu received the B.Eng. degree in marine engineering from the Wuhan University of Technology, Wuhan, China, in 2018, and the M.Eng. degree in marine engineering from the Huazhong University of Science and Technology, Wuhan, in 2021. He is currently working toward the Ph. D. degree in electronic information with the Ocean College, Zhejiang University.

759
760
761
762
763
764
765
766
767



Litong Lyu received the B.Eng. and Ph.D. degrees in mechatronics engineering from Zhejiang University, Hangzhou, China, in 2015 and 2020, respectively.

Since 2020, he has been with the School of Mechanical Engineering, Shijiazhuang Tiedao University, Hebei, China, where he is currently an Associate Professor.

768
769
770
771
772
773
774



Manzhi Qi received the B.Eng. degree in ocean engineering and technology from Zhejiang University, Hangzhou, China, in 2024. He is currently working toward the Ph.D. degree in ocean technology and engineering with the Ocean College, Zhejiang University, Zhoushan, China.



Shizhao Zhou received the B.Eng. and Ph.D. degrees from Zhejiang University, Hangzhou, China, in 2018 and 2024, respectively.

Since 2024, he has been with the School of Mechanical Engineering and Automation, Fuzhou University, Fuzhou, China, where he is currently an Associate Professor. His research interests include advanced control of mechatronic hydraulic systems especially hydraulic manipulators.

775
776
777 Q7
778
779
780
781
782
783
784
785
786
787
788
789
790
791
792
793
794
795
796
797
798
799
800
801



Zheng Chen (Senior Member, IEEE) received the B.Eng. and Ph.D. degrees in mechatronic control engineering from Zhejiang University, Hangzhou, China, in 2007 and 2012, respectively.

From 2013 to 2015, he was a Postdoctoral Researcher with the Department of Mechanical Engineering, Dalhousie University, Halifax, NS, Canada. Since 2015, he has been an Associated Professor with the Ocean College, Zhejiang University, Hangzhou. His research interests mainly focus on advanced control of robotic and mechatronic systems (e.g., nonlinear adaptive robust control, motion control, trajectory planning, telerobotics, exoskeleton, mobile manipulator, precision mechatronic systems, and underwater robots).

786
787
788
789
790
791
792
793
794
795
796
797
798
799
800
801